SELECTIVE DISSOLUTION AND CORROSION OF SOME BINARY NOBLE METAL ALLOYS

BY

P. DURKIN

A thesis submitted for the degree of

Doctor of Philosophy of the University of Warwick

Department of Physics,
University of Warwick.

June 1982

This thesis is dedicated to my parents

Myra and Alan

CONTENTS

ACKNOWLEDGEMENTS

I wish to express my deep and sincere gratitude to my supervisor, Professor A. J. Forty, for his constant encouragement and assistance throughout this study. I am grateful to Drs. A. E. Hughes, A. Atkinson and P. T. Moseley of the Materials Development Division, A.E.R.E., Harwell, for their continued interest and discussion during this work. I would like to thank members of the Department of Physics here at Warwick, for all their help and friendliness during my study. Finally I am indebted to the Atomic Energy Authority, for the granting of a studentship.

DECLARATION

This dissertation is submitted to the University of Warwick in support of my application for admission to the degree of Doctor of Philosophy. It contains an account of my own work performed at the Department of Physics of the University of Warwick in the period from October 1978 to September 1981 under the supervision of Professor A. J. Forty. No part of it has been used previously in a degree thesis submitted to this or any other University. The work described in this thesis is the result of my own independent research except where acknowledged in the text. Accounts of the micromorphological study of the dissolution of silver-gold alloys in nitric acid and of oxide growth during selective dissolution of silver from silver-gold alloys have been published in Phil. Mag. A., 1980, Vol. 42, No. 3, 295-318 and Phil. Mag. A., 1982, Vol. 15, No. 1, 95-105.

June 1982

P. Durkin

ABSTRACT

The aims of the project are to investigate the fundamental processes involved when one component selectively dissolves from a binary metal alloy. This is done with reference to noble metal alloys, particularly silver-gold alloys dissolved in nitric acid. These are prepared as electron transparent single-crystal samples and therefore have a simple initial microstructure which can be viewed directly using transmission electron microscopy. After corrosion very detailed microstructural information can be resolved and this is used to elucidate the processes operating during corrosion itself. A well defined and characteristic morphology is seen to develop on silver-gold alloys which is dependent on the exact extent of corrosion. This can be accounted for by a model involving selective dissolution of silver and re-arrangement of the residual gold in a manner analogous to that occurring during the vapour deposition of thin films on crystal substrates. A corrosion phase develops when silver-gold alloys dissolve in nitric acid and careful examination of its structure and epitaxy using electron diffraction and dark field electron microscopy reveals that it is probably gold I oxide. This indicates that gold is directly affected by the corrosion reaction and therefore provides an indication of the mechanisms by which these alloys dissolve. Evidence of a very aggressive attack on the whole fabric of the alloy during corrosion is given by the observation of dislocations and dislocation networks in all of the systems studied and of mixing of components during corrosion in the copper-gold system. The observations presented lead to the idea that corrosion produces widespread attack of the alloy structure involving the noble component as well as the actively dissolving one. The work demonstrates the importance of surface diffusion processes in the selective dissolution corrosion of the systems under investigation.

ABSTRACT

The aims of the project are to investigate the fundamental processes involved when one component selectively dissolves from a binary metal alloy. This is done with reference to noble metal alloys, particularly silver-gold alloys dissolved in nitric acid. These are prepared as electron transparent single-crystal samples and therefore have a simple initial microstructure which can be viewed directly using transmission electron microscopy. After corrosion very detailed microstructural information can be resolved and this is used to elucidate the processes operating during corrosion itself. A well defined and characteristic morphology is seen to develop on silver-gold alloys which is dependent on the exact extent of corrosion. This can be accounted for by a model involving selective dissolution of silver and re-arrangement of the residual gold in a manner analogous to that occurring during the vapour deposition of thin films on crystal substrates. A corrosion phase develops when silver-gold alloys dissolve in nitric acid and careful examination of its structure and epitaxy using electron diffraction and dark field electron microscopy reveals that it is probably gold I oxide. This indicates that gold is directly affected by the corrosion reaction and therefore provides an indication of the mechanisms by which these alloys dissolve. Evidence of a very aggressive attack on the whole fabric of the alloy during corrosion is given by the observation of dislocations and dislocation networks in all of the systems studied and of mixing of components during corrosion in the copper-gold system. The observations presented lead to the idea that corrosion produces widespread attack of the alloy structure involving the noble component as well as the actively dissolving one. The work demonstrates the importance of surface diffusion processes in the selective dissolution corrosion of the systems under investigation.

CHAPTER 1

General Introduction

1:1 Broad Aims of this work

The bulk of this thesis is concerned with corrosion and selective dissolution in noble metal binary alloys. Selective dissolution is the process in which one constituent of an alloy, the more chemically active, dissolves preferentially and leaves behind a residue of the other, more noble constituent. This is thought to play a very important part in many complex corrosion phenomena, in the aqueous corrosion of alloys in general, in localised corrosion and in stress corrosion cracking and other environment sensitive mechanical properties of alloys. Understanding selective dissolution itself will help in the understanding of these more complex corrosion processes. Experiments have been carefully designed so that selective dissolution can be looked at in isolation from other corrosion processes. In this way, specific information about the processes that occur even on an atomic scale, can be obtained. The work contained here seeks to provide a detailed understanding of the processes involved in selective dissolution of binary alloys and to go some way in showing how these are important in the more complex corrosion phenomena outlined above.

1:2 Corrosion

Most metals occur naturally in some combined state and this can be used to provide a simple definition of corrosion. Corrosion may be described as the thermodynamic tendency of a metal to revert back to some combined state. It goes without saying that since there is such widespread use of metals then this tendency to attain a combined state will be of great technological importance.

Although some metals (thecoinage metals, the platinum metals, mercury)

are found in the Earth's crust in a more or less pure state, many of those which are widely used industrially, such as iron, aluminium and zinc, are highly unstable thermodynamically in the oxidising conditions existing on the Earth's surface. A measure of the tendency of a pure metal to react with its environment is given by its electrode potential. This is the potential difference established between a pure metal and a 1 molar solution of its ions at 25°C. The laws of electrostatics permit only potential differences between two points in a single phase to be measured and so electrode potentials are usually measured relative to the standard hydrogen electrode which is defined as having a standard electrode potential of zero (see for example Tulloch and Stewart (1968)). Table 1.2.1 is a list of standard electrode potentials for some common metals. This electromotive series represents the thermodynamic tendencies or potentials of the reactions listed, the more negative the E_M value then the greater is the tendency for the metal to corrode.

Table 1.2.1. after Stewart and Tulloch (1968)

The Electromotive Series

Equilibrium Reaction	E_M (volts)
$Au^{3+} + 3e \rightarrow Au$	+ 1.7
$2e + \frac{1}{2}O_2 + 2H^+ \rightarrow H_2O$	+ 1.23
$Pt^{2+} + 2e \rightarrow Pt$	+ 1.2
$Hg^{2+} + 2e \rightarrow Hg$	+ 0.85
$Ag^{+} + e \rightarrow Ag$	+ 0.80
$Cu^{2+} + 2e \rightarrow Cu$	+ 0.34
$2H^{+} + 2e \rightarrow H_2$	- 0.00 by definition
$Pb^{2+} + 2e \rightarrow Pb$	- 0.13
$Ni^{2+} + 2e \rightarrow Ni$	- 0.25
$Cd^{2+} + 2e \rightarrow Cd$	- 0.40
$Fe^{2+} + 2e \rightarrow Fe$	- 0.44
$Cr^{3+} + 3e \rightarrow Cr$	- 0.70
$Zn^{2+} + 2e \rightarrow Zn$	- 0.76
$Ti^{2+} + 2e \rightarrow Ti$	- 1.63
$Al^{3+} + 3e \rightarrow Al$	- 1.66
$Mg^{2+} + 2e \rightarrow Mg$	- 2.38

Corrosion processes involve electron transfer, electrons are removed from the dissolving metal (it is oxidised) and taken up elsewhere. This leads to the idea of a corrosion 'cell' where the familiar analogy of an ordinary laboratory cell, the Daniell cell say, is used to describe the closed electrical circuit which must be established if corrosion is to occur.

In the Daniell cell, zinc corrodes to give zinc sulphate. The rate of this corrosion is limited by the rate at which electrons produced in the oxidation (anodic) reaction

$$Zn \rightarrow Zn^{2+} + 2e$$

are taken up by the reduction (cathodic) reaction, which in this case is the deposition of copper at the copper cathode. In the absence of this or some equivalent reduction process the corrosion of zinc would not take place. However, it is well known that a single metal can corrode and therefore different anodic and cathodic areas must exist on the metal. In the Daniell cell the two different metals are anodic and cathodic because of their different electrode potentials, the metal with the more positive potential being cathodic and the one with the more negative potential being anodic. It might be expected that a single piece of zinc would be quite uniform in its properties, but metals are seldom completely pure. If a very small amount of more noble metal impurity were present then the atoms of this metal at the surface would constitute microscopic cathodic areas which could be quite sufficient to permit a measurable rate of corrosion. If the impurity were copper and the dilute corroding acid also contained copper ions then a whole series of microscopic Daniell cells could be envisaged on the surface of the metal. It is well known that zinc will dissolve much more readily in hydrochloric acid if a little copper sulphate solution is added.

Even in the absence of more noble metal impurities metals can still corrode. This can be for a variety of reasons, one important reason being that metal surfaces are not uniform when considered at the microscopic level. Different crystal faces will have slightly different electrode potentials and in a corrosive environment these slight differences can give rise to the anodic and cathodic areas necessary for corrosion to proceed. Strain in the metal can have the same effect, the potential of a strained area being slightly different from that of a surrounding unstrained area. Strains can arise, for example, where rivets pass through a metal structure and extensive corrosion in these areas may represent a serious hazard.

Consider the corrosion of iron, the anodic reaction is:

$$Fe \rightarrow Fe^{2+} + 2e^{-}$$

It is known that iron will corrode under neutral or alkaline conditions, the cathodic process cannot, therefore, be the same as that described for zinc and some other cathodic reaction must be involved. This reaction involves oxygen since iron will not corrode in water if oxygen is carefully excluded.

The cathodic reaction is

$$2H_2O + O_2 + 4e^{-} \rightarrow 4OH^{-}$$

giving rise to the formation of hydroxide ions. If, as expected anodic and cathodic areas of corroding iron are in close proximity iron (II) ions produced at the anode, react with these hydroxide ions resulting in the precipitation of iron (II) hydroxide $Fe(OH)_2$. If sufficient oxygen is present further reactions are possible leading to the formation of a more complex substance of variable composition known generally as rust.

The potential of a cathodic area is, in water, dependent on the concentration of dissolved oxygen. If, therefore, different areas are

exposed to different concentrations of oxygen the oxygen-rich areas will be more cathodic than the oxygen-deficient areas. If a piece of iron is partially immersed in water the oxygen concentration will be greatest at the surface of the water. This area of the metal will be cathodic to the submerged area, corrosion of which will then take place, Fig. 1.2.1. Features on the surface of a completely submerged object (for example a bolt or rivet) can, by limiting the diffusion of more oxygen-rich water, give rise to localized corrosion cells.

Corrosion then occurs because charge transfer reactions are possible. Overall charge neutrality is maintained and anodic processes must be exactly balanced by complementary cathodic processes. It is understanding the nature and distribution of both processes which is the challenge in understanding corrosion.

Approaches to the study of corrosion fall into three broad categories. The first involves consideration of the structure, composition and general metallurgy of a metal and how this changes during corrosion. The second is concerned with the environment of a metal and such things as pressure, temperature, properties and concentration of reactive species. The third concerns the details of the metal/environment interface, for example, how and in what form corrosion products are produced and how they are distributed. It should be possible to examine the microstructural and compositional changes which occur in a metal after corrosion and infer what processes were occurring while the metal was actually corroding. This is particularly true if the initial microstructure of the metal and the chemistry of the corrosion reaction are simple and well characterised. This has been the approach adopted in the study of corrosion described here and very thorough and detailed high resolution investigations of metals after corrosion have been used to elucidate corrosion mechanisms.

The features in a metal which may influence its corrosion behaviour have been listed by Shrier (1976) and are given in Table 1.2.2.

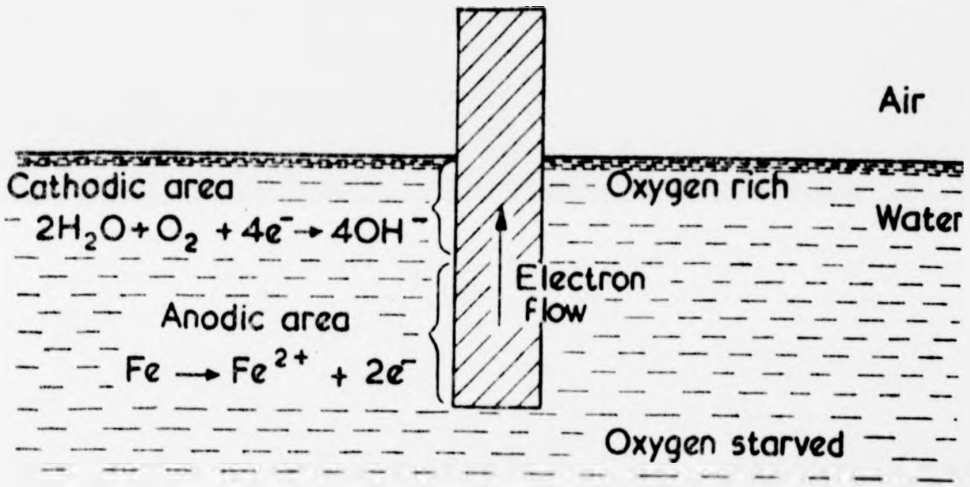

Fig. 1.2.1. Anodic and Cathodic areas on a piece of iron corroding in water. Corrosion takes place below the surface at the anodic (oxygen starved) areas (after Stewart and Tulloch 1968).

TABLE 1.2.2. Heterogeneities in Metals

1 ATOMIC
(a) Sites within a given surface layer; these vary according to the particular crystal plane.
(b) Sites at edges of partially complete layers.
(c) Point defects in the surface layer; vacancies, kink sites, adsorbed molecules, dislocations.
2 MICROSCOPIC
(a) Grain boundaries, usually more active than grain interior.
(b) Phases - metallic, non-metallic, metal compounds, impurities.
3 MACROSCOPIC
(a) Grain boundaries.
(b) Discontinuities on metal surface - cut edges, scratches, discontinuities in oxide films, or in applied coatings.
(c) Bimetallic couples of dissimilar metals.
(d) Geometrical factors - general design, crevices, contact with non-metallic materials etc.

Specimens used in the experiments described in this thesis are fabricated as far as possible without macroscopic imperfections so that they only contain microscopic and atomic heterogeneities. It is worth noting that in the absence of film formation during corrosion, then microstructural singularities can have a more direct influence on corrosion kinetics. It isthought (Shrier, 1976) that structural imperfections influence corrosion behaviour because of compositional changes, due to segregation of solute atoms to these sites. This is demonstrated by comparing the corrosion rates of annealed and cold-worked steel in acid.

The difference cannot be accounted for simply by the increase in stored energy of the cold-worked steel, due to its increased dislocation density but is explained by Foroulis and Uhlig (1964) by segregation of carbon and nitrogen to dislocations so that the cathodic reaction is made easier there. Alternatively, if structural singularities promote an anodic reaction then pitting and other localised corrosion may occur because the area at which the anodic reaction occurs will probably be much smaller than the area at which the cathodic reaction occurs.

Corrosion has been classified into two basic types; wet corrosion and dry corrosion. Expressed very simply, dry corrosion involves a metal/gas reaction and unless corrosion products are volatile then a film forms and if it is continuous it is a barrier to further corrosion. The reaction rate is then controlled by the diffusion of species across this film. In wet corrosion different anodic and cathodic sites are possible and transport of charge can occur in solution as well as in the metal. Metal ions which pass into solution may be hydrated and liberate chemical energy and this can provide a thermodynamic drive for corrosion. If corrosion products are soluble then the corrosion reaction can continue unabated and will obey a linear rate law. Corrosion investigations in this thesis occur in aqueous environments and so fall under the general heading of wet corrosion.

1.3 Some studies of Selective Dissolution

Selective dissolution is a rather specialised form of corrosion. It is an alloy phenomenon furthermore it only occurs when there is a large difference in the reactivities of the constituent metals in the alloy. Dissolution of binary alloys in environments where one component dissolves and the other does not should rapidly stop due to a build up of the non-dissolvable component at the corroding surface. The observation is that

in many instances provided there is sufficient reactive metal (usually > 50 atomic %) then dissolution continues unabated until all of the reactive component is dissolved and only the more noble metal remains, frequently in the form of a porous sponge (Tammann and Brauns, 1931). Clearly some transport mechanism is operating to continually replenish the corrosion surface with reactive metal.

Much of the interest in understanding the processes occurring during selective dissolution arises because it is thought to have a role in the stress corrosion cracking of certain alloys. Stress corrosion cracking is the process by which materials fail due to the combined effect of chemical and mechanical factors. The combination of a stress and an appropriate chemical environment enables rapid propagation of cracks deep into these materials. The cracks may go undetected since they are rarely visible, and cause eventual failure in structures built from susceptible materials. This phenomenon is observed only in alloys and the environments responsible for it are often found to preferentially dissolve one component of the alloy. Graf (1956) noted for homogeneous metal alloys that the susceptibility to stress corrosion cracking appears to be most pronounced when the concentration of the more noble component is less than the parting limit, usually less than 50 per cent. Silver and copper alloyed with gold are susceptible to cracking but gold alloyed with silver or copper is not. Selective dissolution of the active component of these alloys would be expected under a wide range of conditions and Graf noted that cracking nearly always occurs using reagents in which only one component dissolves. A possible exception to this is the cracking of silver-gold and copper-gold alloys in aqua regia in which both components nominally dissolve. However the corrosion of the alloys in aqua regia may also involve the selective dissolution of the less noble component. It is interesting to note that the reacted layer which forms after immersion in aqua regia is quite similar in appearance to the reacted layer which forms when selective dissolution occurs.

Edeleanu and Forty (1960) have proposed a model for the stress corrosion cracking of α-brass in ammonia solution which again involves selective dissolution. Preferential removal of zinc at a crack-tip by the electrolyte is thought to cause embrittlement of the metal around the tip. The porous and embrittled residue of copper can support the initiation of a brittle fracture. If the crack tip velocity is greater than the so-called critical velocity for ductile fracture the crack can continue to propagate until it meets some soft material, for example a slip band, where it becomes arrested. The process of embrittlement followed by crack propagation can then be repeated as before.

Pickering and Swann (1963) were the first to study alloys known to be susceptible to stress corrosion cracking using electron microscopy. They studied copper-gold, copper-zinc, copper-aluminium and zinc-aluminium alloys and found that the corrosion morphology developed in all of these in stress corrosion environments consisted of microscopic tunnels. These same environments are also found to dissolve the less noble component of the alloy preferentially. They concluded that when a susceptible alloy is exposed to a suitable stress corrosion environment the tunnelling morphology, usually developed preferentially at active slip bands when the metal is under stress, is responsible for crack initiation. The alloy fails by a form of ductile fracture as a result of the corrosion tunnelling which continues at the tip of the crack.

As stated previously stress corrosion cracking usually occurs in alloys rather than pure metals and it is important to understand the way in which an alloy dissolves in an aqueous electrolyte. It is especially important to understand those aspects which are not normally found in the anodic dissolution of pure metals. Pickering, in a series of papers, has made a study of the dissolution of alloys. In two studies on copper-gold alloys, (1967a), (1968b), experimental evidence in the form of X-ray and electron diffraction measurements is given to show the formation of new phases,

during anodic dissolution, intermediate in composition between alloy and pure gold. Lattice parameter measurements for various copper-rich alloys after dissolution show a change in composition towards the gold-rich side of the original alloy composition. X-ray intensity in this region increases with increasing dissolution just as the corresponding alloy reflection loses intensity. The position of the maxima in this reflection depends to some extent on the initial alloy composition and in any case it usually corresponds to an alloy containing between 60% and 70% copper. A more gold-rich initial alloy composition gives a maximum in X-ray intensity of the reflection from the "corrosion-phase" corresponding to a more gold-rich composition than that obtained if a less gold-rich initial alloy composition is used. Throughout dissolution the position of this maximum does not shift, indicating that dissolution is occurring from alloy of the original composition. Only in the final stages of dissolution when the specimen is nearly consumed does the position of this maximum move towards the pure gold composition. During these final stages the shape of the X-ray intensity distribution changes from a broad rounded reflection indicating a spread of alloy composition to a sharper reflection indicating a more well-defined alloy composition. These changes in intensity with dissolution are illustrated in figure 1.3.1., taken from Pickering (1967)b, which shows a Cu 5 At% Au alloy dissolved in molar sulphuric acid. Although the actual diffusion distance is small compared with the X-ray sampling depth, Pickering calculates that severe surface roughening occurs if one component of an alloy is preferentially removed; this increases the effective volume of corroded material exposed to the X-ray beam and makes the scattered intensity due to this phase detectable. Electron diffraction measurements, where beam penetration is of the same order as interdiffusion distances, are consequently used to detect phase changes occurring in the first few minutes of dissolution.

Pickering tested the ionisation-redeposition mechanism of selective dissolution which assumes that both alloy constituents are ionised during

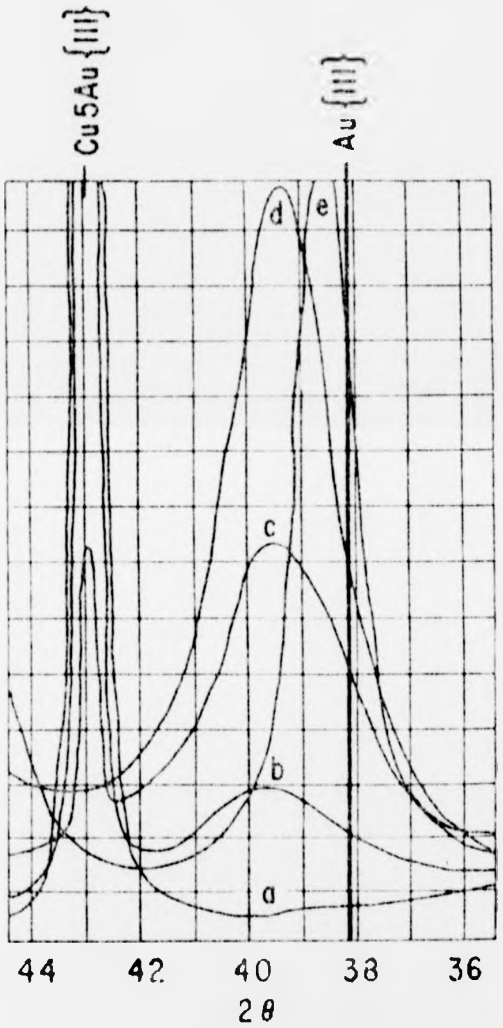

Fig. 1.3.1. Traces of recorded X-ray intensity for Cu 5 at % Au (after Pickering 1967) showing various amounts of dissolution at 5 mA/cm^2 in 1M H_2SO_4 illustrating a broad region of increase diffracted intensity from {111} planes corresponding to the presence of a gradient in composition towards the gold-rich side of the original alloy composition. The 2θ position of pure Au is indicated by the vertical line. Pattern (a) prior to anodic dissolution, (b) 3.0 C/cm^2 passed (c) 12.0 C/cm^2 passed, (d) 48.0 C/cm^2 passed and pattern (e) 96.0 C/cm^2 passed.

dissolution. It will be discussed in greater detail in the next section (1.4). He made electrochemical measurements using a rotating disc and ring combination of electrodes (1967b). A disc of test material is made to dissolve anodically and because it is rotating quickly ions so formed will be swept into the electrolyte where any gold ions can be discharged at the ring electrode by maintaining it at a suitable potential. These tests indicated that no gold ions were being discharged at the ring electrode. Pickering used this to discount the ionisation redeposition mechanism of selective dissolution but Swann (1967), commenting on Pickering's conclusions, states that the tunnelling morphology observed when these alloys dissolve would mean that any gold ionised would be deposited on the sides of the tunnels before it could be swept into the bulk of the electrolyte. The presence of gold fully ionised in the bulk of most electrolytes is highly unlikely. Failure to observe a discharge at the ring electrode simply indicates that no such ions exist in this case. It cannot reasonably be assumed from this that atoms of gold do not become temporarily ionised at the time of dissolution of copper, these gold ions being shortlived and existing only within the first few layers of solution. The ionisation redeposition mechanism of selective dissolution cannot therefore be totally discounted.

At room temperature brass forms a series of homogeneous phases; these are, in order of increasing zinc content, α, β, ν, ε, and η. At certain alloy compositions mixtures of these phases occur, for example (α + β'), (β' + γ) etc. When a single-phase, zinc-rich brass alloy dissolves anodically, not only will X-ray reflections be observed at Bragg angles corresponding to more noble i.e. copper-rich alloy compositions, as in the case of copper-gold alloys, but reflections at Bragg angles corresponding to different phases should also be observed. Pickering made X-ray measurements on several zinc-rich brasses dissolved anodically and was able to identify lines from more copper-rich alloys after they had been dissolved

(1968a). He also observed gradients in chemical composition, within individual phases, towards higher copper concentrations. Metallographic observations of transverse sections of these alloys indicated the formation of a poorly reflecting layer similar to the porous layers formed on partially dissolved copper-gold alloys.

1.4. Selective Dissolution

When a single-phase binary alloy is anodically dissolved two modes of dissolution are possible. First, both elements may be dissolved together and secondly only one element may be dissolved leaving behind the noble component. It is the latter process which is known as selective or preferential dissolution. For this to occur there must be a large difference in the electrode potentials of each metal in the particular electrolyte in which selective dissolution occurs. Selective dissolution is thought to occur when brasses and noble metal alloys dissolve and where a spongy residue of the more noble metal is frequently observed (Tammann and Brauns 1931). For prolonged dissolution transport processes must exist which enable the more reactive metal to be transported to the corroding surface of the alloy and which ensure that the reaction does not become passivated because of a uniform build up of noble metal.

The problem of how dissolution continues under these circumstances can be more clearly understood by considering the analogy of vaporisation of a simple metal in terms of an idealised terrace, step, kink model of its surface. Such an idealised situation is represented in Fig. 1.4.1. During vaporisation atoms may be detached readily from kink sites (K) to form adsorbed atoms along a step at a non-kink site (N) and then diffuse to the terrace to become ad-atoms (A). These eventually desorb into the gas phase. A succession of atoms may be removed from kink sites in this way. The energy required to remove an atom from a non-kink site (N) or to form a kink site (K) is greater. To remove atoms from a step site (S) or

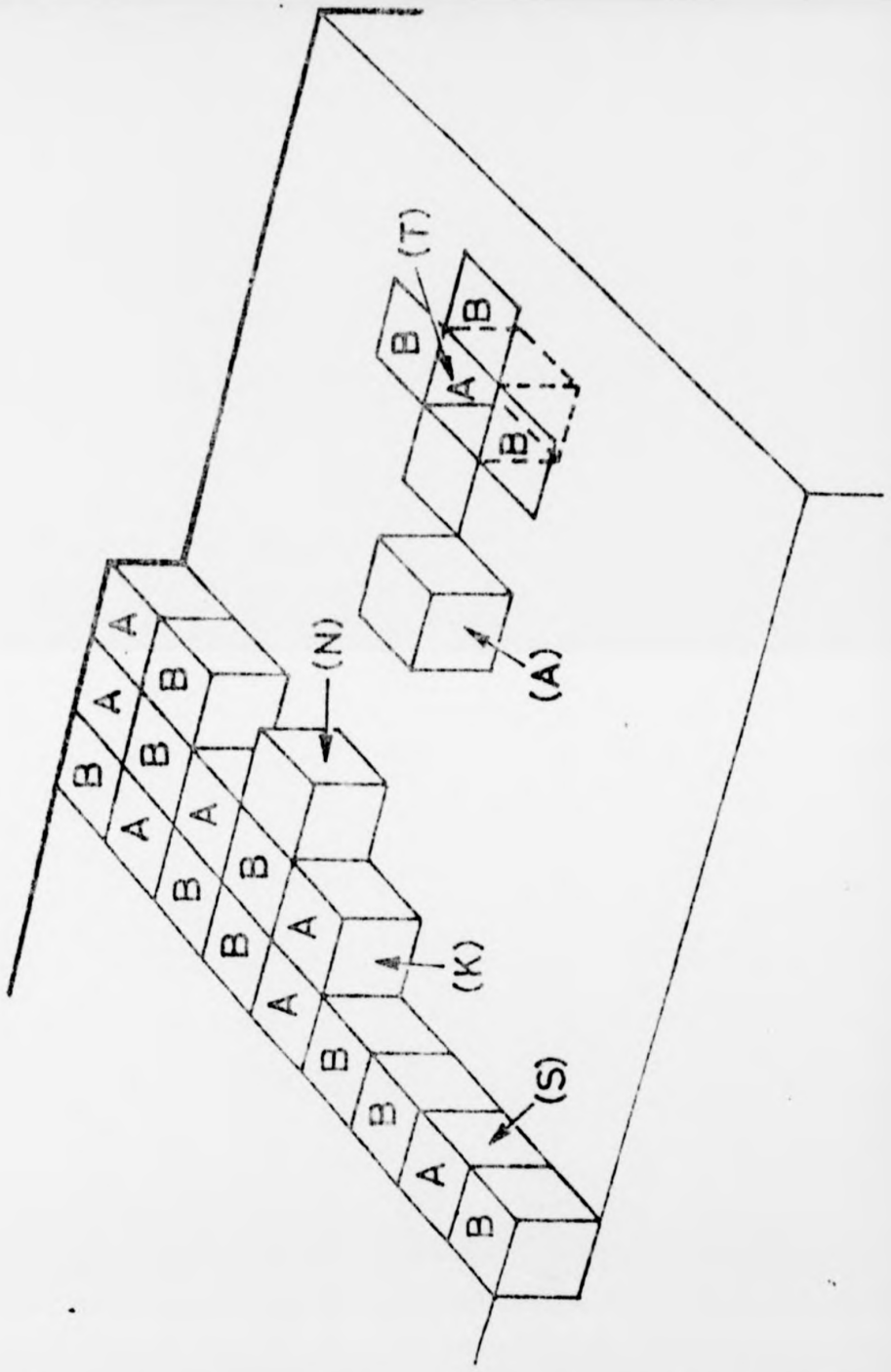

Fig. 1.4.1. An idealised terrace, step, kink, model of the surface of an alloy composed of dissolvable A atoms and noble B atoms. It is a kink site on a surface step, N is a detached atom along a step, A is an adsorbed atom, T is a terrace site.

a terrace site T requires even more energy. These processes, therefore, are thought to be unlikely events unless the temperature is very high, approaching the melting point. The dissolution of a metal is more complex because of the effects of molecular adsorption, oxidation and the formation of ion complexes due to the electrolyte. Selective dissolution of a binary alloy AB represents an even more complex situation. A atoms at kink sites may migrate along a terrace as outlined above and pass into solution. B atoms at kink sites may migrate to non-kink sites and create new kink sites occupied by A atoms. As dissolution proceeds there will be an increasing tendency for B atoms to migrate back to kink sites and, therefore, for kink sites to be completely occupied by B atoms. Eventually a large concentration of B atoms would build up at all kink sites on the alloy surface leading to electrochemical polarisation (i.e. the alloy assumes a potential greater than its equilibrium potential). As the potential increases it may become possible for an A atom at a non-kink site or even at a terrace site to become solvated directly so that corrosion can continue. Even if the chemical activity is high enough for A atoms to be directly removed from the lattice (terrace sites), without continual replenishment of A atoms at the surface of the alloy, corrosion would eventually be halted. There must then be one or more transport mechanisms enabling further A atoms to be anodically dissolved by the solution. The possible mechanisms are outlined below.

When selective dissolution occurs from an alloy one or more of three processes are likely: (i) both metals ionise followed by redeposition of the more noble metal, (ii) only one metal ionises, the remaining metal aggregating by surface diffusion exposing more alloy to be attacked in the same way, (iii) only one metal ionises atoms of both metals move around in the solid phase by volume diffusion.

The ionisation re-deposition mechanism may be looked at by considering, for example, the dissolution of brasses. The anodic reactions will be of the form:-

$$Zn(Brass) \rightarrow Zn^{2+} + 2e^{-} \qquad [1]$$

$$Cu(Brass) \rightarrow Cu^{2+} + 2e^{-} \qquad [2]$$

The re-deposition reaction will be

$$Cu^{2+} + 2e^{-} \rightarrow Cu \text{ (nearly pure)} \qquad [3]$$

If there is no coupling between reactions [1] and [2] then the activity of copper in brass will be less than unity and therefore the equilibrium electrode potential for dissolution will be more noble than that for pure copper (reaction [3]). This is clearly unrealistic. It is reasonable to suggest that there may be some coupling of the anodic reactions affecting the general rate equation for dissolution and lowering the equilibrium electrode potential for copper dissolution from brass with respect to dissolution from pure copper. A model in atomistic terms to account for this coupling of reactions has been suggested by Pickering and Wagner (1967) and is outlined here. When a brass electrode is made to dissolve anodically there is a tendency for zinc atoms to dissolve preferentially, leaving copper atoms free to migrate at random and these may aggregate to form crystallites of practically pure copper. This aggregation of copper implies an activity gradient between migrating and bound copper and the average activity of migrating copper on the surface may be higher than unity. The potential between this copper and solution may, therefore, be less noble than the corresponding potential between bulk copper and solution. If this situation exists zinc and copper ions may both be dissolved and copper re-deposited at the same potential but at a site where the concentration of adsorbed copper is close to that of a bulk copper crystal. There may be other factors which would increase the tendency of atoms of the noble metal to become ionised, for example, Shams and Elmosary (1976), have shown that dissolution of zinc in certain electrolytes is exothermic and that the heat

of reaction generated during dissolution of zinc from brass influences the behaviour of the remaining copper.

The difficulty arising out of the ionisation/redeposition mechanism is that it requires the noble metal to be both dissolving and redepositing simultaneously on the same metal sample. This is accounted for by assuming that the dissolution reaction for the noble component is coupled with that of the reactive metal, lowering the potential at which it dissolves. Pickering (1967) has been unable to detect ions of the noble metal alloy constituent in the bulk solution indicating that if such ions occur they are likely to be transitory and to exist only close to the alloy surface.

The bulk diffusion mechanism assumes that atoms of the reactive metal are continually replenished at the corroding surface from within the alloy. Thus noble metal atoms tend to drift away from the surface and reactive atoms towards it. Pickering (1967, 1968, 1970) has shown that during selective dissolution of copper-gold alloys and zinc-rich brasses, new phases form containing less of the reactive metal than the original alloy. These phases are detected by X-ray and electron diffraction and by electron microprobe analysis. Pickering suggests that the only sensible explanation of these observations is to assume that considerable movement has occurred in the solid phase by volume diffusion.

There is a serious difficulty with this simple explanation which is that bulk diffusion coefficients at room temperature, obtained by extrapolating back from high temperature measurements, are not large enough to account for movement of material over appreciable distances. However, such an extrapolation implies that equilibrium concentrations of vacancies are established at room temperature as at elevated temperatures and the contribution of diffusion along small angle grain boundaries and along dislocations is negligible at room temperature. This need not be the case. Pickering assumes that high concentrations of vacancies and divacancies can form when reactive metal atoms are directly removed from terrace sites on

the surface of a corroding alloy. If this is so then much higher diffusion coefficients are possible for example, the diffusion coefficient for divacancies in copper at 25°C is 1.3×10^{-12} cm^2 s^{-1} giving a mean square displacement after 1000s of $\overline{\Delta X^2} = 2D_{\square\square}t = 2.6 \times 10^{-9}$ which is in the order of 20 atomic distances. This is still however, very low in comparison with the rate of propagation of tunnels in for example, copper-gold alloys (2-300 atomic distances per second Swann 1967) .

This value of $D_{\square\square}$ is also barely sufficient to account for the observed flow of current when the samples are anodically polarised, which is typically 10^{-5} - 5×10^{-4} A. Assuming a high divacancy mole fraction of 10^{-2} a current density of 10^{-4} A cm^{-2} is obtained. Pickering points out that since appreciable surface roughening occurs (Pickering and Swann 1963) the apparent current density may be much greater for the same assumed mole fraction of vacancies.

The observation of new phases formed when preferential dissolution occurs in copper-gold alloys and brasses seem to indicate that the volume diffusion mechanism is operating. For this to be possible it is necessary to invoke diffusion via divacancies. In some cases even this is insufficient to account for the large currents observed to flow during dissolution and the large distances needed to be travelled by atoms to account for the rate of growth of tunnels. It is doubtful, therefore, that volume diffusion by itself is sufficient to fully explain the processes occurring during selective dissolution.

The final mechanism proposed is the surface diffusion mechanism. In outline this is where reactive atoms at the alloy surface are preferentially dissolved, the remaining noble-metal atoms migrating by the much faster process of surface diffusion to expose fresh alloy which can then be attacked as before. It is expected that the remaining noble metal will aggregate together leading primarily to patches of monolayers and eventually

even small three-dimensional crystals of the more noble metal. The principal objection to this mechanism is that since these crystals may be expected to grow in all three dimensions there is the tendency to form a passivating layer of the more noble metal. Further anodic dissolution would, therefore, be halted.

Observations which will be presented in chapter four of this thesis on silver-gold alloys corroded in nitric acid, seem to indicate that a surface diffusion mechanism is operating in the system described there. Calculations by Forty and Rowlands (1981) based on the above observations show that although a layer of unreactive material will form as the less noble component is dissolved, it need not completely cover the alloy surface and thus at selected regions corrosion can continue. This is true for alloys containing more than 50 at.% silver. For more gold-rich alloys coverage is complete and the reaction stops.

It is hoped that this thesis will add weight to the proposal that surface diffusion of residual metal is of primary importance in the dissolution of these alloy systems. Other observations such as the oxidation of gold under certain circumstances and corrosion alloying in the copper-gold system will be given to support the surface diffusion model. There are, however, problems associated with this model, for example, the surface diffusivity of gold extrapolated from high temperature measurements is 1.5×10^{-15} cm^2 s^{-1} and too low to account for the rapid surface migration observed on these samples. It is necessary to assume an interaction between residual noble metal and the electrolyte in order to obtain sufficiently high surface diffusion coefficients.

The various models for selective dissolution will be further discussed towards the end of this thesis and in the light of observations presented herein. A clearer indication of their relative merits should then be possible.

1.5. Summary of the Work Contained in this Thesis

In the following chapter the manufacture and structure of the alloy specimens used for this work is dealt with, from their fabrication in a vacuum coating unit to mounting ready for viewing in an electron microscope. Chapter three is concerned with the techniques used to study the specimens, for example, electron microscopy, electron diffraction and E.D.A.X. chemical analysis. Chapter four gives an extensive account of the microstructural and micromorphological changes that take place when alloys spanning the entire composition range are corroded. It illustrates that silver-gold alloys corroded under open circuit electrochemical conditions in nitric acid offer a particularly good system for studying selective dissolution. The structure and corrosion behaviour of copper-gold alloys are discussed in chapter five, in particular, the observation of corrosion induced alloying which is indicated by some of the observations given there. Similarities between the two alloy systems are also stated. Chapter six reports a detailed study of the distribution and crystal structure of a chemically separate corrosion phase which develops under certain conditions; its identification as gold I oxide is postulated. Chapter seven draws together all the observations presented in the thesis. A model to account for selective dissolution and rapid re-distribution and re-crystallisation of residual gold based on chapter 4, is reported. A further more sophisticated model arising from the more speculative assumptions based on observations in chapters five and six is also presented. The final chapter gives a summary of the thesis along with suggestions for future experiments arising from work reported here.

References - Chapter 1

Edeleanu, C., and Forty, A. J., (1960), Phil. Mag., 5, 1029.

Foroulis, Z. A., and Uhlig, H. H., (1964), J. Electrochem. Soc., 111, 522.

Forty, A. J., and Durkin, P., (1980), Phil. Mag. A, 43, 171.

Graf. L., (1950), Stress Corrosion Cracking and Embrittlement, ed. W. D. Robertson, (N. York, J. Wiley and Sons) pp48-60.

Pickering, H. W., and Swann, P. R., (1963), Corrosion, 19, No. 11, pp369-389.

Pickering, H. W., and Wagner, C., (1967)a, J. Electrochem Soc. 114, 698.

Pickering, H. W., (1967)b, Proceedings of the Conference of Fundamental Aspects of Stress Corrosion Cracking, Edited by R. W. Staehle, A. J. Forty, and D. van Rooyan (Houston N.A.C.E.), p.159.

Pickering, H. W., (1968)a, J. Electrochem Soc., 115, 143.

Pickering, H. W., (1968)b, J. Electrochem Soc., 115, 690.

Pickering, H. W., (1970), J. Electrochem Soc., 117, 8.

Robertson, W. D., and Bakish, R., (1956), Acta Met., 3, 282.

Shams El-Din, A. M., Elmosary, A. A., (1976), Corr. Sci. 16, 8, 485.

Shrier, L. L., (1976), Corrosion, Vol. 1 (London: Newnes-Butterworths) p.167.

Swann, P. R. and Duff, W. R., (1970) Met. Trans, 1, 73.

Swann, P. R., (1967), Proceedings of the Conference on Fundamental Aspects of Stress Corrosion Cracking, Ed. R. W. Staehle, A. J. Forty and D van Rooyan (Houston: N.A.C.E.) p175.

Tammann, G., and Brauns, E., (1931), Z. anorg. allg. Chem., 200, 209.

Tulloch, D. S., and Stewart, D., (1968), Principles of Corrosion and Protection, Macmillan London.

Vermilyea, D. A., (1967), Proceedings of the Conference on Fundamental Aspects of Stress Corrosion Cracking, Ed. R. W. Staehle, A. J. Forty, and D. van Rooyan (Houston; N.A.C.E.) p.176.

CHAPTER TWO

Preparation of Thin Films

2.1 Specimen Requirements

The approach to the problem of elucidating corrosion processes adopted for this work has been to make a high resolution electron microscope study of the micromorphology that develops on alloys after they have been corroded and to infer from this the changes that occur in the alloys during corrosion. The best way of achieving microstructural resolution approaching the atomic scale is using a transmission electron microscope. This means that specimens must be electron transparent. There are several ways of preparing electron transparent metal foils, the main ones being: vapour deposition (evaporation and sputtering onto a suitable substrate), electrodeposition, electropolishing, and ion beam thinning. Films deposited from the vapour tend to have a structure which is dependent on the conditions of preparation and so may be unrepresentative of the bulk material. Electrochemical etching and ion beam thinning have the advantage of starting with the bulk material. Frequently however, films prepared by electrochemical deposition methods are contaminated with oxide or other residues of the electrochemical reaction. This means that they would have only a limited application in corrosion studies as it is necessary to know that any chemical products which may appear on specimens are due to corrosion and not specimen preparation. Ion beam thinning is slow and time consuming, severe problems associated with preferential sputtering of one component of the alloy can occur if alloys are being thinned. Both electropolishing and ion beam thinning processes produce surfaces which may be rough on the atomic scale and therefore not ideal for high resolution studies of the microscopic structural changes that might occur during a corrosion reaction.

For the purposes of the work presented here specimens were prepared by

vapour deposition techniques. The fact that they are sometimes unrepresentative of the bulk material when they are prepared in this manner has been used to advantage in that it was possible to prepare single crytals of alloys with a resulting simplification in their microstructure. This method of specimen preparation has been particularly useful since it was quick and relatively easy to perform, and films produced had quite good reproducibility and were of high quality. Specimens were fairly easy to handle and capable of being mounted for viewing in an electron microscope with relative ease. The description of specimen preparation to follow (section 2.4) will show that it was a relatively simple matter to strip films from their substrates, wash them and mount them on electron microscope grids ready for examination.

In a study of the micromorphology of corroded alloys it is important to be able to separate pre-existing structural imperfections in metals and those which result from corrosion. It is also an advantage to prepare specimens with an initial microstructure that is as simple as possible in order to make interpretation of the corrosion morphology relatively straight-forward. The specimens used for this work have been prepared with these requirements in mind. The constituent metals in the alloys used for these studies must have a large difference in their single electrode potentials in order for selective dissolution to be their dominant mode of dissolution under a wide range of conditions.

Silver-gold alloys corroded in nitric acid offer a very good system for a micromorphological study of selective dissolution. Silver and gold are completely miscible and alloy together as a single face-centred-cubic phase across the complete compositional range. Silver and gold have practically identical atomic sizes with less than a 0.02% change in crystal lattice parameters from silver through all the alloys to gold. This means that there is very little lattice strain and consequently no significant

microstructural rearrangement arising from lattice parameter changes during corrosion. There is a large difference in the single electrode potentials of silver and gold (0.8V) and silver dissolves readily in nitric acid under open circuit conditions whereas gold is not dissolved at all. It will be shown in a later chapter that there is evidence to suggest that in silver-gold alloys anodic dissolution of silver may create conditions leading to a coupling of reactions whereby residual gold can be, at least partially solvated. This is a complicating, but also very interesting possibility. Another feature of this system is that, due to the high solubility of the corrosion product (silver nitrate), no insoluble corrosion product should form and changes in microstructure will be due only to any transport processes occurring in the alloy. It is thought, however, that the transport of residual gold during corrosion is not a simple diffusion process but involves formation of gold I oxide as an intermediate metastable phase which then decomposes, re-distributing gold on the alloy surface. In some circumstances, the oxide remains long enough to be observed after corrosion and may be regarded as a pseudo corrosion product.

The other alloy system discussed in this thesis, copper-gold, does not have the simple phase diagram of silver-gold and it is not possible to draw such unambiguous conclusions from microscopic studies of its alloys, where large changes in lattice parameter can occur. In the case of copper-gold alloys several structural ordering processes can occur as the composition varies. One severely limiting result of this variation of lattice parameter with composition in these alloys is that electron micrographs frequently contain a high density of moiré fringes which map out the small fluctuations in chemical composition which occur. This leads to much of the micro-structural detail, which would otherwise appear on a micrograph being obscured.

2.2 Description of the Equipment for Vacuum Evaporation

The equipment for preparing specimens was an N.G.N., twelve inch coating unit of the type illustrated in figure 2.2.1. This comprised a vacuum chamber evacuated in the normal way by a rotary and diffusion pump combination. Roughing and backing pressures were measured on a thermocouple gauge and low pressure was measured on an N.G.N. Penning gauge. The thermocouple gauge heads were situated in the backing and roughing lines and the Penning gauge head was situated behind the manually operated baffle between the diffusion pump and evaporating chamber. The evaporating chamber itself contained three live electrodes and two earth electrodes, the live terminals were fed from three independent power sources. The evaporating sources were tungsten metal filaments heated electrically by a variable low-voltage power supply.

Vapour from the hot filament was directed downwards onto an atomically smooth substrate, usually a slip of freshly cleaved mica. This was held at an appropriate temperature by mounting it on a stainless steel hotplate. The arrangement is shown in figure 2.2.2. The construction of the hotplate is shown schematically in figure 2.2.3. and comprises a 240 V, 65 mA (15 W) heating element embedded in two blocks of stainless steel. These blocks were screwed into a stainless steel plate and the resulting assembly was fastened through ceramic connections to a stainless steel base. The ceramic connections ensured thermal and electrical insulation from the base. A Pt/Pt 10% Rh thermocouple was embedded into one of the stainless steel blocks and secured by one of the fastening screws; the thermocouple wires were covered with ceramic insulation and connected to two of the terminals on a fourway lead-through built into the evaporating chamber. This enabled the temperature of the substrate to be measured continuously. The heating element connections were also insulated with ceramic beads and connected to two separate terminals fed from a transformer-

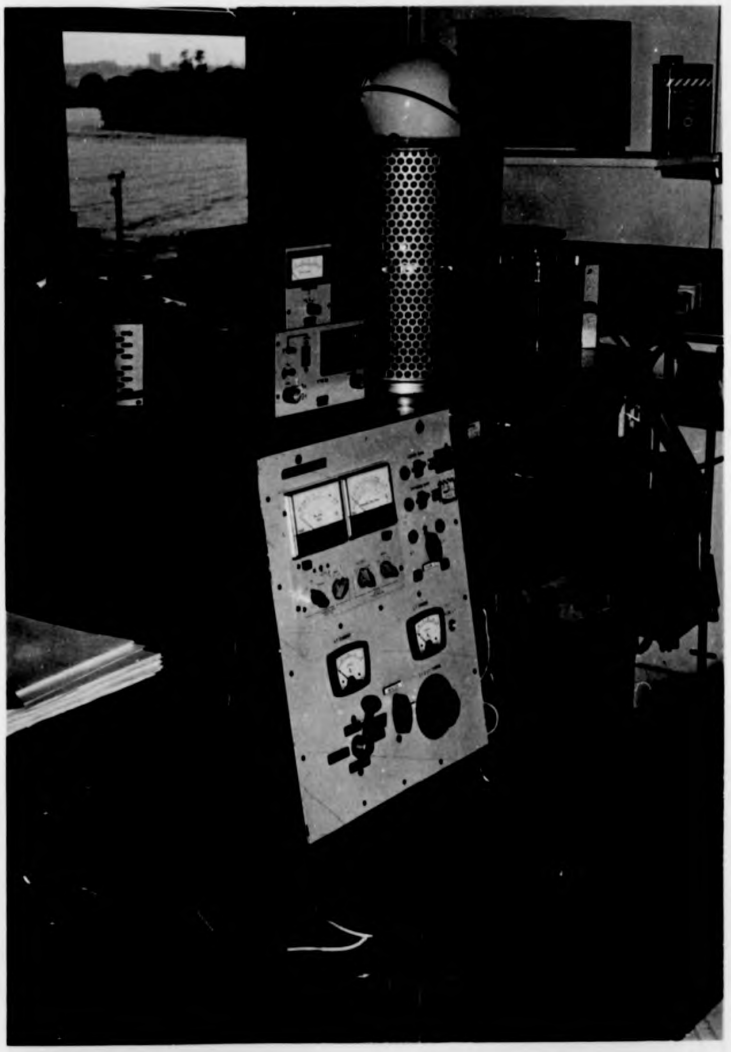

Fig. 2.2.1. Photograph of the N.G.N. 12 inch Vacuum Coating Unit used to prepare thin films.

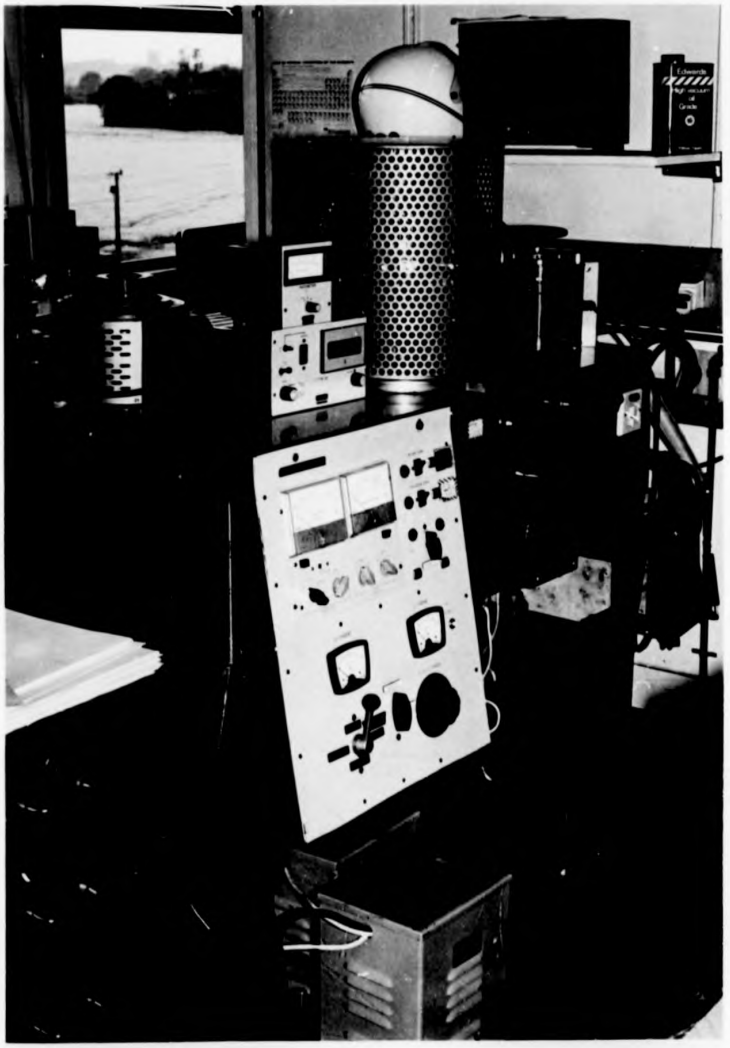

Fig. 2.2.1. Photograph of the N.G.N. 12 inch Vacuum Coating Unit used to prepare thin films.

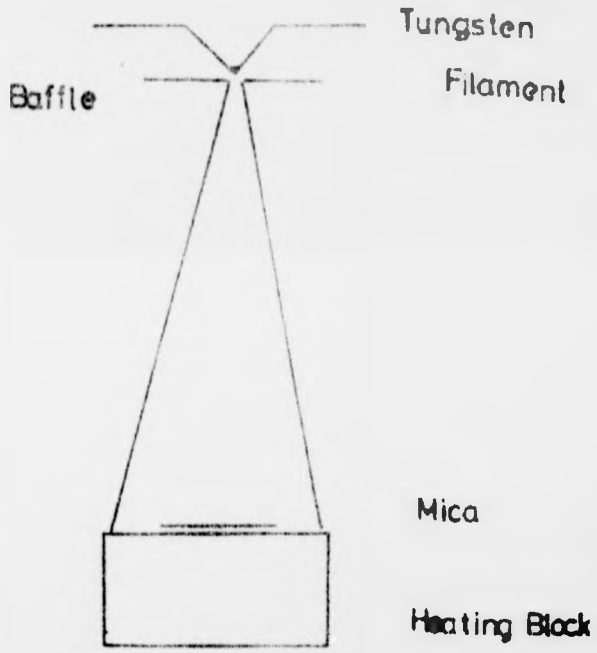

Fig. 2.2.2. Showing the arrangement of the various components in the evaporating chamber.

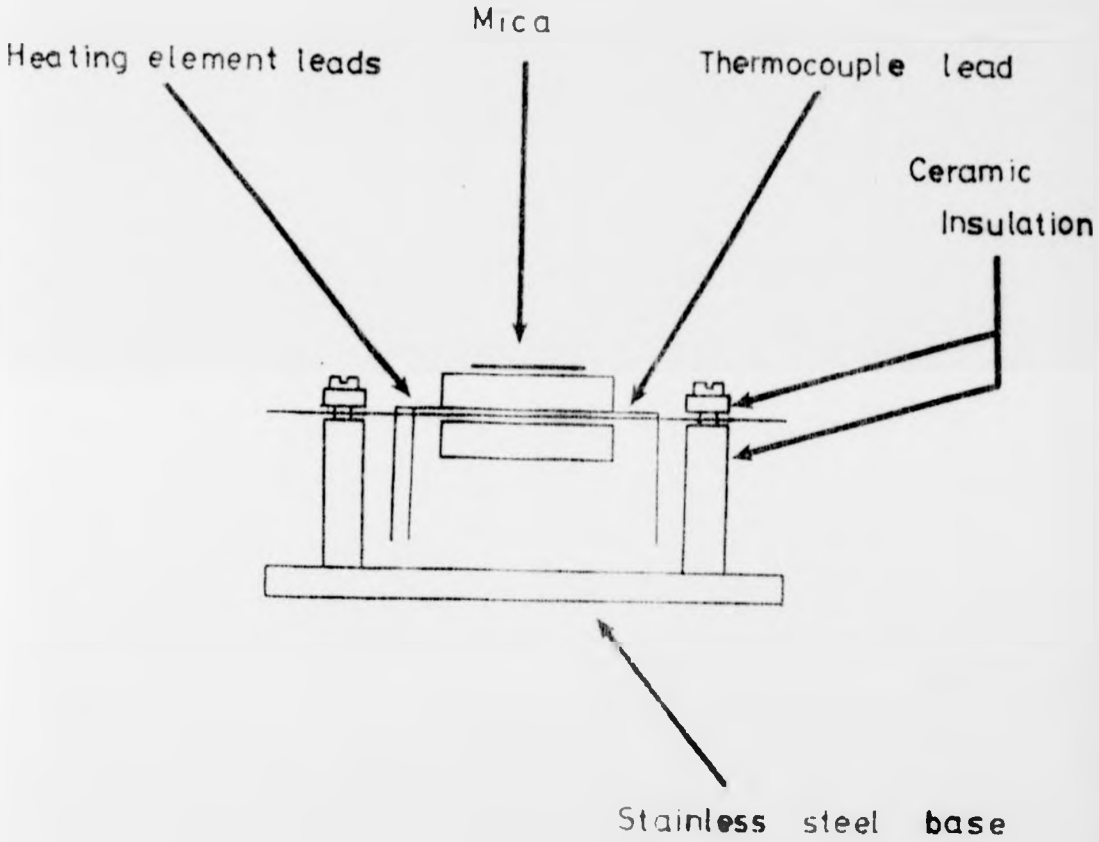

Fig. 2.2.3. Showing the construction of the hotplate used for heating mica during specimen preparation in the evaporating chamber.

controlled mains supply.

Specimen thickness was measured using a film thickness monitor (Edwards FTM 2D type) which gave a digital display of film thickness. Its operation was as follows: A quartz 'monitor crystal' of the type used in R.F. control circuits and with a frequency of 6.0 MHz, was positioned in the vacuum chamber so that vapour was deposited on the substrate and on a defined area of the crystal surface. This was connected by tinned copper wire connections to the remaining two terminals of the fourway lead-through. A second, reference crystal, with a frequency of 6.5 MHz was contained in the main unit outside the vacuum chamber. The difference in frequency between the two crystals was mixed with a variable oscillator and filtered to produce a final difference frequency of between 0 and 150 kHz. The mass of the deposited material caused a reduction in the natural resonant frequency of the monitor crystal, causing an increase in the final difference frequency. This change was converted to a D.C. signal which changed the digital display. The sensitivity of the digital display to this signal was calibrated in density units to enable film thicknesses from a range of different materials to be read out directly.

Deposition rate was measured using an Edwards Ratemeter attached to the thickness monitor. The rate of depositon can influence many film parameters and, most importantly, determine the alloy composition when films are prepared by simultaneous evaporation from two or more sources. An output from the measuring circuit was fed into an F.E.T. amplifier with highly stable characteristics. Capacitance at the input and resistance feedback produced a differentiating action so that a constantly rising thickness produced a steady output on the ratemeter.

The system developed for this work enabled the simultaneous deposition of up to three metals and the monitoring of their combined deposition rates.

The vapour beams were directed onto the heated substrate by defining apertures. Two manually operated shutters could be rotated into positions to select the metal or metals that were to be deposited. In-situ monitoring of the film thickness was possible. The system was designed to be as flexible as possible and allow for a wide range of alloys of various compositions to be fabricated.

2.3. Description of Equipment for Ion-Beam Sputtering

In sputtering, a target of the material to be deposited is bombarded with energetic ions which cause ejection of the surface atoms. Ejected atoms can then be condensed on a substrate in a similar way to evaporated atoms. The advantages of sputtering over evaporation are that there will be no alloying between the filament and the evaporant, it is possible to sputter metals that would not evaporate until very high temperatures were reached, and it is possible to deposit alloys with an accurately known composition. Rates of deposition can be varied by changing current density in the ion beam or by changing the energy of the ions. Generally, deposition rates are lower than in the case of evaporation and, although the rates can be controlled accurately, problems with oxidation and contamination can occur if reactive metals are being sputtered. In many sputtering systems the operating pressure is higher than that in corresponding evaporating systems because of the residual gas from the ion gun. This was largely overcome in the particular ion guns (Ion Tech) used in the system described here.

These were saddle-field ion sources which had very small dimensions ($\sim$ 4-5 cm) and the plasma once formed was confined within the source. The electrostatic saddle-field configuration induced electrons to follow long oscillatory trajectories, without recourse to a magnetic field, within a small volume. Consequently it was possible to generate quite large ion currents (40-60 μA) whilst using cold cathodes and working at relatively

low pressures (10^{-4} torr). The anode of the gun was enclosed by the cathode and hence extraction electrodes were not required. The beam emerged from a slot or hole in the cathode. The shape of the beam was defined by the shape of the aperture.

Three types of gun, all employing argon ions, were used in the sputtering unit used to prepare specimens for this work; an Ion Tech B21bW gun which had a 10 mm slot in the cathode and produced a wide beam for polishing and cleaning substrates ready for deposition; Ion Tech C11W and B11W guns which were fine beam sources, the emergent ions being largely concentrated into a beam of 2 mm diameter. Each of these guns was connected to an Ion Tech B50 power supply which matched the electrical requirements of these Saddle Field Ion Sources. The power supply was current regulated, having a high output impedance of the order of 5×10^{6} ohm. The B11W guns differed from the C11 guns only in that they contained a monitor plate which sampled ion current and was connected to an ion current meter in the B50 power unit. The ion current produced in the guns could therefore be continuously monitored. All of these guns described above were water cooled.

The vacuum system for sputter-deposition consisted of an eighteen inch work chamber evacuated by an Edwards E.D.M. rotary pump and 'Diffstak' diffusion pump. The 'Diffstak' range of pumps do not have liquid nitrogen cold traps to stop backstreaming into the evaporating chamber. It is claimed that a cold trap is not necessary for its successful operation. An Edwards hot filament Pirani 10 gauge was used for measuring roughing and backing pressures and an Edwards Penning 8 gauge was used for measuring low pressures.

Inside the work chamber there were three work stations corresponding to the following operations; crystal substrate cleaning; deposition of a metallic crystalline substrate; and deposition of the alloy. A photograph of the sputtering unit is given in figure 2.3.1. and the relative positions

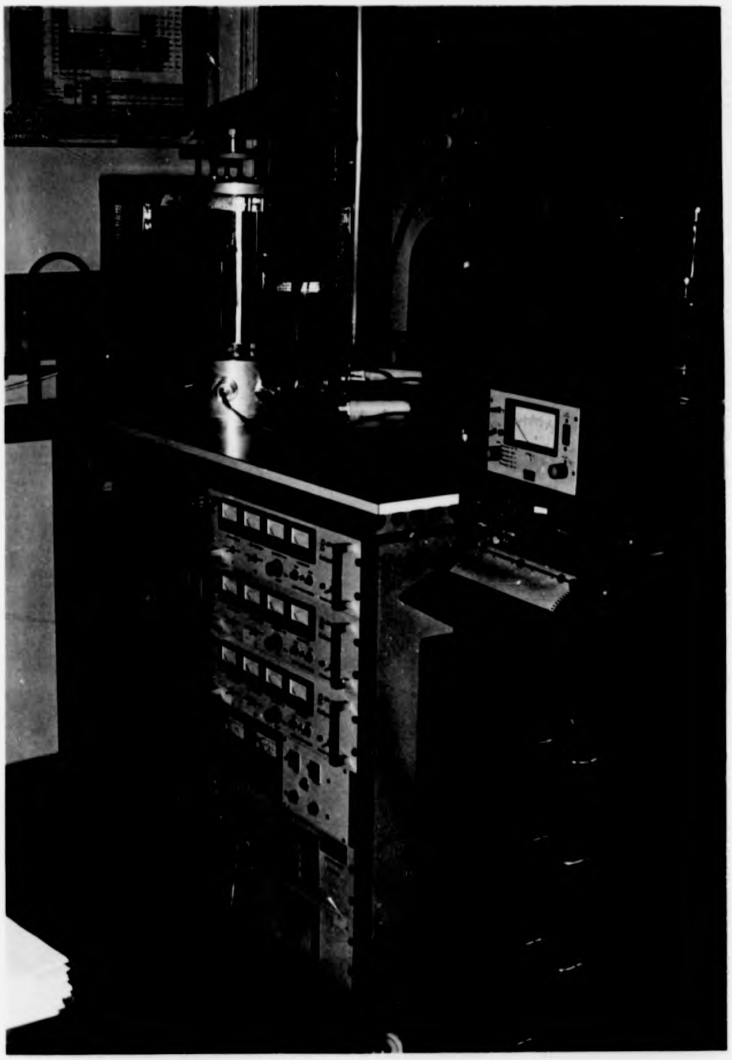

Fig. 2.3.1. Photograph of sputtering unit used to prepare ion beam sputtered films.

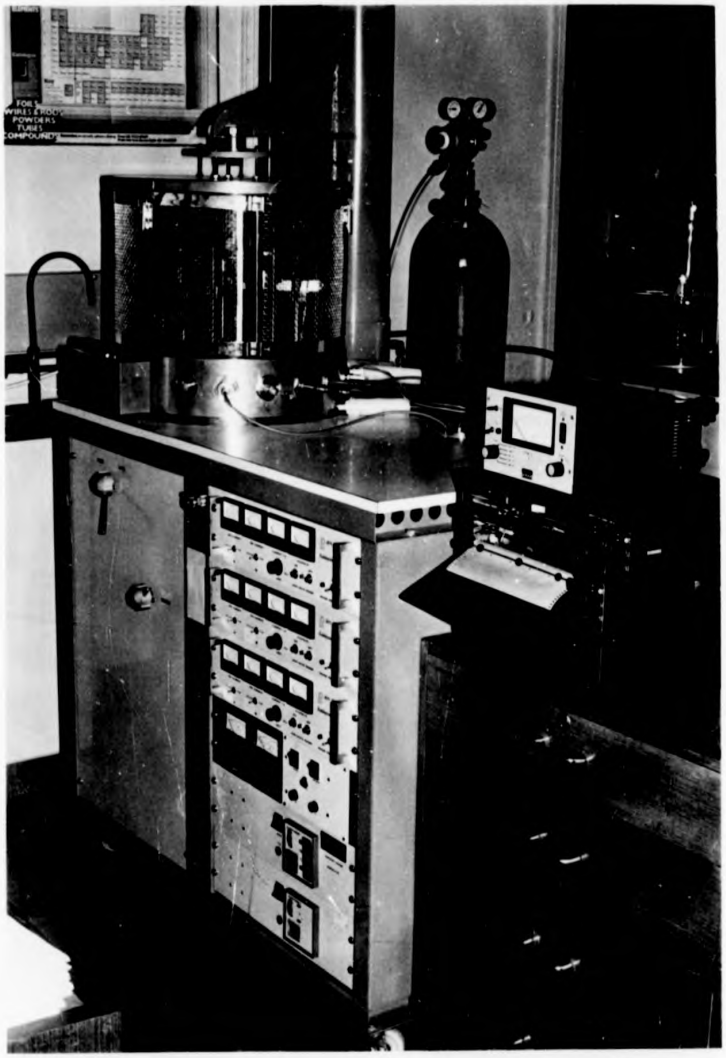

Fig. 2.3.1. Photograph of sputtering unit used to prepare ion beam sputtered films.

of ion-guns sputter target and substrate are shown in figure 2.3.2.

The substrate, for example a slip of freshly cleaved mica, was held in one of three metal recesses on a large stainless steel circular plate. This was supported at its centre by a positioning mechanism which allowed the substrate to be manually rotated and indexed in position at each of the three work stations. There was a shutter which was also position-indexed so that it was held in a position which shielded the substrate from sputtered metal when the guns were switched on but no metal was required to be deposited.

All guns were supplied with cooling water delivered in stainless steel pipes. The ion guns were fed from power supplies which were positioned outside the evaporating chamber with interconnections which made it possible to select any combination of ion cleaning or ion sputter sources. They were also fed with high purity argon with separate needle valves to regulate the gas supply to each of the total of six guns independently.

The substrate heater was a 15 W heating element sandwiched in two stainless steel blocks (Fig. 2.2.3). The lower block was machined to sit firmly in position above the mica substrate to ensure good thermal contact with it. The substrate heater had been designed in very compact form in order to fit within the restricted space available above the substrate without obstructing the ion sources. Since the substrate was rotated from one work station to another during specimen preparation the power supply to the heater had to be fed to it by radial connection from the axis of the indexed circular plate. This minimised twisting and crossing of the wire connections during rotation of the plate. The connections were $^{1}/_{8}$" gauge copper wire insulated with ceramic beads. The temperature of the heater could be pre-set using a Eurotherm digital power supply to the heating element and a (Pt/Pt 10% Rh) control thermocouple.

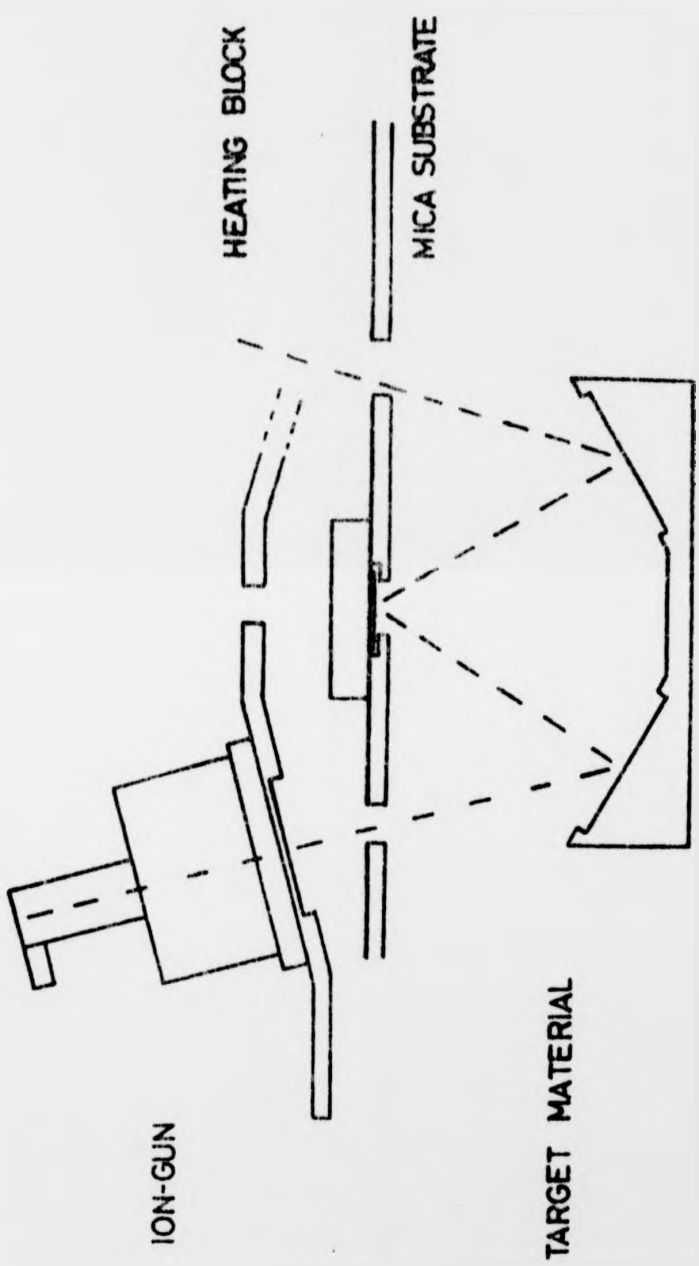

Fig. 2.3.2. Showing the relative positions of ion guns, targets and substrate in the vacuum chamber of the sputtering unit.

During operation of a gun the ion beam was directed down through a hole in the stainless steel plate supporting the substrate and onto the target material to be sputtered (Fig. 2.2.5). The ejected atoms diffused away from the target area and were deposited on the heated substrate above it. The distances between the ion-gun targets and the substrate were kept to a minimum and the angles between them were carefully chosen in order to optimise deposition rates. There was insufficient space to mount a quartz crystal adjacent to the substrate and in situ monitoring of film thickness in the way outlined in the previous section was therefore not possible. Film thicknesses were controlled by deposition times and ion-beam currents and voltages which when pre-set for successive specimen preparations gave consistent film thicknesses. Deposition rates had been calibrated by depositing metals onto weighed substrates over long periods.

2.4. Specimen Fabrication

Most of the alloys used in the studies on silver-gold have been prepared by a technique of depositing vapour from a hot filament onto a suitable substrate. This was an extension of earlier work by Pashley (1959a), (1959b) and Pashley and Stowell (1963) on the preparation of single crystal gold films. Substrates used for growing single crystals needed to be very smooth themselves on the atomic scale. Freshly cleaved muscovite mica was used for the films prepared for this work. This technique yielded good quality specimens having smooth (111) surfaces with a silver-gold composition that could be controlled by the relative rates of deposition of the component metals (Forty and Durkin 1980).

Silver was evaporated from a tungsten wire basket filament containing a 2 mm diameter silver wire about 1 cm long. To minimise the effect of radiant heating from this filament, which would raise the surface temperature of a film during preparation, suitable shields were necessary. The arrangement of the filament, shield, substrate heater and mica is illustrated in

figure 2.2.2. A filament/substrate distance of about 15 cm was used. The substrate heater has been described in the previous section. Pashley (1959) found that the presence of tin, arsenic or tellurium, which are sometimes added to alloys to improve their machining properties, could contaminate the mica substrate and impair the subsequent growth of single crystals of silver. Great care was therefore taken to ensure that the metals used in the construction of the heater were pure and free from those particular contaminants. Good quality stainless steel was found to be completely satisfactory.

The optimum substrate temperature at which to deposit silver films as good single crystals was between 250 and 300°C. Films grown under these conditions showed a minimum of double positioning twinning, no {111} twinning and very large crystal sizes. The surfaces were optically smooth and the crystalline epitaxy was defined by:

$$(111)_{Ag}\ [1\bar{1}0]_{Ag}\ \Big|\Big|^{\ell}\ (001)\text{mica}\ [010]\text{mica}$$

or

$$(111)_{Ag}\ [\bar{1}10]_{Ag}\ \Big|\Big|^{\ell}\ (001)\text{mica}\ [010]\text{mica}$$

The occurrence of these two possibilities is known as double positioning. The first step in the preparation of an alloy of, say, silver-gold was to deposit a single crystal film of silver approximately 1200 Å thick onto the mica substrate held at a temperature of 285°C in a good vacuum (10^{-5} - 10^{-6} torr). A deposition rate of about 10 Å s^{-1} produced a good single crystal with a mirror smooth (111) surface. This was an excellent surface on which to grow gold since the misfit for parallel orientation was only 0.02%. Consequently a second layer of approximately 200 Å of gold was deposited onto silver at a rate of 1 Å s^{-1} under the same conditions of vacuum and substrate temperature. The gold film was again a good single crystal, epitaxial with the silver film. Finally, a deposit of about 400 Å of silver-gold alloy was laid down on top of the gold layer

by simultaneously evaporating silver and gold at the appropriate rates, and at a combined rate of between 1 and 5 Å s^{-1}. The individual deposition rates of silver and gold obviously determined the composition of the alloy formed. Thus the Au 50 At % Ag alloy was formed if both silver and gold were deposited at 1 Å s^{-1}; the Au 75 At % Ag alloy required deposition rates of, say, 1 Å s^{-1} for gold and 3 Å s^{-1} for silver. After deposition the composite specimen was then floated on a bath of dilute nitric acid with the silver-gold film uppermost so that the silver substrate was slowly dissolved and the mica eventually became detached to leave the alloy floating on the surface on its gold supporting film. The gold film served the dual purpose of providing a buffer against direct exposure of the alloy to acid during the process of stripping it from the mica/silver substrate and also providing a support for the alloy after corrosion. The stripping process is illustrated in figure 2.4.1.

Copper-gold alloys prepared in the same manner as that outlined above for silver-gold showed extensive moiré effects when viewed in the electron microscope due to the over-lapping of alloy and gold crystal lattices. One way of avoiding this was to evaporate copper-gold alloy of the required composition directly onto a single crystal of silver on mica, this having been prepared in the usual way. The assumption was made that dissolution of silver during stripping would not affect the subsequent corrosion behaviour of the copper-gold alloy. The extent of corrosion in alloys prepared in this way depends on the strength of acid used for stripping and the length of time the specimen was in contact with the acid. Control of the extent of this unwanted corrosion was therefore not so easy in these alloys. It should be pointed out that corrosion during stripping in silver-gold alloys was frequently observed due to penetration of the nitric acid solution through small holes in the supporting gold film. This unwanted corrosion was localised around the holes and could therefore be readily recognised. Further corrosion could, of course, be carried out by exposure of the free surface of the alloy to different concentractions of nitric acid.

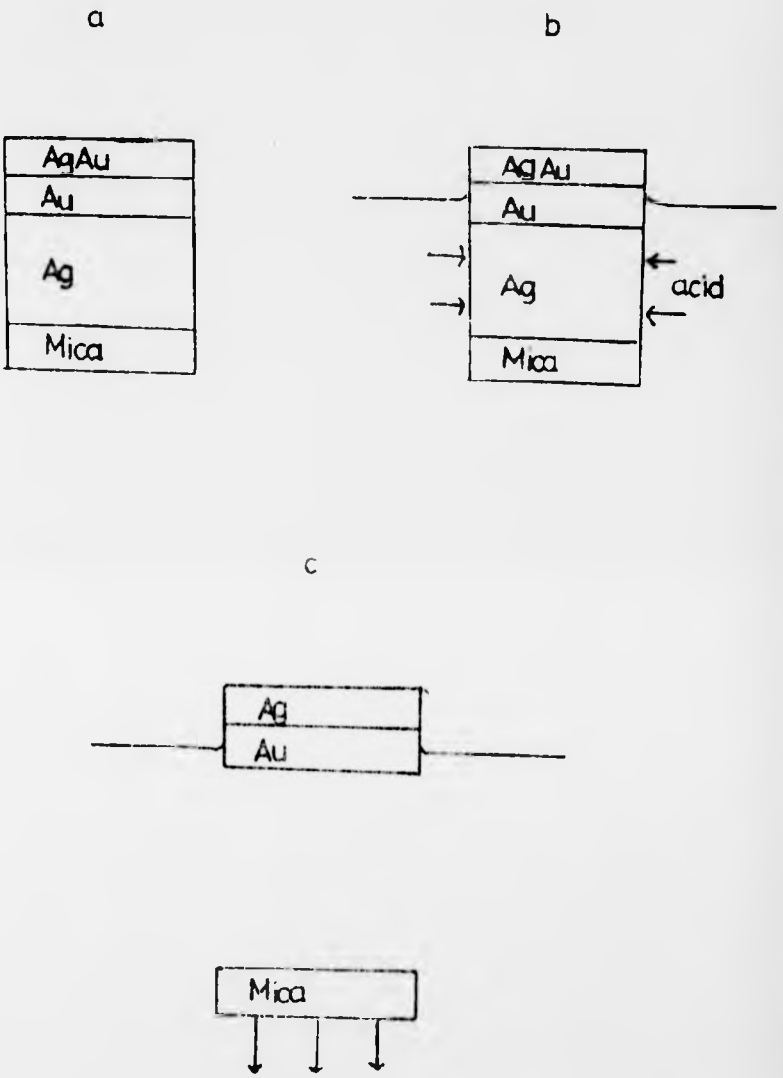

Fig. 2.4.1. Showing the stripping process. (a) Shows the various layers in the composite sample, (b) shows acid attack at the underlying silver layer and the "buffering" action of the gold layer, (c) shows the mica detached and the alloy film freely floating ready for washing.

2.5. Structure and Morphology of these Films

An assessment of the structure and composition of the alloy films before corrosion is important if unambiguous conclusions concerning the corrosion morphology are to be drawn from the subsequent microscopic studies. Consequently the films were examined, before being stripped from the substrate, by scanning electron microscopy and X-ray micro-analysis. The results of these prior examinations were correlated with observations of the films by transmission electron microscopy and X-ray analysis after stripping. This yielded important information about the effects of pre-existing structural defects (e.g. holes) and local compositional variations, on the subsequent corrosion.

An examination by transmission electron microscopy and electron diffraction of the composite gold and silver-gold films prepared by the procedures outlined above showed that they were good quality single crystals in a (111) orientation. The principal microstructural features were structural fault boundaries and holes. Silver and gold deposited on mica cleavage surfaces grew as island films which coalesced as more material was deposited to form coherent films. Island nuclei existed in two distinct but crystallographically equivalent orientations which were twin related with $[1\bar{1}0]_{Ag}$ parallel to [010]mica and $[\bar{1}10]_{Ag}$ parallel to [010]mica as described earlier. This produced a structural misfit, a so-called double-positioning boundary, when the islands in two different orientations eventually merged to form a continuous film. It was infact an incoherent twin boundary (Pashley and Stowell 1963).

The other main microstructural features were small holes (0.05 → 0.1 μm diameter) which penetrated the composite specimens. These were predominantly associated with double positioning boundaries and frequently occurred at the intersections of boundaries. They were thought to arise from the imperfect coalescence of island nuclei, probably due to impurities and

imperfections in the mica substrate. That they existed in the film when it was first prepared on the mica substrate and did not arise as a result of exposure of the films to acid can be seen by comparing figs. 2.5.1 and 2.5.2. Figure 2.5.1 shows a scanning electron micrograph of a 33% Au silver-gold alloy before it had been removed from its substrate. The specimen therefore consisted of a mica base, supporting layers of silver, gold and silver-gold alloy. The micrograph was recorded using the Z-contrast mode which enhanced the variations in atomic composition present in the film. This was typical of micrographs from alloys of various other compositions. It shows dark, rounded features whose size and distribution is readily comparable with that of holes observed when the specimen was stripped from its composite substrate and viewed using transmission electron microscopy. This can be seen by comparing figure 2.5.1 with figure 2.5.2 which is the TEM image of the same specimen. The implication from this similarity between the size and distribution of holes in TEM images and the size and distribution of the dark rounded features in the SEM images was that they correspond to the same feature i.e. holes. Two samples were made, following the method of preparation described earlier. The first was a layer of pure silver (1000Å) on mica, the second was a layer of pure gold (300Å) on pure silver (1000Å). SEM images from both samples were analogous to the SEM images from samples where a further layer of alloy had been subsequently deposited. Thus the dark features in these images were formed in the initial stages of specimen fabrication and existed at all stages of the preparation.

It is however, possible that these dark features were some solid state artefact containing silver, which would dissolve during the stripping process leaving the holes which were observed in TEM images. The most likely explanation of these features seems to be that they were holes formed during the deposition of the films. The SEM images were formed using backscattered electrons so it was expected that holes in the film

0·5μ

Fig. 2.5.1.. Scanning electron micrograph (Z contrast mode) of silver-gold alloy on gold, silver mica substrates, showing holes and d.p. boundaries in the composite film.

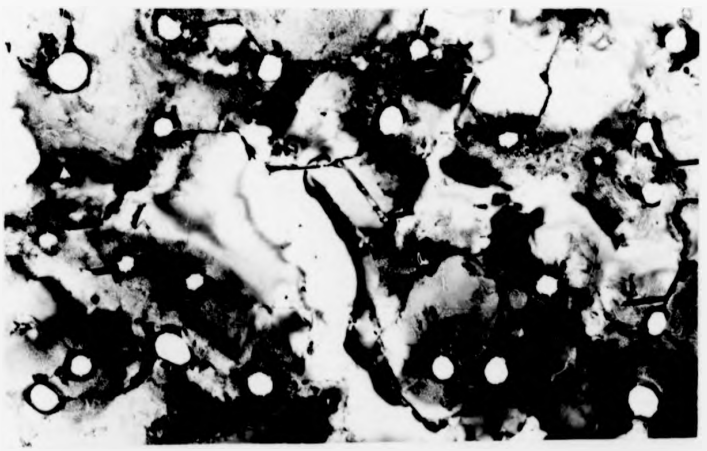

05 μ

Fig. 2.5.2. Transmission electron micrograph of the same specimen showing double positioning boundaries and holes.

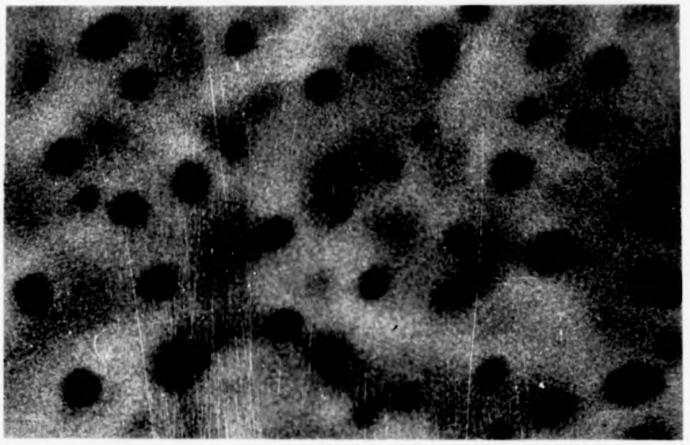

Fig. 2.5.1. . Scanning electron micrograph (Z contrast mode) of silver-gold alloy on gold, silver mica substrates, showing holes and d.p. boundaries in the composite film.

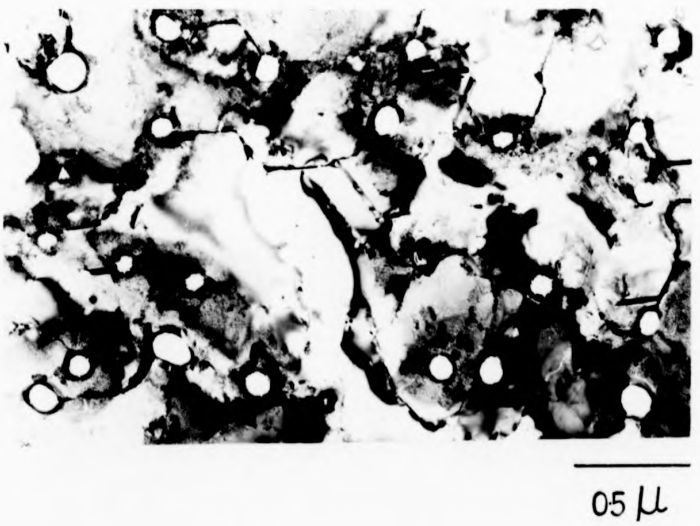

Fig. 2.5.2. Transmission electron micrograph of the same specimen showing double positioning boundaries and holes.

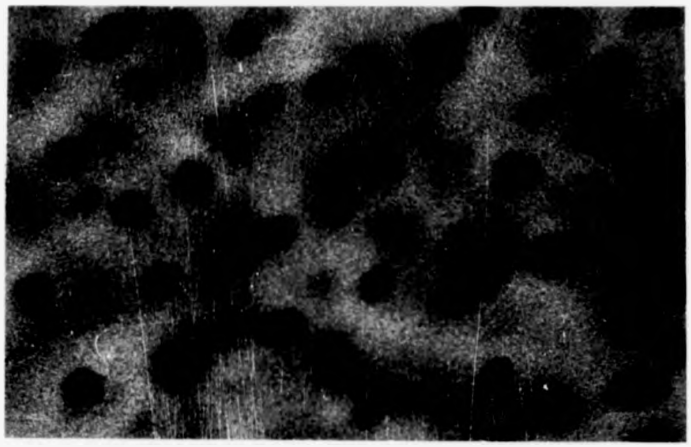

0·5μ

Fig. 2.5.1.. Scanning electron micrograph (Z contrast mode) of silver-gold alloy on gold, silver mica substrates, showing holes and d.p. boundaries in the composite film.

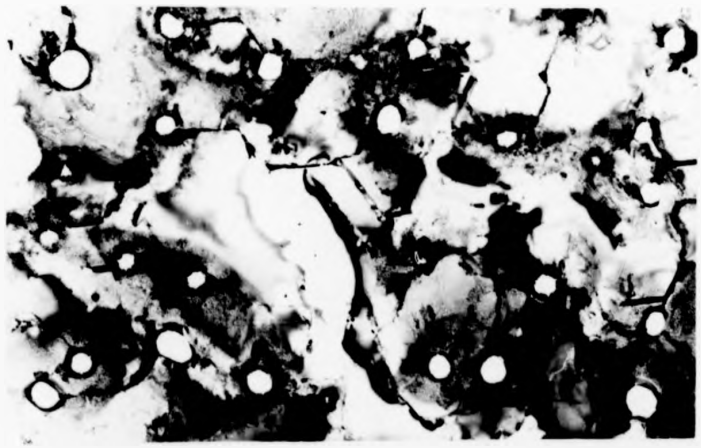

05 μ

Fig. 2.5.2. Transmission electron micrograph of the same specimen showing double positioning boundaries and holes.

should appear dark relative to other regions. EDAX analysis of similar samples observed in the transmission electron microscope revealed silver enrichment around the holes (typically 10 to 15 atomic %). In addition enrichment of silver (up to 10 atomic per cent) was observed in the vicinity of the double-positioning boundaries.

The conclusion that the holes observed in TEM images of these samples were formed during specimen preparation rather than by chemical etching in the acid during stripping was further supported by investigations of how the size and density of holes varied with alloy composition. These results are given in table 2.5.1 and show that there was no apparent correlation between the size of a hole and the composition of an alloy.

Table 2.5.1. Showing the average hole diameter for various alloy compositions

Ag-Au Alloy Composition	Average hole diameter (Å)
11% Au	1270
20% Au	796
25% Au	950
33% Au	1500
50% Au	420
70% Au	660
100% Au	440

Segregation of silver to holes and double-positioning boundaries was responsible for preferential corrosion at the holes and the double-positioning boundaries, as will be evident later (see Chapter 4). By comparison dislocations and stacking faults also present in the films had only a secondary influence on the corrosion morphology.

SEM micrographs of copper-gold alloys again indicated the presence of dark-features at all stages of sample preparation. Local variations in copper concentration also occurred at boundaries and holes though not so uniformly and consistently as in the case of silver-gold alloys. The copper concentration in these regions was not usually significantly different from that in the bulk of the alloy.

2.6. Auger Depth Profiling

In addition to the variation in composition across an alloy film there was also a variation with respect to depth within the film. Auger electron spectroscopy has been used to provide information about this. It is a surface-sensitive technique and a depth profile of the internal composition of a specimen can be obtained by progressively removing layers of material by ion beam bombardment and recording an Auger emission spectrum after each removal.

If a beam of electrons with energies in the region of 1-2 keV is incident on a material, secondary emission in the form of Auger electrons will occur with a fairly strong intensity. An incident electron causes an electron from a core state within an atom to be ejected. This leaves a hole which will be filled by a second electron dropping from a higher energy level releasing a well-defined amount of energy which is characteristic of that particular atom. This excess energy can be used to eject a third electron which will also have a characteristic energy dependent on the atomic energy levels involved in this Auger transition. X-ray fluorescence will also tend to occur as a competing process, but for light elements and low incident electron energies Auger electron emission is the dominant process. For heavier atoms Auger processes dominate if the primary electron beam has an energy below 1000 eV. Furthermore, the Auger process involves low energy electrons and only those emitted from atoms close to the surface can escape without inelastic scattering and contribute

to the elastic spectrum. Thus the technique is surface-sensitive.

The Auger electron energy spectrum is superimposed as a series of relatively small peaks on a background of secondary electrons. The spectral peaks are usually distinguished from the secondary electron noise using a phase sensitive detection method and displaying the differentiated signal. The peak-to-peak amplitudes of the differentiated peaks can be used as an indication of surface concentration but several serious problems are encountered in the quantitative interpretation of Auger spectra. Sputter rates are difficult to determine particularly for alloys with locally varying compositions. The rate may not remain constant during an experiment. Moreover preferential sputtering of one or more element or elements is usual, leading to surface enrichment of components having a lower sputtering rate. There is the so-called "knock-on" effect viz. impinging gas ions could "knock" surface atoms into the lattice thus enlarging the apparent thickness of the zone containing these atoms. Interdiffusion may also occur, enhanced by the presence of sputter-induced defects and local heating caused by the ion beam.

The sensitivity of detecting silver in silver-gold alloy, say, may not be equal to the sensitivity of detecting silver in pure silver. This is called a matrix effect. There are two processes which may contribute to the matrix effect, first, primary electrons backscattered from within the bulk solid may have sufficient energy to generate Auger electrons near the surface. Different elements will have different backscattering efficiencies and variations in the composition of an alloy, say, can cause variations in the relative yield of Auger electrons from a particular element over and above the variation expected simply from the change in the mole fraction of the element being measured. In addition there is a variation of sampling depth for different peaks on an Auger spectrum. The escape depth for each peak will be determined by the energy of the Auger

electron and the nature of the bulk material.

A major difficulty in undertaking quantitative analysis in conjunction with ion-beam sputtering is that a microtopography frequently develops on a sputter-etched surface. It may become faceted or ridged, show steps or cones of material. The extent of surface damage is critically dependent on the ion flux and the angle of the incident beam of ions. Glancing incidence will tend to minimise surface degradation. The presence of a surface topography will reduce depth resolution since several levels of the sample are being simultaneously sampled in a given spectrum. In practice the loss of depth resolution, due to the variation in escape depths for Auger electrons of different energies, is obscured by the more pronounced loss of resolution due to degradation of the surface by the sputter-etch process. A non-uniform flux of sputtering ions can also cause a severe loss of depth resolution particularly if a large fraction of the sputtered area is being sampled. In many instances this can be overcome by sputtering a large area either by using a large beam or by rastering a small beam, and sampling only a small uniform portion of the sputtered area.

To minimise the development of surface topography during sputter-etching relatively low energy (300 eV) argon ions were used for the experiments described here. Furthermore specimens were single crystals and so faceting due to preferential sputtering of a particular crystal orientation should not occur. Samples had atomically smooth surfaces (Cherns 1974) which should also tend to reduce uneven sputtering.

Peak to peak heights of the gold 66/69 eV and silver 351/356 eV double peaks were used to provide concentration ratios for silver and gold. Correction was made for the sensitivity of the gold signal relative to the silver signal. Errors in concentration measurements due to matrix effects and surface topography have been estimated at between 10 and 15% (for example Davis et al 1977). Ho et al in their study on the silver-gold system indicate that silver will be preferentially sputtered which will lead to an increase in gold concentration in the remaining material. Also, under

a wide range of conditions silver segregation to the "free" surface is generally observed. They estimate the altered layer thickness i.e. the width of the layer influenced by the sampling process to be between 15 and 30 Å.

Figure 2.6.1. shows a depth profile for silver-gold specimens obtained in the manner outlined above. There was an enrichment of the silver content close to the free surface of the alloy, followed by zones having approximately the predicted composition of the alloy. In the sample shown here the alloy was deposited initially at a 50:50 Ag-Au composition followed by a further deposit at 60:40 Ag Au. In another depth profile, shown in Fig. 2.6.2. the specimen was a 67% silver, 33% gold alloy onto which a layer of pure gold, 35Å thick had been deposited. The gold-silver region remote from an interface with the other layers was roughly consistent with its nominal alloy composition. There was evidence of a Kirkendall effect (Christian, J. W., 1965) at the first alloy interface. It was not evident at the second interface. For both samples the boundaries between the alloy and the gold substrate appeared broadened by diffusion, and there was a significant concentration of silver throughout the gold substrate. It is possible that this was simply a result of the sampling process which, as discussed above, can lead to difficulties in interpreting Auger spectra. Some mixing over and above that due to sputter etching seems indicated, for example, silver was observed throughout the 100-200 atomic distances of the nominally pure gold supporting layer compared with the 10-20 atomic distances expected from the "knock-on" effect. Consequently interdiffusion between layers and the attendant change in alloy composition seems indicated. The observation of segregation of silver to the surface of samples is clearly demonstrated and supports similar observations elsewhere, (Fain and Macdonald 1974, Ho et al 1977). A high concentration of silver at the free surface can have a profound influence on the kinetics of the corrosion reaction due to its autocatalytic reaction with nitric acid,

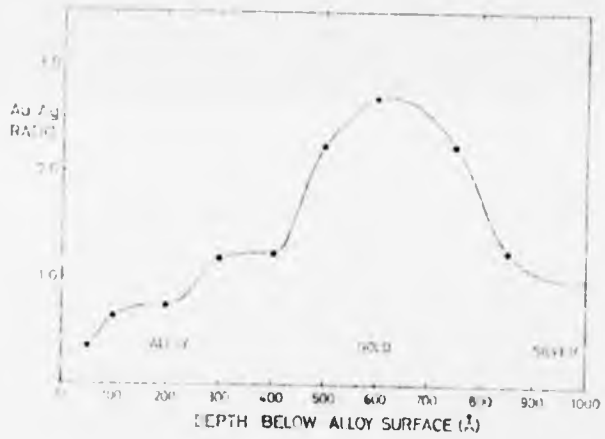

Fig.2.6.1. Depth composition profile (after Forty and Durkin 1981) taken through a silver-gold alloy on gold and silver substrates by Auger electron spectroscopy. The compositions are given in terms of atomic ratios.

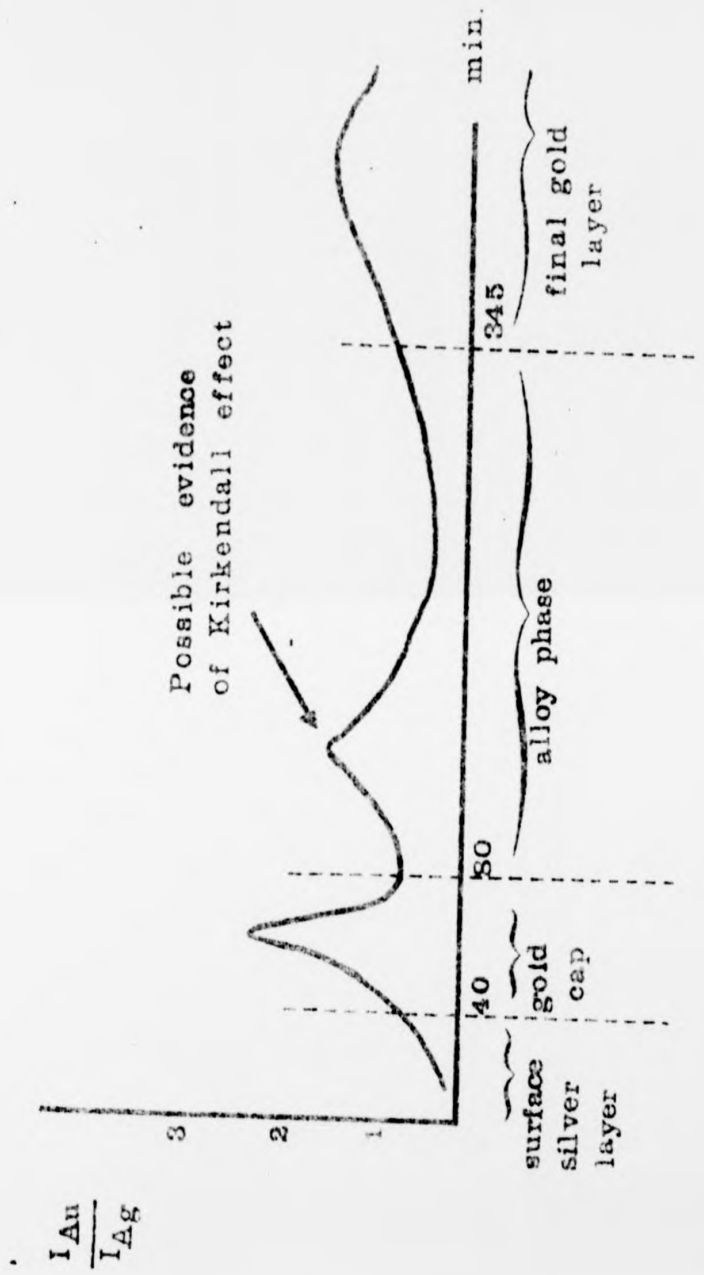

Fig. 2.6.2. Auger depth profile of a 67% silver, 33% gold alloy on to which a layer of pure gold, 35 Å thick, had been deposited. The boundaries between the alloy and the gold 'cap' and the gold supporting film are broadened by diffusion. The gold-silver ratio of the alloy in regions remote from an interface with other layers is roughly consistent with its nominal alloy composition.

which will be discussed further in chapter six of this thesis.

Carbon, oxygen and sulphur were contaminants observed on Auger spectra before any etching had occurred. The concentrations of carbon and sulphur were consistent with the levels of contamination frequently observed in these experiments (Johnson, Private Communication). In the case of the sample illustrated in Figure 2.6.2. a high initial concentration of oxygen was also observed this was judged to be higher than would be expected (Johnson 1979) and may indicate a small degree of oxide formation.

Auger Depth profiling is potentially a very valuable technique for examining local changes in elemental concentrations. Until the various sources of uncertainty arising from the technique are better characterised only large incremental changes in concentration will be resolved with any certainty. The results described here show silver surface enrichment and seem to indicate that the distribution of silver in the composite specimens is widespread. The discrete layers of gold, silver and alloy in the sample predicted from the preparation procedure, are then better considered as graded into gold-rich and silver-rich zones.

REFERENCES: Chapter Two

Christian, J. W., (1965), The theory of transformations in metals and alloys, Pergamon Press Ltd., Oxford.

Cherns, D., (1974), Phil. Mag. 30, 549.

Coburn, J. W., Ray, E. (1974), Crit. Rev. Solid State Sci., 4, 561.

Davis, L. E. et al (1976), Handbook of Auger Electron Spectroscopy Published by Physical Electronics Industries Inc. Minnisota.

Fain, F. C., and Macdonald, J. M. (1974), Phys. Rev., B9, 5099.

Forty, A. J., (1981), Gold Bull., 14 (1).

Forty, A. J., and Durkin, P. (1980), Phil. Mag. 42, 295.

Ho, P. S., Lewis, J. E., and Howard, J. K., (1977), J. Vac. Sci. Technol., 14, 322.

Johnson, P. D., (1979) Private Communication.

Pashley, D. W., (1959)a Phil. Mag., 4, 316.

(1959)b Phil. Mag., 4, 324.

Pashley, D. W., and Stowell, M. J., (1963), Phil. Mag., 8, 1605.

CHAPTER THREE

Microstructural Analysis

3.1. Transmission Electron Microscopy

The electron microscope is often compared to the optical microscope since electrons have wave properties and can be focussed using suitable magnetic lenses. Fig. 3.1.1. shows the lenses and cardinal points of both optical and electron microscopes. In each instrument, illumination from the source is focussed by the condenser lens on to the specimen. A first magnified image is formed by the objective lens and this is further magnified by a projector lens and in some cases two projector lenses, on to a fluorescent screen (electrons) or a ground glass screen (light).

The resolution of an electron microscope is much better than its light optical counterpart. In an optical microscope under optimum conditions the limit of resolution, called the diffraction limit is due to the wavelength of light and no further improvement is possible. An accelerated electron beam has a wavelength given by:

$$\lambda = \sqrt{\frac{150}{v}}$$

where v is the accelerating potential. For a typical accelerating voltage of 100 kV, $\lambda = 0.04$ Å, however, lens aberrations reduce this theoretical limit of resolution to between 1 and 10 Å in a typical microscope.

Contrast in images formed with a light microscope is due to absorption of light by the object. In the electron microscope it is due to the complex processes of electron scattering. Electrons may be scattered elastically and if a crystalline solid is being examined a coherent beam of electrons which suffer no loss of energy is formed. The magnitude of the scattering factor increases slowly with atomic number, being roughly proportional to $Z^{1/3}$ for fast electrons. (For X-rays the scattering factor is directly proportional to Z). In addition electrons may be inelastically scattered

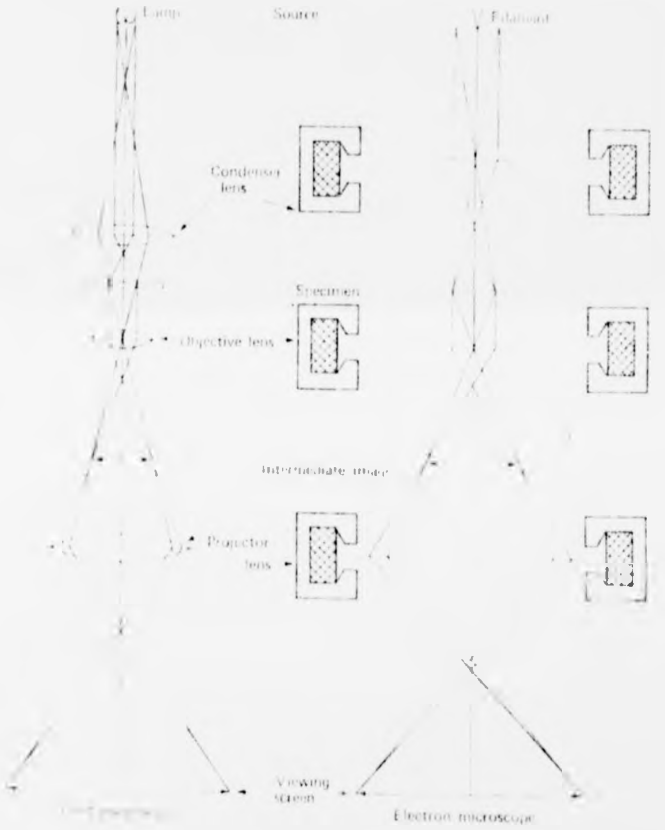

Fig. 3.1.1. Lenses and cardinal points for light and optical microscopes (after Agar 1974).

losing energy. This can arise from an interaction with conduction electrons (plasmon scattering), or because of thermal vibrations which perturb the perfect periodic potential of a crystal. In contrast to the elastic scattering, this inelastic scattering varies as Z.

Thus elastic and inelastic scattering contribute to the Z contrast of an image.

Thicker parts of a specimen or those composed of elements of higher atomic number, will deplete the transmitted beam more (i.e. they will scatter more electrons outside the range of angles admitted by the objective lens aperture). This gives rise to absorption contrast which also increases with increasing sample thickness. Thicker samples, however, bring about low image intensity and loss of resolution. Elastically scattered electrons passing through the objective aperture correspond to a variation in the phase of the wave leaving the lower surface of the specimen rather than to a variation in amplitude. Intensity is therefore uniform and contrast is not usually visible. It is possible to produce phase contrast since the phases of scattered waves are affected by lens aberrations and the degree of defocus of the objective lens. Obtaining information from out of focus images is potentially useful for increasing the effective resolution of the microscope and may represent a better approach to the resolution problem than improving the instrument itself.

The main contribution to contrast in most electron microscope images is diffraction contrast. This contrast is produced by allowing only either the transmitted beam or one diffracted beam to pass through the objective aperture. Thus it arises only from elastic scattering processes. In a region of the specimen in which the lattice planes are bent (for example in the vicinity of a dislocation), the local diffracted intensity increases and this will appear dark or light depending whether the transmitted or diffracted beam is imaged. The width of an image produced in this way

depends on the area distorted, but is usually in the order of 100 Å. Electrons in a backscattered wave are in the correct configuration (i.e. on the other side of the reflecting planes at the Bragg angle), to be re-scattered into the incident beam direction. The dynamical theory incorporates multiple elastic scattering effects and inelastic effects, both of which can modify the observed contrast considerably.

A full description of the dynamical theory of image formation is given elsewhere (for example Bowen and Hall 1975, Hirsch et al 1965). In essence the theory considers that at any depth Z in a crystal electrons can be represented by two waves, a wave travelling in the incident direction and an associated diffracted wave. It is sometimes useful to extend this idea of considering a transmitted and a diffracted beam coupled together by the diffraction of electrons from one to the other and think in terms of two separate solutions to the appropriate wave equation, each in itself consisting of a related direct and diffracted wave component. This is called the Bloch representation, the two solutions being known as Bloch waves which propagate independently through the crystal. Thickness fringes can be considered as the beating together of two Bloch waves producing an oscillation in the wave intensity. The thickness increment between such fringes is called the extinction distance and is at a maximum when the crystal is orientated at the Bragg reflecting condition. The extinction distance is critically dependent on orientation and multiple scattering events in the crystal.

Diffraction contrast is responsible for the observation of dislocations in electron microscope images. The displacement R due to any dislocation is to the first order approximation parallel to the burgers vector b. The contrast depends on g.R, which will be zero everywhere if g.b is zero. The Bloch formulation provides a simple explanation of why dislocations have dark contrast in both bright and dark field conditions and why oscillatory

contrast can arise when dislocations occur near the surface of a material (Bowen and Hall 1975).

Voids in crystals may be imaged in the out of focus condition. The contrast then consists of a weak absorption component and a phase contrast component due to the defocus, the latter giving Fresnel fringes at the edge of the void. The principal dark fringe is commonly used to delineate the edge of the void, usually in the under focus condition. Many workers take the inside edge of the dark fringe to be the void edge. The fringe position is in practice remarkably insensitive to size and orientation of void, and defocus (Foreman et al 1979). Some of the features seen on corroded silver-gold alloys are similar to voids. According to the present hypothesis they are infact thought to be channels and pits on the alloy surface. Careful examination of any fringe contrast at the edges of these features could reveal whether they are voids or pits. It would, however, require a very careful and detailed examination.

Under normal, bright field conditions an image is formed from un-diffracted electrons, scattered electrons being excluded by the objective aperture. If electrons from a diffracted beam are used to form an image, a dark field image will be seen. The simplest way to obtain a dark field picture is to displace the objective aperture until it is centred around the beam which is to be imaged so that it excludes all other beams. Images formed in this way are of poor quality, since they are formed from off axis electrons and consequently the effect of lens aberrations is increased. A better way of obtaining dark field images is to electrically tilt the electron beam until the diffracted beam being used for imaging passes along the microscope axis. It should then be subject to no more aberration than an ordinary bright field image. Tilting the beam can produce astigmatism in the beam before it reaches the object, this being more likely as tilt angles get larger. A special set of controls to correct for this is usually fitted.

Dark field imaging is a very powerful technique because it enables information from a particular family of planes to be imaged independently. Diffracted beams which are not expected in a particular diffraction pattern can be used and in this way those features in the image which give rise to them are thus identified directly.

A feature characteristic of electron lenses is a great depth of field, which arises because of their small angular aperture. For most samples the depth of field is usually greater than their thickness and a specimen will appear equally sharp throughout its thickness.

Most of the conventional TEM images recorded in this work were obtained using a JEOL 100 C microscope. This has a side entry eucentric tilting goniometer stage. It operates at 100 kV and can be fitted with an energy dispersive X-ray (EDAX) analyser. Other images were obtained using a JEOL JEM 7 microscope which is fitted with a heating stage so that in situ annealing of specimens is possible.

3.2. Electron Diffraction

A crystalline specimen will diffract electrons at well defined angles θ dependent on electron wavelength and crystal lattice spacings in accordance with Bragg's law,

$$n\lambda = 2d \sin\theta \quad .$$

Electrons accelerated through high voltages have a very small de Broglie wavelength and consequently the Ewald sphere of reflection (radius $1/\lambda$) is very large compared with the dimensions of the reciprocal lattice of a sample. At the origin of reciprocal space the curvature of the sphere is slight and it may be considered as a plane section through the reciprocal lattice, centred at the origin. It thus intersects many reciprocal lattice spikes and often an electron diffraction pattern from a single crystal is the section in the reciprocal lattice appropriate to the zone axis along which the electron beam is passing.

Obtaining electron diffraction patterns in an electron microscope is a fairly simple matter. Diffracted electrons are brought to focus in the back focal plane of the objective lens (fig. 3.1.1). In the normal mode of operation the image formed by the objective lens lies in the object plane for the first projector lens. This is usually called the intermediate lens. The strength of this intermediate lens can be reduced until the object plane coincides with the back focal plane of the objective lens. In this mode of operation the diffraction pattern from the object will be imaged by the intermediate lens and then magnified by the remaining projector lens. In the JEOL 100C the image plane or the diffraction pattern can be selected for viewing by pushing the appropriate button to give the required intermediate lens current. It is possible, by placing an aperture at the objective lens image plane to isolate a small region of the object. This will then be the region giving rise to any diffraction pattern transmitted by the selector aperture. This is known as selected area diffraction. There are errors in this selected area technique which arise from the spherical aberration of the objective lens and incorrect focusing of the objective lens. These lead to appreciable errors for third and higher-order beams (see, for example Hirsch et al 1965).

The ease with which electron diffraction patterns are obtained is a very useful feature of a transmission electron microscope. It enables the operator to see at a glance whether a sample is polycrystalline or a single crystal and whether more than one phase is present. The use of a specimen stage in a microscope enables 3-dimensional information about the reciprocal lattice to be obtained (rotating the specimen with respect to the electron beam is equivalent to rotating the Ewald sphere through reciprocal space), and a complete structural analysis is possible from this information.

Imperfections in the crystal will have an effect on the reciprocal lattice. Thermal vibrations produce a diffuse back-ground and a corresponding

decrease of Bragg intensity. Point defects will also have the same effect. Bending of the crystal will cause a radial spread of the intensity distribution in reciprocal space perpendicular to the incident electron beam. The case of dislocations can be complicated. The rapidly varying strains near the dislocation core give rise to tails in the diffraction pattern; the slowly varying long range strain field gives rise to broadening. Stacking faults cause streaking of reciprocal lattice points, the length of the streaks increasing with the number of faults. If the stacking fault plane is not parallel to the plane of the foil, then two spots are observed due to streaking perpendicular to the plane of the foil and perpendicular to the plane of the faults. A fuller description of the effects of imperfections on the reciprocal lattice is given in Hirsch et al 1965 or Pinsker 1953.

Reciprocal lattice points for a crystal in the form of a thin plate are elongated along the direction normal to the plate, to give reciprocal lattice spikes. The total spike length is inversely proportional to the thickness of the plate, down to a minimum spike length when the thickness reaches the extinction distance. Thus the geometry of the diffraction pattern can be influenced by crystal shape and it is crucial to know how the sphere of reflection intersects elongated or broadened reciprocal lattice spikes.

3.3. Scanning Electron Microscopy

The principle of the scanning electron microscope is closely comparable to that of a closed circuit television system. In the television camera, light from the object forms an image on a special screen, and the signal from the screen depends on the image intensity at the point being scanned. The signal is used to modulate the brightness of a cathode-ray tube display. The original image will be faithfully reproduced if the camera and display

rasters are geometrically similar and synchronous and if the time for signal collection and processing is short compared with the time for the scan to move from one picture point to the next.

In the scanning electron microscope the object itself is scanned with the electron beam and the electrons emitted from the surface are collected and amplified to from the video signal. The emission varies from point to point on the specimen surface and so an image is obtained. Many different specimen properties cause variations in electron emission and thus, although information might be obtainable about all these properties, the images need intepreting with care. The resolving power of the instrument cannot be smaller than the diameter of the electron probe ($\sim$ 50 Å) scanning across the specimen surface. In most systems a practical resolution of 150-250 Å is normal. A small probe is obtained by focussing an electron beam using electron lenses. The lenses are therefore probe forming rather than image forming. Magnification in the scanning microscope is determined simply by the ratio of the sizes of rasters scanned on the specimen surface and on the display screen.

Three lenses are usually used to condense the electron beam, although fewer lenses may be employed when "bright" types of electron gun are used (e.g. those incorporating lanthanum hexaboride filaments). The final condenser lens must have low aberrations if the smallest probe sizes are to be achieved. However, its magnetic field should not extend into the specimen chamber. It must operate at a focal length of 10 mm or more, in order that the specimen can be moved about and the emitted electrons collected. These requirements tend to result in increased aberrations. For the smallest probe sizes the lens aperture must be adjusted to an optimum size compatible with the scan system, typically around 100 microns in diameter. The probe divergence will thus be low, resulting in a large depth of focus. This is a very useful feature of the scanning electron microscope.

There is a basic noise level in the video signal visible on the screen. This is because the emission of electrons from a hot filament is a random process subject to statistical variations. This fundamental noise level cannot be reduced and may be increased by the processes of electron emission from the specimen, electron detection and amplification. The result is that a variation in signal level may be partially obscured by a variation in noise level. The arbitrary criterion usually adopted for visibility is that the signal variation is greater than five times the noise variation.

Signals from specimens in the scanning microscope are collected using a detector designed by Everhart and Thornley which converts the very small signals (of the order of 10^{-12} A) into a flux of photons using a scintillator. A photomultiplier then amplifies this signal, converting it back to an electrical signal. This produces noise free amplification of up to 10^{6} x which is virtually 100% efficient and has a band width of 10 MHz. If the detector entry grid is positively biased low energy secondary electrons will be detected, if it is negatively biased these will be repelled and only backscattered or reflected electrons will be detected. Thus two modes of image formation are readily obtainable.

3.4. X-ray (EDAX) Analysis

When electrons strike a metal surface many interactions occur, among them the production of X-rays. X-ray energies are characteristic of a particular element and if analysed can provide information about which elements are present in a specimen. Counting X-rays in a spectral distribution should give quantitative information about the elements present. However, the relationship between the intensity of X-rays and concentration of the corresponding element is complex.

It is common practice to use an X-ray detection system in conjunction with an electron microscope, so that the concentration and distribution of elements in a sample can be determined. In the work presented here use was made of an EDAX (energy dispersive analysis of X-rays) detection system. As the name suggests, this equipment can detect and display simultaneously the intensities of all X-ray energies leaving the specimen. These systems use lithium-drifted silicon crystals to detect X-rays and have to be kept at liquid nitrogen temperatures. X-rays entering the crystals create electron-hole pairs. The number of these pairs is proportional to the X-ray energy. The associated charges are collected and passed into a multichannel analyser where pulses are separated in terms of amplitude and stored in memory channels corresponding to these amplitudes. Measurement time must be very rapid since emitted X-rays of different energies arrive at the detector virtually simultaneously. The resulting energy spectrum is then displayed on a cathode ray oscilloscope forming a V.D.U. output from the multichannel analyser.

Energy dispersive analysis of X-rays offers certain advantages over the other major technique for collecting X-rays, wavelength dispersive analysis of X-rays. The EDAX system has good collection efficiency measuring the whole spectrum simultaneously. It requires only short collection times and is effective at low beam currents. It can be used for roughened as well as smooth surfaces. There are, however, some disadvantages. It is poor at detecting light elements, a Be window in front of the detector absorbs low energy X-rays. Its detection limits are high. Peak to background ratios are low due to the collection of spurious X-rays generated from the components of the microscope due to scattered electrons and fluorescent effects. There is also high inherent 'noise' in the electronic detection process used in this system.

As previously stated quantitative X-ray analysis is complex. If absolute concentrations are required, then it is usually necessary to use standards. It is simpler to determine the ratio of two concentrations since the corrections for each component will be similar. Quantitative information is often presented in this way.

As electrons enter a sample a number of processes occur which affect the production and collection of X-rays from the sample. The concentration, Cx, of an element x can be given by:

$$Cx = \frac{kIx}{C_Z C_A C_F}$$

where Ix is the X-ray intensity from the sample, k is a constant which is given by the ratio of concentration to X-ray intensity for a standard of X under the same operating conditions. C_Z, C_A and C_F are correction factors to account for the effects of atomic number, X-ray absorption, and X-ray fluorescence respectively. These make up what is known as the ZAF correction procedure for use in microanalysis of bulk specimens (Philibert and Tixier 1968). Such correction procedures are often very complex and are frequently carried out with the aid of a computer.

Most of the correction factors mentioned above do not apply to thin specimens because of the lack of backscatter and electron energy loss. Absorption and fluoresence corrections can also be ignored. In a transmission electron microscope the volume of material producing X-rays is fairly accurately defined. Since specimens are very thin (less than 1000Å) it is just the product of the electron beam diameter and foil thickness; beam divergence over such short distances is negligible. This leads to a concentration ratio obtained from:

$$\frac{C_1}{C_2} = \frac{P_2}{P_1} \times \frac{I_1}{I_2} \quad ,$$

C_1 and C_2 = concentration of components 1 and 2

I_1 and I_2 = measured intensities of 1 and 2

P_1 and P_2 = correction factors for 1 and 2.

The correction factors take account of differences in ionisation cross-section and fluorescent yield between elements and detector efficiency. These have been tabulated for most X-ray energies detected on EDAX equipment. Thus concentration ratios can easily be obtained from intensity measurements. It is important when obtaining spectra that statistically meaningful results are obtained. It must be possible to differentiate counts at the peak position from counts at the background position. Long counting times are desirable but errors due to contamination deposition, instrument drift, beam current fluctuations and extraneous electronic noise must also be considered.

Valuable information about the segregation of silver to holes and double-positioning boundaries in the thin films and other microstructural features is obtained using these techniques and a correlation between this segregation and the subsequent corrosion behaviour of these alloys can be established. The spatial resolution of the electron probe is typically, 2-300Å and highly-resolved information about the distribution of elements is possible. This is particularly relevant to corrosion studies where changes in composition can have a profound influence on the corrosion behaviour of a material.

REFERENCES - Chapter Three

Agar, A. W., (1974), Practical Methods in Electron Microscopy, Vol.2, Ed. A. M. Glauert, North-Holland Publishing Co., London.

Belle, J. A., (1979), Electron Microscopy and Microanalysis of Crystalline Materials.

Bowen, K. D., and Hall, C. R., (1975), Microscopy of Materials: Modern Imaging Methods Using Electron X-ray and Ion Beams, MacMillan Press.

Coslett, V. E., (1946), Introduction to Electron Optics, Oxford: Clarendon Press.

Everhart, T. E., and Thornley, R. F. M., (1960), J. Sci. Instrum., 37, 246.

Foreman, A. J. E., Harrach, H. V., and Saldin, D. K., (1979), Inst. Phys. Conf. Ser. No 52, p.225, Institute of Physics, Bristol.

Hirsch, P. B., Howie, A., Nicholson, P. B., Pashley, D. W. and Whelan, M. J., (1965), Electron Microscopy of Thin Crystals, Butterworths, London.

Philibert, J., and Tixier, R., (1968), Quantitative Electron Probe Microanalysis, K. F. J. Heinrich ed. (N.B.S. Special Pub. 298, Washington, D. C.), p.269.

Pinsker, Z. G., (1953), Electron Diffraction, London, Butterworth.

Weinberg, F., (1970), Tools and Techniques in Physical Metallurgy, Marcel Dekker, Inc. New York.

Wischnitzer, S. (1970), Introduction to Electron Microscopy, Pergamon Press, New York.

CHAPTER FOUR

Micromorphological Observations of Silver-Gold Alloys Corroded in Nitric Acid

In this chapter TEM observations of the micromorphology of corroded alloys are described. The alloys had a wide range of compositions and were treated with acids of different concentrations. Silver-gold alloys developed a characteristic morphology when treated in nitric acid. The particular morphology that formed was the result of a combination of all corrosion system parameters: alloy composition, acid strength, and exposure time. The observations are used to illustrate the idea of a developing corrosion morphology, the degree of development corresponding to the extent of corrosion. This again was a function of the parameters mentioned above. Measurements of island growth with time are given to support this idea of development of the micromorphology with increasing corrosion.

4.1. Silver 50 Atomic per cent Gold Alloys Corroded in Nitric Acid

Figure 4.1.1. shows the typical morphology that developed when a 50% gold, 50% silver alloy was corroded for approximately one minute in 50% nitric acid (percentage by volume of HNO_3 sp. gravity 1.42 diluted in de-ionised water). The main feature was a two-dimensional development of irregularly shaped ribbons of metal. These ribbon regions appeared darker than the channels separating them. Another example of a specimen stripped from its mica/silver substrate and exposed freely to 50% nitric acid solution is shown in figure 4.1.2. This micrograph is useful because it contains examples of the three basic morphologies that developed on these alloys. The first type of morphology illustrated at site A consisted of islands which had a diameter of the order of 500 Å or less; frequently

Fig. 4.1.1. Transmission electron micrograph of a 50:50 silver-gold alloy corroded in 50% nitric acid for 60 s.

Fig. 4.1.1. Transmission electron micrograph of a 50:50 silver-gold alloy corroded in 50% nitric acid for 60 s.

Fig. 4.1.2. Transmission electron micrograph of island and channel structures on the surface of 50:50 Ag-Au alloy after exposure to 50% nitric acid for 1 min. A, island structure; B, ribbon development; C, connected island structure and pits; D, misfit dislocation. The inset is a typical diffraction pattern for a corroded specimen.

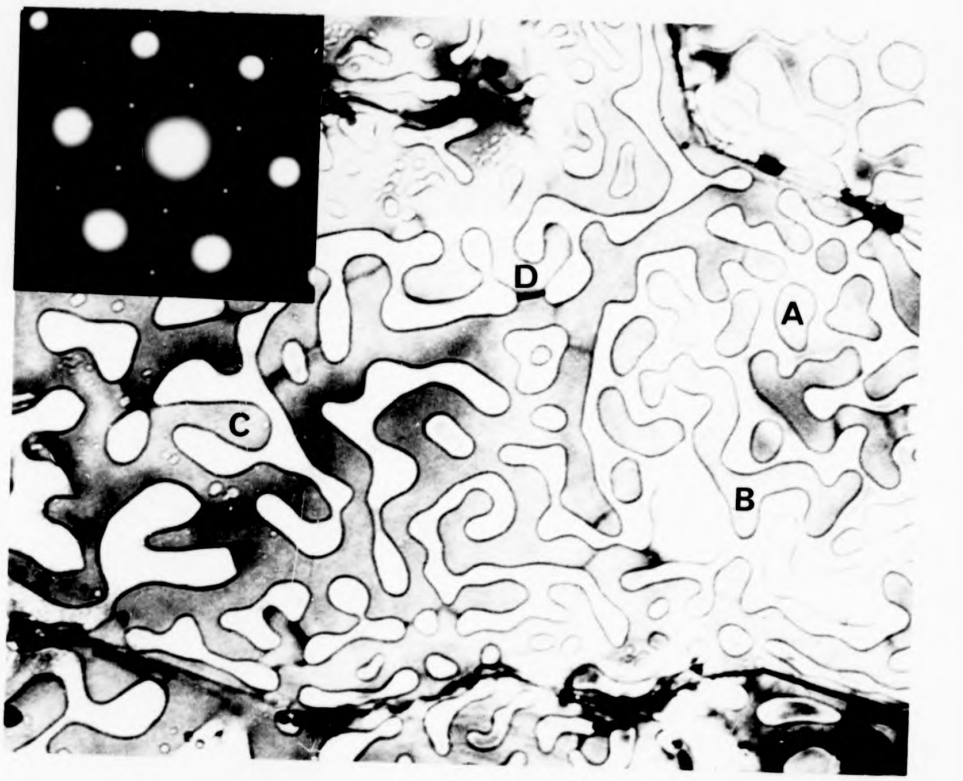

Fig. 4.1.2. Transmission electron micrograph of island and channel structures on the surface of 50:50 Ag-Au alloy after exposure to 50% nitric acid for 1 min. A, island structure; B, ribbon development; C, connected island structure and pits; D, misfit dislocation. The inset is a typical diffraction pattern for a corroded specimen.

islands were smaller (~ 100 Å) and separated by correspondingly larger areas of less strongly absorbing material. Growth of these islands on certain areas of the specimen produced a coarsening of the first morphology, such that the islands merged together into a ribbon-like development interleaved with channels, and this is illustrated at B. Further growth of these ribbons caused them to merge at certain points forming an interconnected structure enclosing sections of channels which were thus reduced to isolated and irregularly shaped pits, shown at C in figure 4.1.2. From a study of many such specimens it was concluded that as this third type of morphology developed the pits slowly shrank in diameter and penetrated deeper into the specimen.

The three basic morphologies can be summarised as: first, the island morphology which consisted of separate and roughly equiaxed islands up to approximately 500 Å in diameter; second the ribbon/channel morphology which had irregularly shaped ribbons forming a maze-like pattern interleaved with channels; finally the pit morphology where channel regions had been "pinched-off" leaving isolated pits which extended deep into the alloy.

The electron diffraction pattern from a 50% gold alloy corroded in this way is shown as an inset to figure 4.1.2. This was essentially the pattern expected for a single crystal of face-centred-cubic gold or silver-gold alloy with a (111) orientation and with the incident electron beam parallel to a [111] direction (i.e. one of the four sets of {111} planes was perpendicular to the electron beam). This gave rise to the six intense $2\bar{2}0$ type first-order reflections shown in the pattern. Additional and much weaker spots very close to the forbidden 111 reflections were visible and were thought to arise because of double diffraction effects which occurred in the region of the double-positioning boundaries. These consisted of two overlapping twin-related orientations of the alloy, (Pashley and Stowell, 1963). Essentially a 111 type reflection from material in one twin

orientation was then diffracted by material in the second orientation. The spot in the reciprocal lattice corresponding to this two stage reflection now cut the Ewald sphere and contributed to the diffraction pattern of this specimen. Only a small fraction of the total volume of material contributed to this reflection and therefore it had a low intensity. A later study by Cherns (1974) suggests that monatomic steps on the surface of films grown in this way, may also contribute to the intensity of these reflections. The S.T.E.M. mode of operation on the J.E.M. 100C, which uses a very fine beam probe, was used to obtain micro-diffraction patterns from areas on the sample in the order of the beam diameter (50Å). The patterns from island regions and from non-island regions were similar to the pattern shown in figure 4.1.2. This indicated that there was a very close epitaxial relationship between islands and the underlying alloy. Diffraction patterns for corroded specimens frequently showed further additonal spots, the most intense of these being arranged in pairs around forbidden 111 reflections. An explanation for these is given in chapter six of this thesis.

The contrast between island and channel regions was quite marked probably due to the different thicknesses of these regions. Edge diffraction and phase contrast in themselves would only account for a very small loss of intensity visible in the resulting image and Forty (1982) has suggested that complex double and triple diffraction in the region of the islands can provide a better explanation of the pronounced differences in contrast between island and channels observed on micrographs such as those shown here. One interesting feature of the morphology was the presence of a dark line around the edge of islands or the ribbon-like strands of material which developed on these specimens. The reasons for the presence of this dark line are not fully understood. It may be a Fresnel fringe due to a complicated phase effect arising from the change in alloy thickness in the vicinity of the edge of the island or channel.

An attempt was made to detect any difference in composition which might have existed between the island and channel regions. The S.T.E.M. facility with EDAX available on the J.E.M. 100C was used for this purpose. Although significant changes in the relative amounts of silver and gold were readily detected on a more macroscopic scale across the surface, measurements made on this scale were not so reliable. This was partly because of the difficulty of positioning the electron beam accurately and wholly within an island or channel region and partly because of the rather large amount of gold in the supporting film which made it difficult to discriminate between small local changes in the silver-gold ratio. In addition, beam divergence which was pronounced for the highly condensed electron probe used in this mode (a 50Å diameter probe typically spreading to ~ 150Å as it passed through an alloy several hundred angstroms thick) tended to exacerbate the difficulties of positioning and accuracy mentioned above.

The micromorphology changed dramatically if the alloy was annealed after its initial exposure to nitric acid. In the experiments described here annealing was carried out *in situ* in a J.E.O.L. J.E.M. 7 transmission electron microscope fitted with an externally-controlled heating stage so that the specimen could be observed continuously as the heat treatment progressed. Figure 4.1.3. shows the new micromorphology that developed when a pre-corroded specimen was heated to 450°C, held at this temperature for a few minutes and then cooled to room temperature again. This showed that island and channel regions appeared to have grown together to form a continuous surface cover whereas the channel regions had shrunk to form small pits trapped at the junctions between islands. The brightness of these pits in the electron image suggested that they were considerably deeper than the original channels. An interesting observation on these pits was that they were frequently crystallographic in shape as shown in Fig. 4.1.4. which was a corroded alloy given the same annealing treatment as described

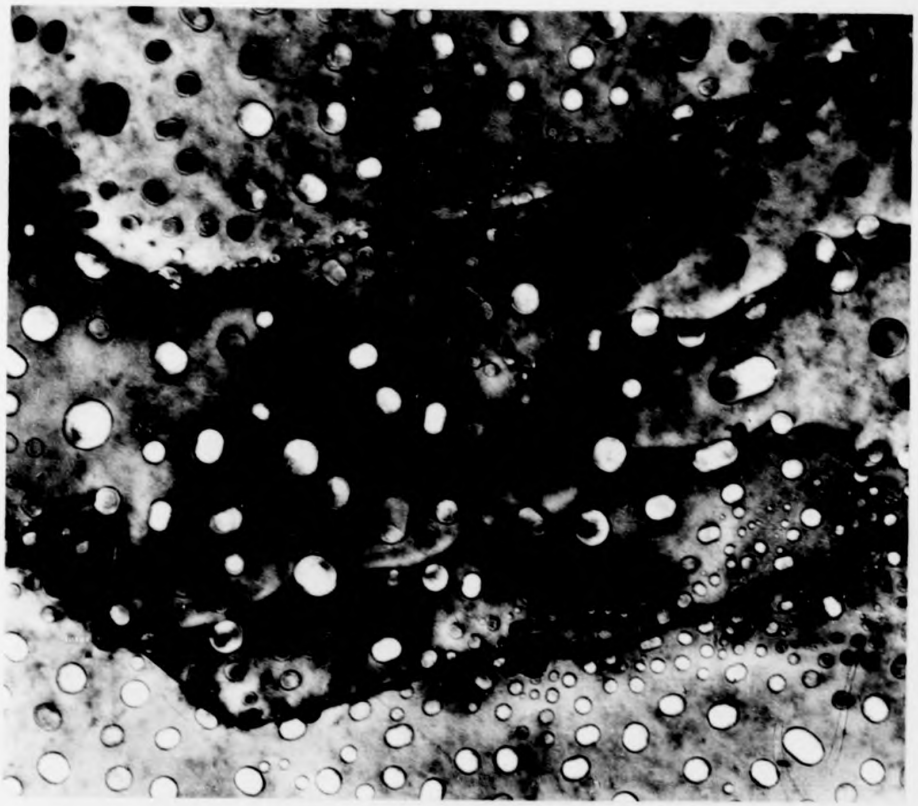

Fig. 4.1.3. Transmission electron micrograph of 50:50 Ag-Au alloy after corrosion in 50% nitric acid and annealing at 450°C.

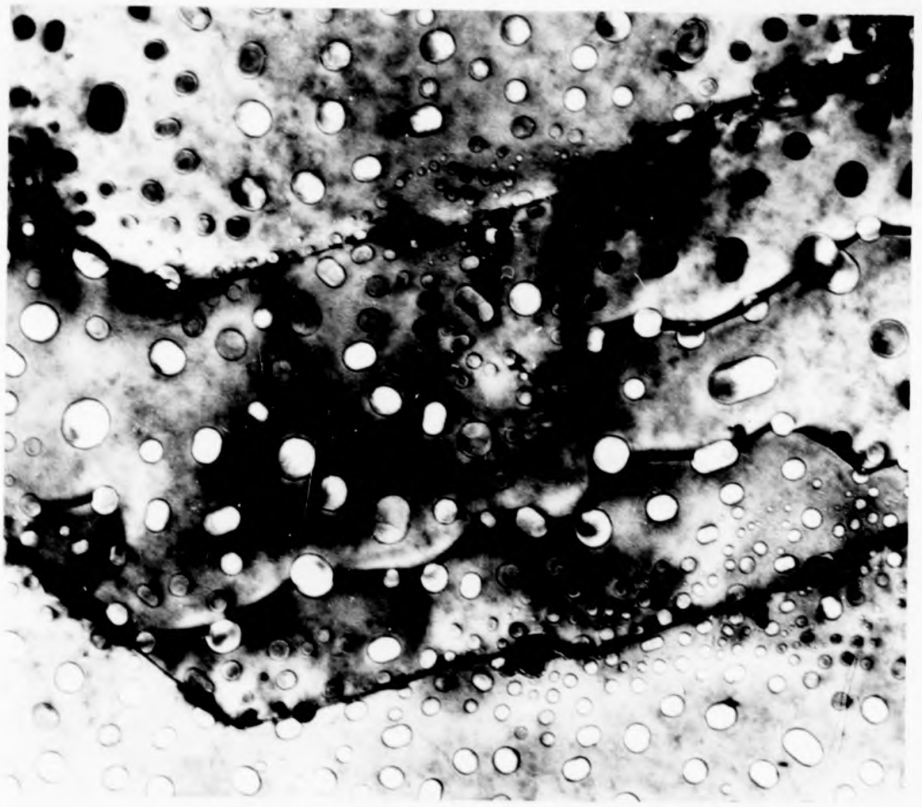

Fig. 4.1.1. Transmission electron micrograph of 50:50 Ag-Au alloy after corrosion in 50% nitric acid and annealing at 450°C.

Fig. 4.1.4. A 50:50 Ag-Au alloy after corrosion in 50% nitric acid and annealing at 450°C. The edges of the annealed pits are parallel to the principal <110> directions in the metal.

Fig. 4.1.4. A 50:50 Ag-Au alloy after corrosion in 50% nitric acid and annealing at 450°C. The edges of the annealed pits are parallel to the principal <110> directions in the metal.

above but for a more prolonged period. The edges of the pits were parallel to the principal <110> directions (i.e. the close packed directions) in the metal. The mechanisms whereby the growth of island and ribbon regions led to the "pinching-off" of channel regions is illustrated in figure 4.1.5. which shows an earlier stage of development where merging of islands was incomplete.

A striking example of how the morphology changed when specimens were annealed is shown in figure 4.1.6.; 4.1.6. (a) shows a 50:50 alloy corroded in 50% nitric acid and 4.1.6.(b) and (c) show different areas of the sample after it had been annealed at 250°C. Evident in figure 4.1.6 (b) was the marked reduction in pit size frequently found in the vicinity of double positioning boundaries. This was thought to be due to enhanced corrosion disordering and re-structuring of the surface in these regions and was associated with a greater relative concentration of silver in these regions as found by E.D.A.X. analysis (Chapter 2). The increased chemical disordering was thought to give rise to a greater frequency of island nucleation in these regions so that the residual pits were consequently more numerous but smaller. If the corrosion process led to a roughening of the alloy surface on an atomic scale then the more chemically active regions i.e. silver-rich regions became relatively more disordered leading to a faster re-ordering which tended to produce narrower but deeper pits. It might be concluded therefore that the annealed structures mapped out the change in chemical activity across the alloy surface. Figure 4.1.6. (c) shows extinction contours within pit regions. These arise because the intensities of diffracted and transmitted electron beams are periodic throughout the depth of a specimen (as described in chapter three). Allowing for many-beam dynamical effects, in orientations of high symmetry, such as in this case, the extinction distance for pure gold is approximately 70 Å (Hirsch et al 1965). Assuming that the extinction distance for gold alloys is similar to that for pure gold then the micrograph indicates that in this example

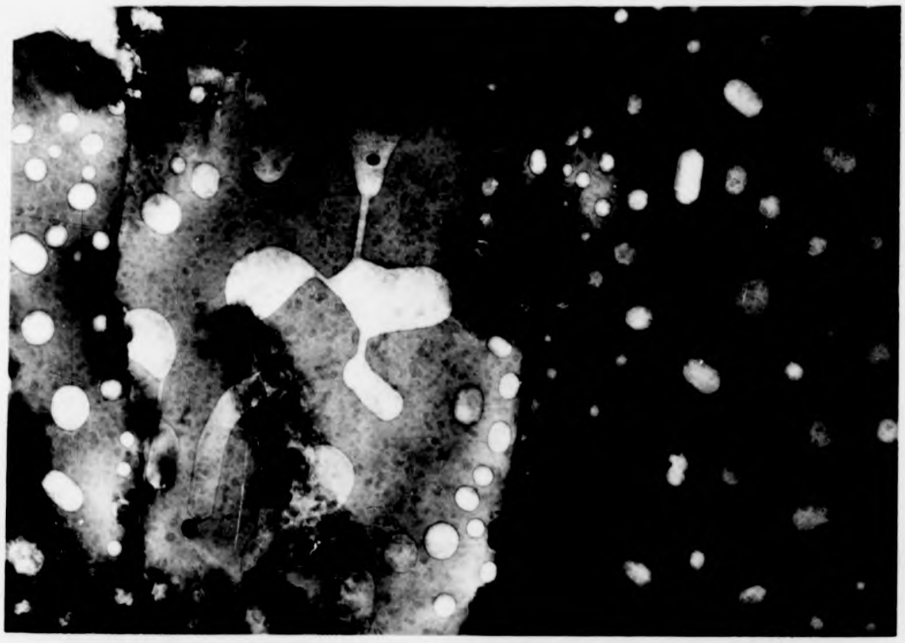

Fig. 4.1.5. Transmission electron micrograph of 50:50 Ag-Au alloy after corrosion in 50% nitric acid and annealing at 450°C showing the final stages of pit formation by the merging of islands as annealing proceeds.

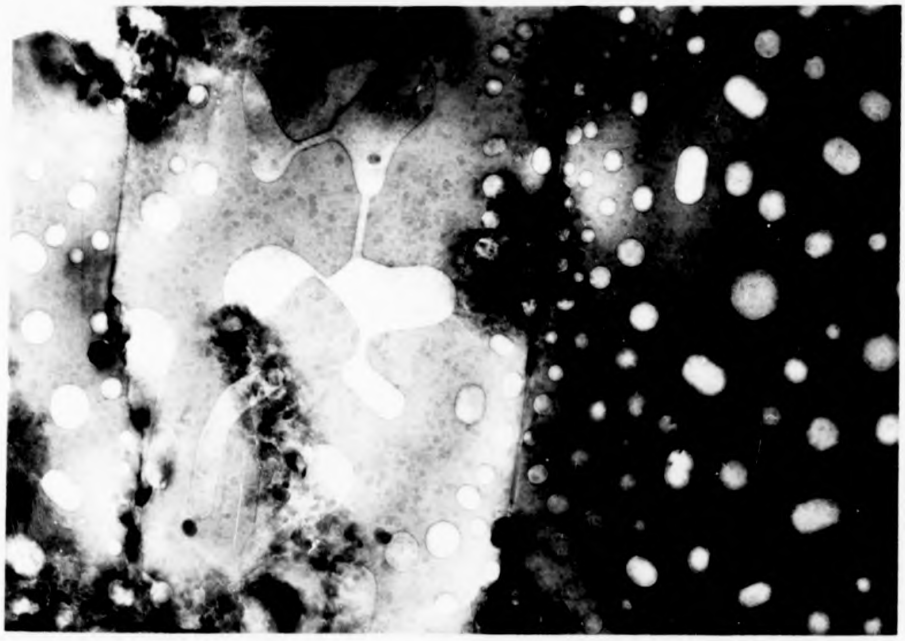

Fig. 4.1.5. Transmission electron micrograph of 50:50 Ag-Au alloy after corrosion in 50% nitric acid and annealing at 450°C showing the final stages of pit formation by the merging of islands as annealing proceeds.

(a) Transmission electron micrograph of a 50:50 alloy corroded in 50% nitric acid.

(b) Transmission electron micrograph showing a different region of the sample shown in (a). Note the marked reduction in pit size in the vicinity of double positioning boundaries.

(c) Transmission electron micrograph also illustrating pit formation and showing extinction contours within pit regions.

0·1μ

(a) Transmission electron micrograph showing a region of the sample which has been severely corroded in [illegible] solution.

(b) Transmission electron micrograph showing a ditferent region of the sample shown in (a). Note the marked reduction in pit size in the vicinity of double positioning boundaries.

0·1μ

(c) Transmission electron micrograph showing a [illegible] pit [illegible] extinction contours within [illegible] regions.

pits vary in depth between less than 100 and more than 300 Å. Typically their depths are approximately one extinction distance or less.

Another interesting feature of the corroded and annealed alloys was the formation of dislocations which lay in the (111) plane of the film. These appeared to be associated with the pits. It is thought that these dislocations were built in during corrosion, or annealing, when neighbouring islands grew together with a crystallographic mismatch. (An example of this in a specimen that had simply been corroded can be seen at D in figure 4.1.2.). It should be stated that handling specimens before they were observed in the electron microscope may have introduced dislocations into the structure. More striking examples were found after the more extensive island growth that occurred during annealing. For example, figure 4.1.6. (b) was a particularly good example showing dislocation lines which appeared to be anchored firmly on the annealing pits. Also on this micrograph and on figure 4.1.4. was a cellular network of dislocations presumably formed as a result of the annealing process. A possible explanation for this (Forty and Durkin 1981) was that the rapid re-forming of the surface by this severe treatment had resulted in a large number of dislocations which had climbed together as a result of the high concentration of vacancies in the surface layers of the heavily corroded specimen to form networks. Similar networks have been observed by Pashley (1959) in gold films, prepared by evaporation onto a silver film substrate, stripped by floating the composite film on 35% nitric acid and then annealed at 500°C. It will be shown later in this chapter that dislocation networks could readily be formed in silver-rich alloys by exposure to weak acid (35%) even without annealing.

Summary of the observation made so far

Many of the micromorphological features which appeared generally on silver-gold alloys corroded in nitric acid could be seen in some form on the 50:50 (Ag:Au) alloys corroded in 50% nitric acid as described above. Observations made on this system provided a standard with which other

alloy systems could be compared. These observations suggested that the corrosion reaction caused a disordering of the surface, probably by selective dissolution of silver. Re-ordering or re-distribution of the residual material seemed to occur by a nucleation and growth process. This material re-structuring of the surface was accelerated by annealing. The island morphology showed a striking resemblance to that found in the nucleation and growth of epitaxial films of silver and gold on crystalline substrates (Pashley, Stowell, Jacobs and Law 1964). The idea of a surface re-ordering involving similar processes would provide a basic model with which to view the observations made this far and in the remainder of this chapter.

4.2. The Micromorphology of 50:50 Silver-Gold Alloys Corroded in Strong Acid

In general, attack by more concentrated acid produced a micromorphology which was equivalent to that found when a 50:50 Ag-Au alloy had been exposed to 50% nitric acid and then annealed for some time at 450°C. Figure 4.2.1. shows a 50:50 alloy corroded for 10s in 100% HNO_3 where the more advanced transformation of the channel to the pit morphology was clearly visible. Figure 4.2.2. is a similar example in which the transformation to the pit morphology was more complete.

A number of experiments have been performed in which a specimen corroded in strong acid was examined after annealing to progressively higher temperatures. For example, figure 4.2.3. (a) shows the effect of corrosion in concentrated (100%) nitric acid on 50:50 Ag-Au alloy; figures 4.2.3. (b); 4.2.3. (c) and 4.2.3. (d) show the same area of the specimen after annealing it progressively to 150°C, 300°C and then 450°C. There were inevitably changes in the diffracting conditions in any one part of the specimen during annealing and these resulted in the changes of contrast in the micrographs. This tended to make a comparison of the micrographs difficult and therefore a marker has been placed at the same region of the specimen on each micrograph to assist viewing. The morphology

Fig. 4.2.1. Transmission electron micrograph of a 50:50 Ag-Au alloy stripped in 100% HNO_3 showing the transformation from a channel to a pit morphology.

Fig. 4.2.1: Transmission electron micrograph of a 50:50 Ag-Au alloy stripped in 100% HNO_3 showing the transformation from a channel to a pit morphology.

Fig. 4.2.2. Transmission electron micrograph of a 50:50 Ag-Au alloy stripped in 100% nitric acid. The transformation to a pit morphology is almost complete.

Fig. 4.2.2. Transmission electron micrograph of a 50:50 Ag-Au alloy stripped in 100% nitric acid. The transformation to a pit morphology is almost complete.

Fig. 4.2.3. The effect of corrosion in concentrated 100% nitric acid on 50:50 Ag-Au alloy. (a) immediately after corrosion, (b) after subsequent annealing at 150°C, (c) annealing to 300°C, and (d) after finally annealing at 450°C.

M1.0

(b)

(c)

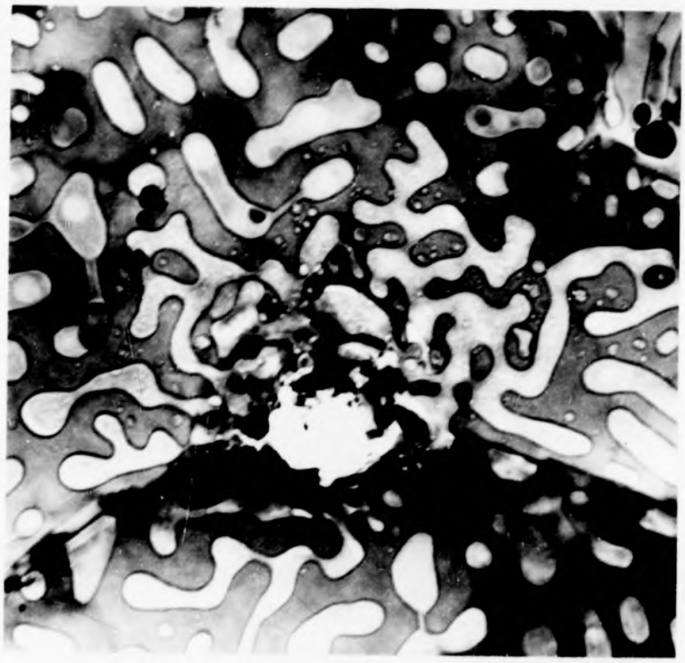

(c)

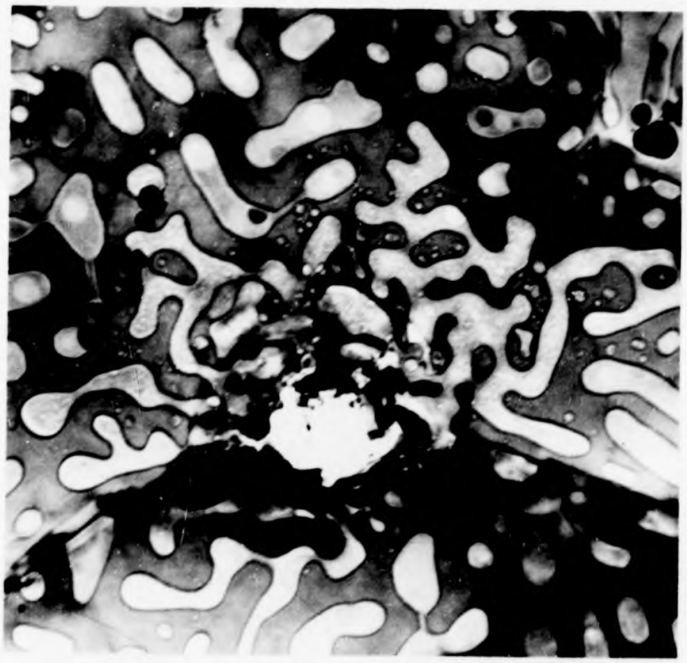

(d)

in the close vicinity of the marker gives a good indication of the changes which occurred generally as a result of annealing. There appeared to be a steady but quite noticeable, progressive change in morphology at the lower annealing temperatures (150°C and 300°C) which seemed to indicate that the stronger acid caused more "corrosion disorder" so that there was evidence of re-ordering even at these low temperatures. Annealing to 450°C (fig. 4.2.3. (d)) caused widespread transformation to the pit morphology. This micrograph also illustrated the interesting feature of corrosion dislocation networks which were clearly influenced by the specimen micromorphology adding weight to the idea that these networks were formed during the severe annealing treatment described in the previous section (4.1). Figure 4.2.4. shows the same specimen after it had been annealed to 600°C. In this case transformation to the pit morphology was complete.

4.3. The Micromorphology of 50:50 Ag-Au Alloys Corroded in 35% Nitric Acid

An examination of these specimens after stripping and immersion in 35% nitric acid frequently revealed two superimposed island morphologies, as shown in figure 4.3.1. It was thought that corrosion occurred at the original silver/gold interface during stripping as well as at the free surface of the alloy during deliberate corrosion. In this case weaker acid presumably did not completely dissolve the alloyed zone at the interface during stripping but left a residual island morphology. All the previous observations (4.1 and 4.2) were made on specimens that were stripped and immersed in stronger acids which apparently did not leave such a clearly observable residue at the silver/gold interface. The residual morphology at the silver/gold interface was often completely removed by further exposure to 35% nitric acid.

A very important observation made on a 50:50 alloy exposed to 35% nitric acid is shown in figures 4.3.2 (a) and 4.3.2(b). These show that the island morphology observed at the free surface of the alloy could be modified by

Fig. 4.2.4. This micrograph shows a 50:50 Ag-Au alloy corroded in 100% nitric acid and annealed to 600°C.

0·1 μ

Fig. 4.2.4. This micrograph shows a 50:50 Ag-Au alloy corroded in 100% nitric acid and annealed to 600°C.

Fig. 4.3.1. Tranmission electron micrograph of 50:50 Ag-Au after stripping and corroding in 35% nitric acid. Note the overlapping micromorphology corresponding to corrosion at the gold/silver interface as well as the alloy surface.

Fig. 4.3.1. Tranmission electron micrograph of 50:50 Ag-Au after stripping and corroding in 35% nitric acid. Note the overlapping micromorphology corresponding to corrosion at the gold/silver interface as well as the alloy surface.

Figure 4.3.2. The effect of time of exposure of a 50:50 Ag-Au alloy surface to 35% nitric acid. (a) after stripping from substrate and exposure to acid for 30 s and (b) after re-exposure for a further period of 30 s.

(a)

0·1 μ

(b)

(a)

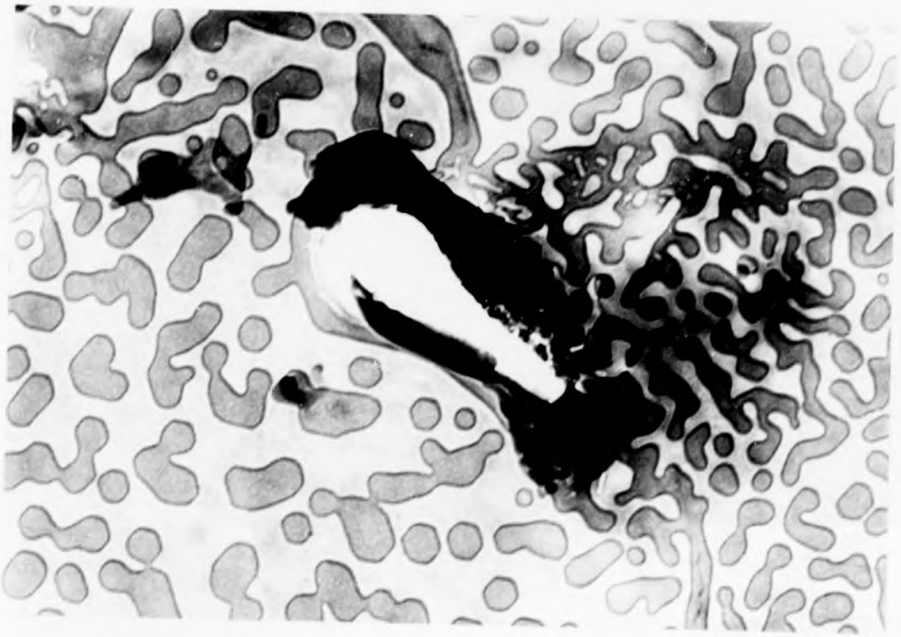

0·1 μ

(b)

further exposure to the acid. Figure 4.3.2(a) shows the structure that developed after an initial immersion of 30s and figure 4.3.2(b) shows how this was modified by re-exposure of the corroded surface for a further period of 30s. The two micrographs in figure 4.3.2. were taken from the same specimen area as is indicated by the pre-existing hole clearly visible in both micrographs. This also acts as a suitable reference point from which to compare morphologies. During the second exposure the morphology already developed by the first exposure was developed further. However very little significant change occurred after subsequent exposures. This development of the morphology by re-immersion in acid was a difficult observation to repeat. Usually the morphology that developed during initial exposure was somehow stabilised against further modification by re-exposure to acid. This might be expected for alloys exposed to strong acid when corrosion was more extensive but it has not been possible to make this observation even for alloys exposed to weak acids for only very brief periods. It will be shown later that there is evidence of a thin epitaxial overlayer, possibly gold I oxide, formed on the alloy surface during corrosion and that this may be responsible for stabilising a particular morphology as described above. For the purposes of continuity this observation of an overlayer will be dealt with in chapter six and no further reference will be made here to gold oxide. The results that were obtained showing the development of the morphology after re-immersion in nitric acid will be summarised in the final section (4.9) of this chapter.

Although difficult to reproduce, the observation of a development in morphology after re-exposure to acid provided substantial support for the idea that the corrosion morphology developed as a result of selective dissolution of silver and the redistribution and reforming of residual gold by surface diffusion, island nucleation and growth. Re-distribution would depend on the rate at which silver atoms were dissolved which, in turn, depended on the composition of the alloy and on the strength of the acid (i.e. the

chemical activity of the system). The re-forming process would also depend on temperature and the kinetics of silver dissolution. The processes of selective dissolution of silver and re-distribution of the residual gold were therefore interrelated to some extent. For the present, however, it will be evident that the morphology observed must depend on alloy composition as well as acid strength and time of exposure. It could be predicted, for example, that to observe any corrosion morphology at all for gold-rich alloys they must be exposed to concentrated acid. On the other hand, the early stages of corrosion, that is island formation, would be detectable for silver-rich alloys even if dilute acid was used. These predictions are confirmed to some extent by the observations described in the next four sub-sections which deal with alloys of different compositions.

4.4. The Micromorphology of 33:67 Ag-Au Alloys Corroded in Nitric Acid

These gold-rich alloys exhibited very little morphological change even after exposure to strong acids. This was in keeping with ideas on parting limits discussed in Chapter 1 which indicate that if the noble metal component in an alloy exceeds approximately 40% then no corrosion occurs. With 50% acid there was evidence of pit formation in the close vicinity of holes in the film, where the silver content was found by EDAX to be relatively higher ($15\% \pm 5\%$), presumably as a result of diffusion and segregation from the underlying thick layer of silver. This is illustrated in figure 4.4.1. Exposure to stronger acid (100%) also produced a morphology confined to the vicinity of holes but in this case it was slightly more extensive. Figure 4.4.2. shows the type of island micromorphology developed in this case. The morphology obtained could once again be modified by annealing and figure 4.4.3. shows the usual pitted structure obtained by annealing, again confined to hole regions. It was usually necessary to anneal these specimens to well over 450°C in order to obtain a fully developed pit morphology. Considerable rearrangement of the alloy at the edges of holes was also evident in comparison

Fig. 4.4.1. Shows a 67% Au, Ag-Au alloy corroded in 50% nitric acid corrosion is localised around hole regions.

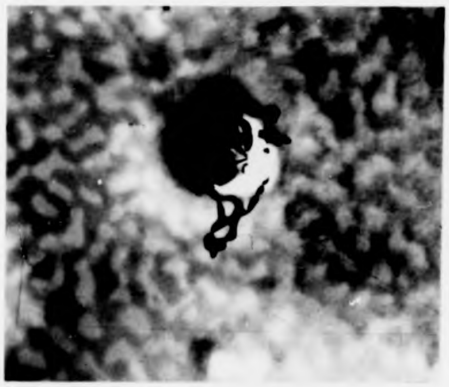

0·1 μ

Fig. 4.4.2. A gold-rich (67% Au) Ag-Au alloy corroded in strong acid (100%) showing increased attack by acid in the vicinity of holes compared with that observed when weaker acid is used.

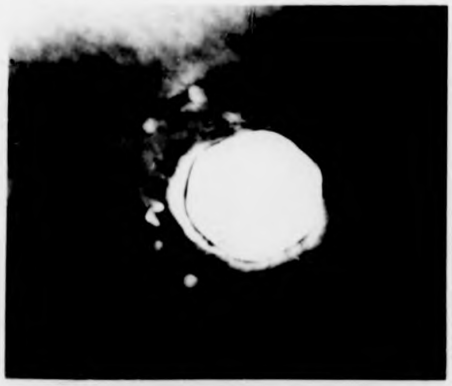

Fig. 4.4.3. This is a 67% Au, Ag-Au alloy which has been annealed to over 450°C. The corrosion morphology is correspondingly more developed.

Fig. 3.4.1. Shows a 67% Au, Ag-Au alloy corroded in 50% nitric acid. Corrosion is localised around hole regions.

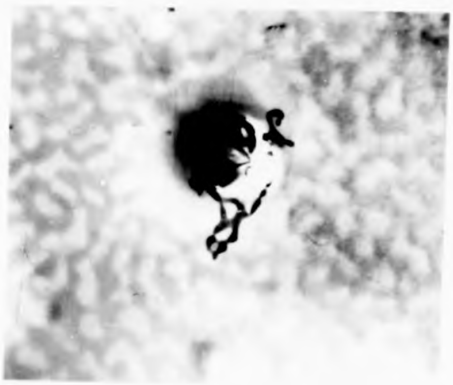

0·1 μ

Fig. 3.4.2. A gold-rich (67% Au) Ag-Au alloy corroded in strong acid (1:1) showing increased attack by acid in the vicinity of holes compared with that observed when weaker acid is used.

Fig. 3.4.3. This is a 67% Au, Ag-Au alloy which has been annealed to over 1000°C. The corrosion morphology is correspondingly more developed.

with unannealed specimens.

4.5. The Micromorphology of 67:33 Ag-Au Alloys Corroded in Nitric Acid

With these silver-rich specimens the characteristic island and channel morphology was readily developed by exposure to weak (35%) nitric acid. This is illustrated in figure 4.5.1. where exposure to acid had occurred through a hole in the film during the stripping process. A degree of development of the island morphology towards a pitted structure was also evident in this micrograph. This was similar to the structure found for 50:50 Ag-Au alloys exposed to very strong acid or annealed at high temperature. The pitted structure could be highly developed by allowing the corroded specimen to 'age' at room temperature for several days. For example, figure 4.5.2. shows a specimen after ageing for one week. Alternatively, a similar morphology could be produced by annealing at an elevated temperature. Stronger acids had a severe effect on these silver-rich alloys. Figure 4.5.3. shows a 33% Au alloy stripped in 80% nitric acid. Attack was extensive and particularly well developed in zones around the double-positioning boundaries connecting the holes in the film. These regions were silver-enriched relative to the bulk alloy by 10 ± 5 atomic percent silver over 100-200 atomic distances across the boundary. Away from the boundaries the lesser developed type of pit morphology was observed.

Attack was even more severe when a 33% alloy was exposed to 100% acid and this is shown in figure 4.5.4. In this specimen pits were very well developed and were present throughout the material in a random and complicated fashion. A porous structure was observed which might be thought to be similar to the gold spongy residues observed elsewhere (see for example Tammann and Brauns (1931)).

It is interesting that such extensive island growth and pit formation occurred for the 67:33 alloy even without a subsequent annealing treatment. This was probably a reflection of the greater chemical activity of this silver-rich alloy which gave rise to a more extensive dissolution of silver

0·1μ

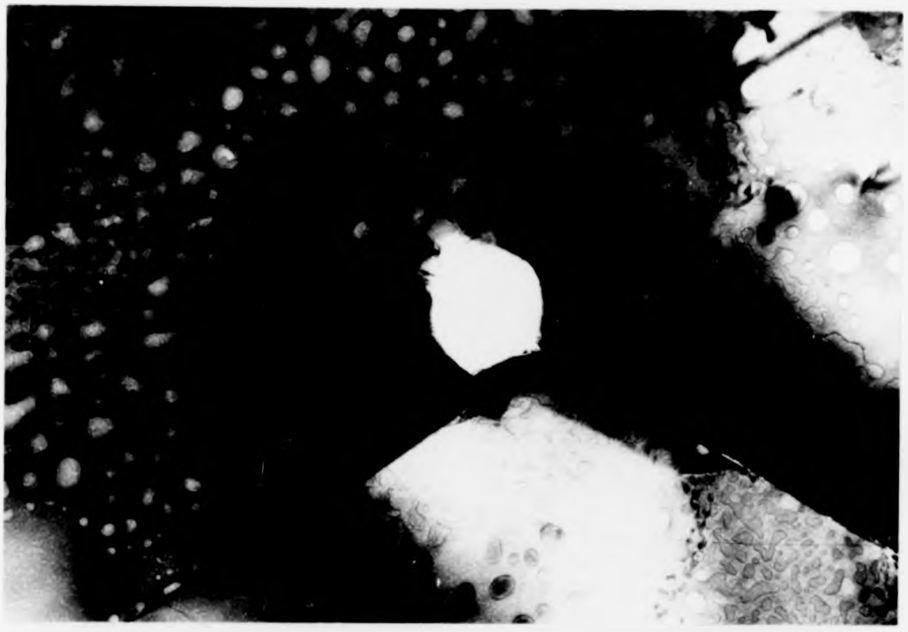

Fig. 4.5 .1. Transmission electron micrograph of 67:33 Ag-Au after corrosion in 35% nitric acid. Note the island and channel structure and the pit development.

0·1μ

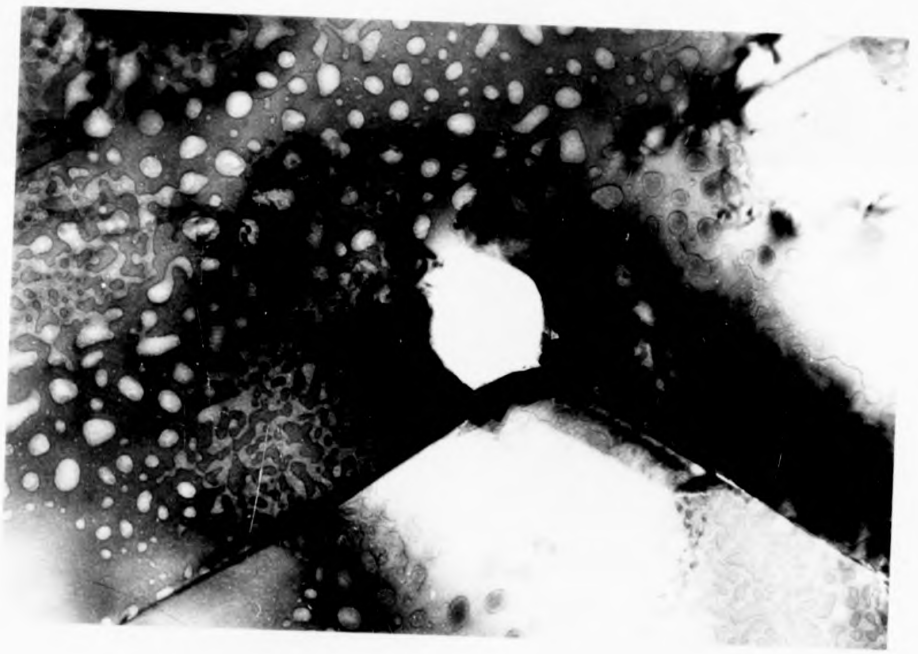

Fig. 4.5 .1. Transmission electron micrograph of 67:33 Ag-Au after corrosion in 35% nitric acid. Note the island and channel structure and the pit development.

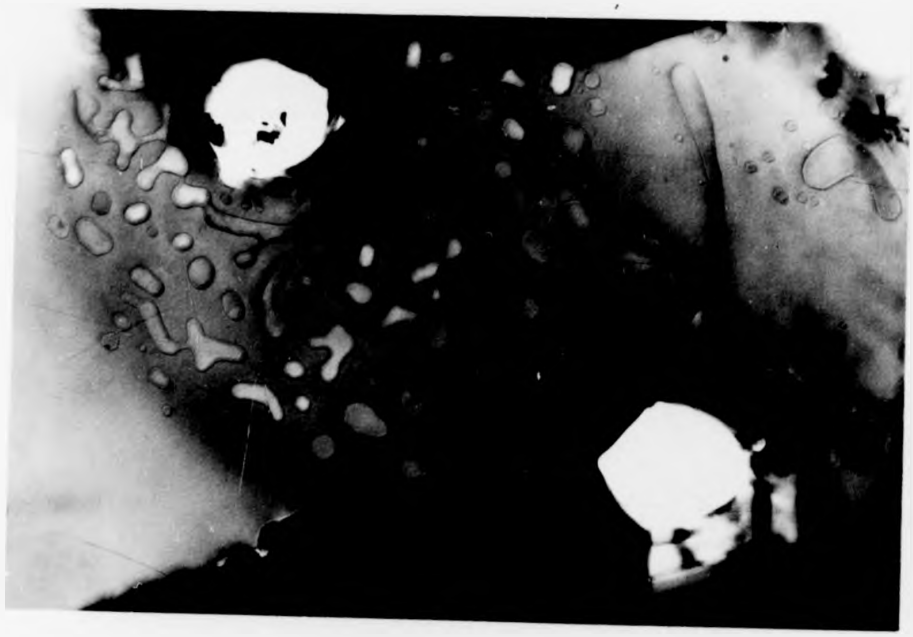

Fig. 4.5.2. Extensive pit development in a corroded surface of 67:33 Ag-Au after room temperature annealing for one week.

Fig. 4.5.2. Extensive pit development in a corroded surface of 67:33 Ag-Au after room temperature annealing for one week.

0·1μ

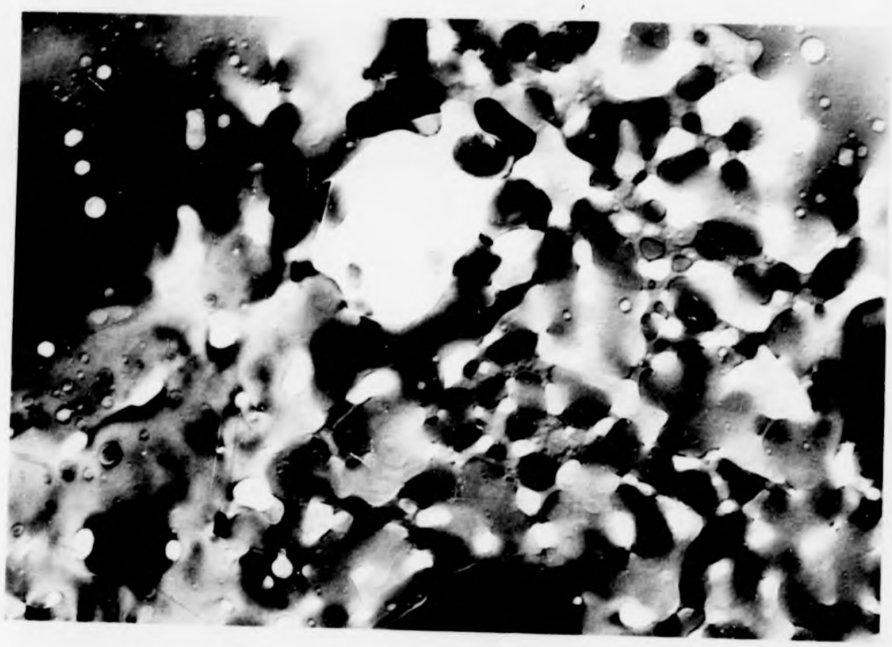

Fig. 4.5.3. shows a 33% Au alloy stripped in 80% nitric acid.

0·1μ

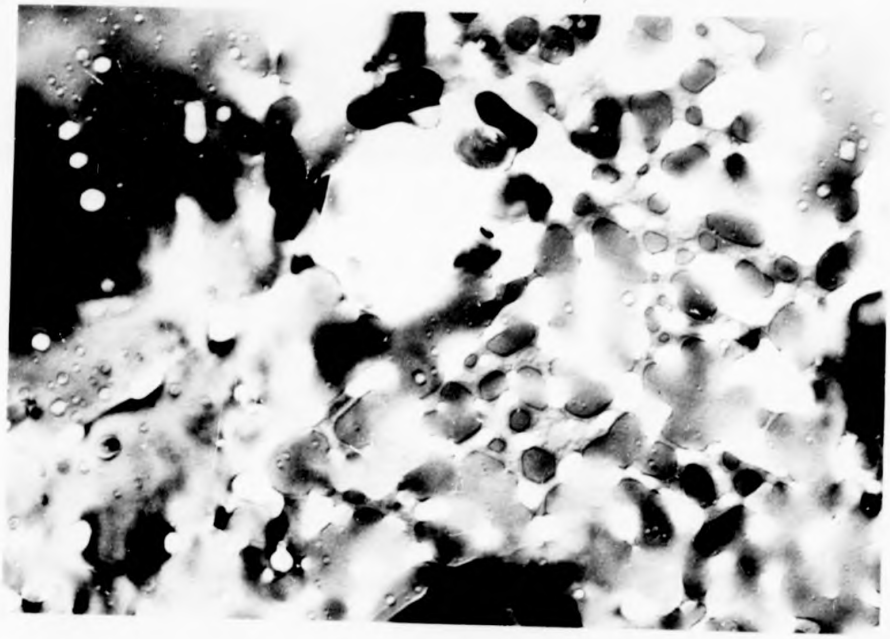

Fig. 4.5.3. shows a 33% Au alloy stripped in 80% nitric acid.

Fig. 4.5.4. Showing very severe attack occuring in 100% acid for a 67:33 Ag-Au alloy.

Fig. 4.5.4. Showing very severe attack occuring in 100% acid for a 67:33 Ag-Au alloy.

which subsequently led to more rapid redistribution and reordering of gold.

Diffraction patterns taken from these specimens frequently showed extra unexpected reflections as outlined in section 4.1. Simple tests to find out the effect of annealing and the strength of the corroding acid on the intensity of these reflections were performed. The results indicated that increasing the strength of the corroding acid tended to reduce their intensity; annealing the specimens after corrosion also reduced their intensity and during high temperature annealing (450°C and above) they rapidly disappeared completely. These observations will be discussed further in Chapter six; for the present it is sufficient to observe that the extra diffraction spots appeared to be associated with the island and channel morphology, gradually fading as pit structures developed.

4.6. The Micromorphology of 75:25 Ag-Au Alloys Corroded in Nitric Acid

Well-defined island, channel and pit morphologies were again observed on these alloys. Observations made after exposure to acids of various strengths and for various times showed that more "developed" morphologies occurred even more readily for these alloys, presumably because of the increased silver content. Figure 4.6.1. shows small islands formed on 75:25 Ag-Au alloy after a short exposure of a few seconds in 35% nitric acid. There is also evidence on this micrograph of an underlying superimposed morphology similar to that observed on 50:50 alloys corroded in 35% acid (section 4.3.).

After prolonged exposure to 35% nitric acid more extensive island growth and coalescence were observed and this is illustrated in figure 4.6.2. which shows an alloy after an exposure of a minute. It is interesting to note in figure 4.6.1. that the greater density of island nuclei and the more extensive growth and coalescence of these (fig. 4.6.2.) occurred in the vicinity of double-positioning boundaries. This further supports the suggestion (section 4.1) that the silver-enriched regions around the double

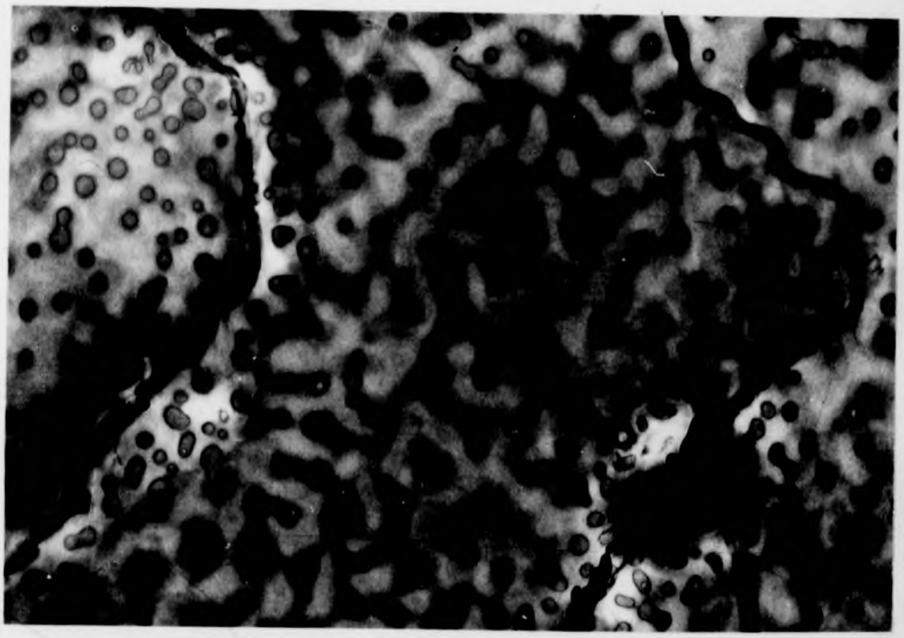

Fi g. 4.6.1. Small islands formed on 75:25 Ag-Au alloy after a short exposure to 35% nitric acid.

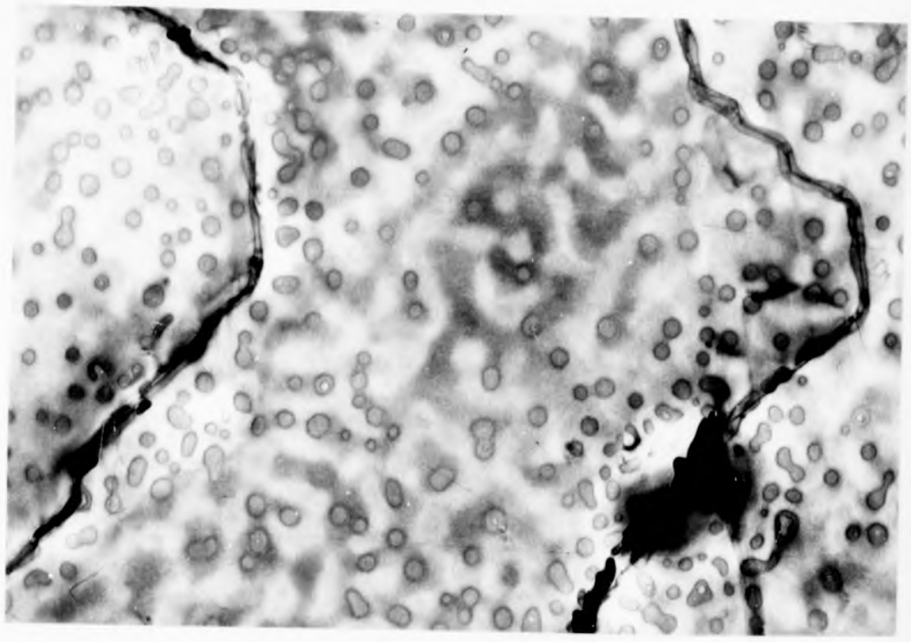

Fig. 4.6.1. Small islands formed on 75:25 Ag-Au alloy after a short exposure to 35% nitric acid.

Fig. 4.6.2. The micromorphology of 75:25 Ag-Au alloy after prolonged exposure to 35% nitric acid. Note the occurrence of more extensive island growth and coalescence compared with fig. 4.6.1.

0·1 μ

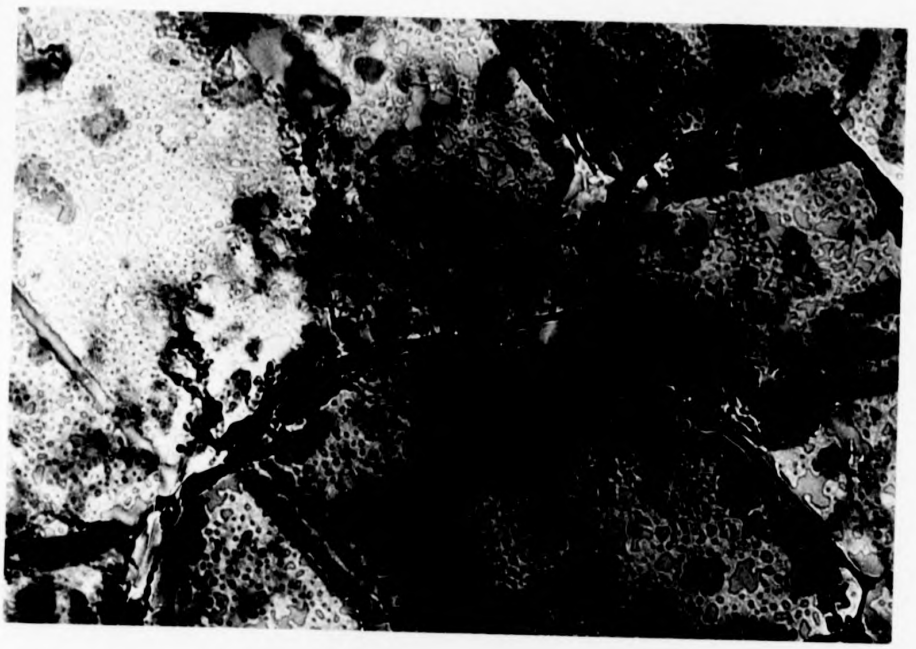

Fig. 4.6.2. The micromorphology of 75:25 Ag-Au alloy after prolonged exposure to 35% nitric acid. Note the occurrence of more extensive island growth and coalescence compared with fig. 4.6.1.

positioning boundaries were more extensively corroded and consequently the residual gold was more readily reordered to give well developed morphologies. These films often contained linear diffraction fringes which followed 111 traces in the alloy and which were greatly influenced by the presence of islands. Forty (1982) has suggested that they indicate the arrest of slip bands in the alloy at the interface between the metal and a surface film, presumably a thin layer of the gold I oxide mentioned earlier.

4.7. The Micromorphology of 90:10 Ag-Au Alloys Corroded in Nitric Acid

For these very silver-rich alloys no evidence of an island or pitted morphology could be found, even with very dilute acid (10% nitric acid). However, the marked variation of electron absorption contrast, as can be seen in figure 4.7.1., indicated an extensive variation in the thickness of the film, suggesting that severe corrosion had occurred. Networks of dislocations lying in the (111) plane of the film, such as those shown in figure 4.7.2., were frequently found with this alloy after exposure to 35% nitric acid. They were thought to arise as a result of surface re-ordering, possibly by a process similar to that described in section 4.1., but an alternative explanation could be that they were a consequence of vacancy injection during silver dissolution. Some of the dislocation lines were in an irregular zig-zag configuration which might indicate that a vacancy-assisted climb process was involved in the formation of the networks. The absence of islands on these surfaces may simply reflect the small concentration of gold in these alloys or may indicate a difference in the electrochemistry of these systems.

4.8. Summary of the Observations on the Corrosion Morphology of Silver-Gold Alloys Corroded in Nitric Acid

Three distinct alloy morphologies have been observed which depend in detail on alloy composition and strength of corroding acid. These have been

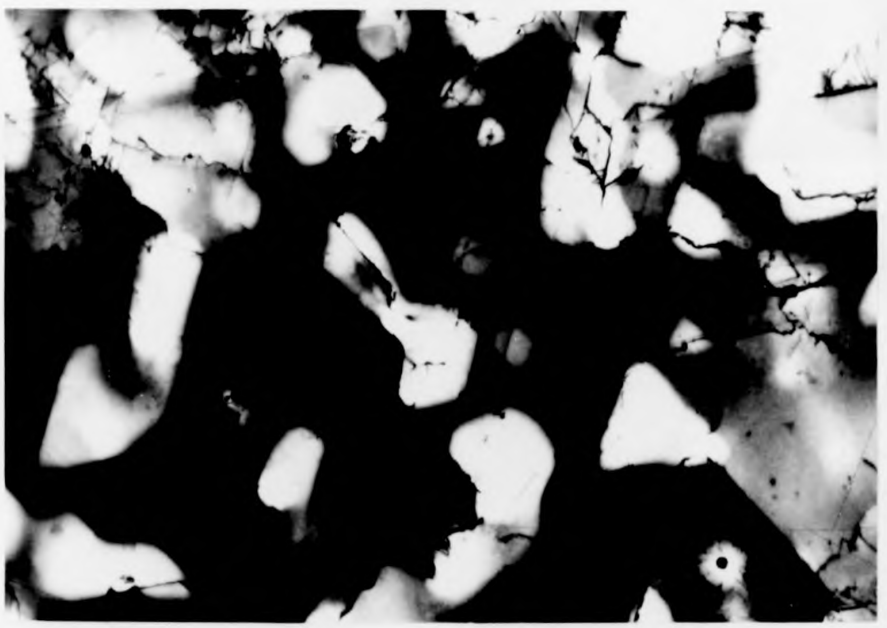

Fig. 4.7.1. Showing the marked variation in electron absorption contrast commonly found when alloys with low gold contents are corroded. This is a 90:10 Ag-Au alloy corroded in 35% acid.

Fig. 4.7.1. Showing the marked variation in electron absorption contrast commonly found when alloys with low gold contents are corroded. This is a 90:10 Ag-Au alloy corroded in 35% acid.

Fig. 4.7.2. Transmission electron micrograph showing dislocation networks and 'helical' dislocation in 90:10 Ag-Au after corrosion in 35% nitric acid.

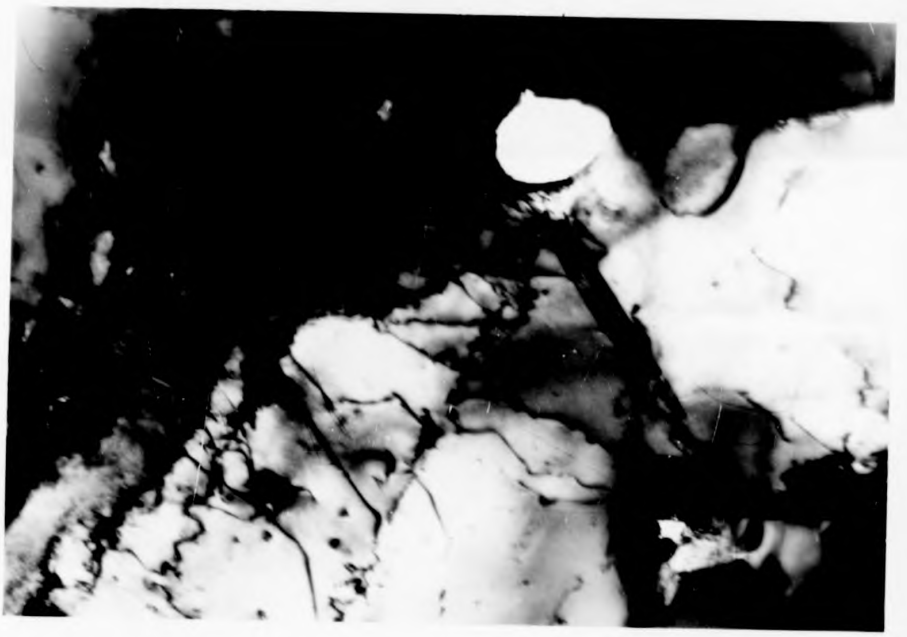

Fig. 4.7.2. Transmission electron micrograph showing dislocation networks and 'helical' dislocation in 90:10 Ag-Au after corrosion in 35% nitric acid.

described in the preceding sections. A general view of the type of morphology that developed was well illustrated by figure 4.5.1. which showed the effect of localised corrosion on the surface of a 67:33 Ag-Au alloy following penetration of nitric acid (35%) through a hole in the film during the stripping process. This demonstrated particularly well how the corrosion morphology, and in particular the island structure, was related to the original alloy surface over which the acid had flowed. The material in the vicinity of a hole was, of course, silver-rich as a result of diffusion from the silver substrate and this, in part, explained the localised attack by the dilute acid in this region. Clearly some metal (silver) had been removed by the corrosion and the material remaining (gold and possibly a little silver) was in the form of islands. The previous sections seemed to indicate that the islands spread as corrosion proceeded whilst the channels between them shrank but deepened. The pit morphology which finally developed as a result of the partial coalescence of the islands was clearly evident near the edge of the corroded region, in this case.

The tendency towards a pit morphology increased as the silver content of the alloy increased and as the strength of the acid increased. For example, the island morphology was readily replaced by a pit structure in the 67:33 Ag-Au alloy, even when dilute acid was used (see Fig. 4.5.2). Alternatively, a decrease in silver content, as in the case of 50:50 Ag-Au, led to a more stable island morphology (Fig. 4.3.2 (a)) which could only be modified towards the pit structure by a prolonged exposure to acid (Fig. 4.3.2.(b)), or by using very strong acid (see Fig. 4.2.3. (a)), or by heating the corroded alloy to a few hundred degrees centrigrade (see Figure 4.1.3.).

In very silver-rich alloys (90:10 and 95:5 Ag-Au) neither islands nor pits were observed, even when very dilute acid was used. The only micro-structural evidence of the corrosive attack was the marked variation in thickness of the alloy and the formation of dislocation networks, which were typical of the final stages found in the morphological development when the less silver-rich alloys were corroded.

The gold-rich alloys (33:67 Ag-Au were more resistant to corrosion and the only observable morphology was confined to the vicinity of holes in the film where the silver content was known to be greater. The pitted structure in these regions was the result of extensive disorder produced in the silver-enriched alloy by the concentrated acid used in this case.

A progressive development of the micromorphology observed on these alloys from island to pit structures seemed to be indicated. The formation of these structures was critically dependent on the combination of alloy composition, acid strength and temperature as outlined in this chapter. The similarities between observed morphologies and those found for vapour-deposited and electrochemically-deposited gold indicated that similar nucleation and growth processes were occurring during corrosion, and in the light of this a model is proposed which goes some way to account for the observations outlined here. This will be dealt with in chapter 7 of this thesis.

4.9. Measurements to show the Development of Corrosion Micromorphology with Increased Acid Exposure

In the last section the observations of corrosion micromorphology on silver-gold alloys were summarised. Structures observed were very similar to those observed for epitaxial gold deposits on cleavage surfaces (Pashley 1964). This leads to the idea that corrosion proceeds via a surface disordering reaction in which silver is removed. This is followed by a re-forming of the residual material by surface diffusion in much the same way as the nuclei of the deposited metal grow during thin film growth by vapour deposition. This model can account in part for the general development of morphology which is summarised in the previous section.

In order to support the idea that there is a development of the corrosion morphology with increasing acid attack, measurements of island size versus length of exposure in acid are given here. Information of this kind is extremely difficult to obtain. It requires the same area of foil to be located in the electron microscope after it has been removed, corroded

rewashed and put back into the microscope.

Where this procedure was successful the results confirmed the ideas of development described above and provided a degree of support for the proposed models for the corrosion of these samples (Chapter 7).

Three samples of a specimen of 50 atomic % gold, silver-gold alloy were viewed directly after they were stripped in 35% nitric acid. Great care was taken to avoid acid contact with the upper alloy surface. They were then subsequently completely immersed in the same acid for 15 s and a further 15 s and the same region was viewed after each immersion. A ruler was placed across enlarged micrographs of these specimens and the diameters of any islands which touched a 10 cm line were measured. An average island size was obtained in each case by several lines on each micrograph. These results are given in table 4.9.1.

Table 4.9.1. Mean Island Diameter (measured on enlarged micrograph (mm)) for different times of exposure to 35% nitric acid.

	Specimen 1	Specimen 2	Specimen 3	Using all 3 results
After Stripping	no islands	no islands	no islands	no islands
Immersion for 15 s $\bar{x}$	1.34	1.40	1.72	1.38
n	44	66	44	154
σ_n	0.56	1.78	0.65	0.68
Immersion for 30 s $\bar{x}$	2.35	2.11	2.39	2.14
n	76	91	92	259
σ_n	1.6	1.13	1.81	1.17

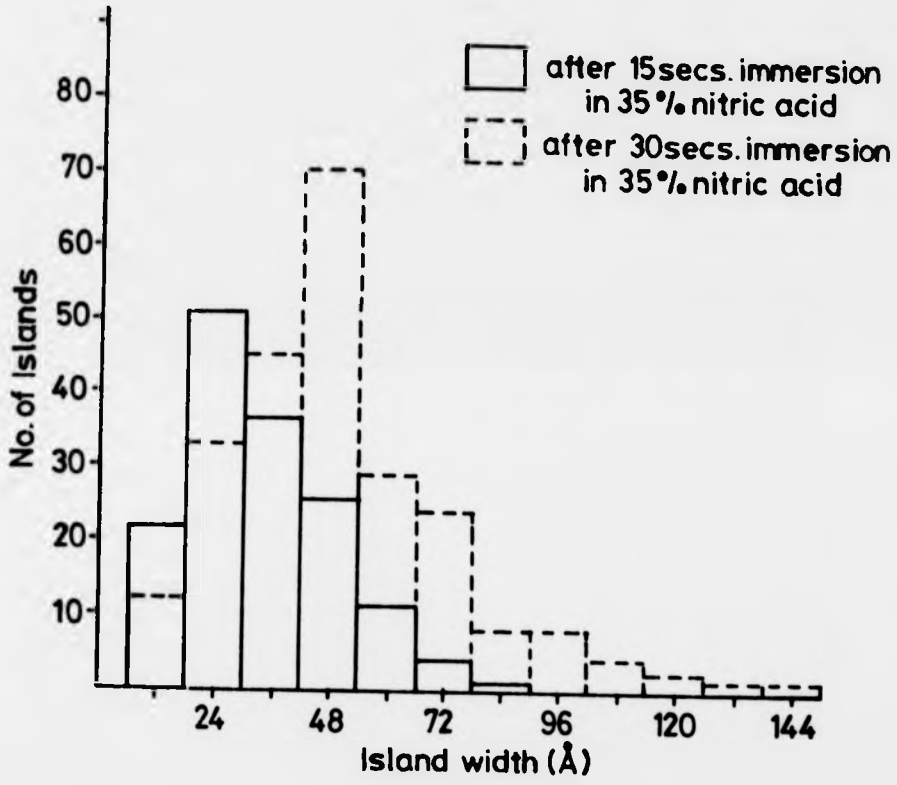

Fig. 4.9.1. A histogram showing how the number of islands with a particular diameter varies with time of exposure to 35% nitric acid.

Measurements were taken on regions away from holes and boundaries. They clearly demonstrate that there has been a growth in average island diameter ($\bar{x}$) and also in the number of islands (n) with increasing acid attack. A histogram showing the number of islands and island size is given in Fig. 4.9.1. which illustrates more clearly the changes which have occurred because of further acid attack. No islands were observed on specimens which had simply been stripped in acid (in regions away from holes and boundaries). After 15 s immersion islands were observed with an average diameter of 33 Å (obtained by combining measurements from all three specimens). After a further 15 s immersion the number of islands had increased by 60% and the average island diameter was now 51 Å.

These measurements have been used to test the Forty Rowlands model (Forty and Rowlands 1981). This is an analytical model based on the observations given in this chapter. The discussion of this and other models for the corrosion of these alloy systems is left until chapter 7. Further discussion of the measurements described above is also included in Chapter 7.

References: CHAPTER FOUR-

Cherns, D., (1974), Phil. Mag. 30, 549.

Dickson, E. W., Jacobs, M. H., and Pashley, D. W., (1965), Phil. Mag., 11, 575.

Durkin, P. and Forty, A. J. (1979), Inst. Phys. Conf. Ser. No. 52, Proceedings of E.M.A.G. Conference.

Evans, U. R., (1969), The Corrosion and Oxidation of Metals, Scientific Principles and Practical Applications, p.325, Edward Arnold Ltd., (London).

Forty, A. J., (1961), Phil. Mag. 6, 587.

Forty, A. J., and Durkin, P., (1981), Phil. Mag. A, 42, 295-318.

Forty, A. J. and Rowlands, G., (1981), Phil. Mag. A, 33, 171.

Forty, A. J., (1982), Microdeformation images of T.E.M. images of silver-gold alloys corroded in nitric acid, submitted for publication in Phil. Mag.

Hirsch, P. B., Howie, A., Nicholson, P. B., Pashley, D. W., and Whelan, M. J., (1965), Electron Microscopy of Thin Films, Butterworths, London.

Pashley, D. W., (1959)a, Phil. Mag. 4, 316 (1959)b, Phil. Mag. 4, 324.

Pashley, D. W., and Stowell, M. J. (1962), Proceedings of the Fifth International Congress for Electron Microscopy, edited by S. S. Breese, (London, New York, Academic Press), P.G.G.1; (1963), Phil. Mag. 8, 1605.

Pashley, D. W., Stowell, M. J., Jacobs, M. H., and Law, T. J., (1964), Phil. Mag. 10, 127.

Shoab, K., and Segall, R. L., (1969), Proc. Roy. Soc. A, 314, 129.

Swann, P. R., (1971), Proceedings of the Conference on the Theory of Stress Corrosion Cracking in Alloys, edited by J. C. Scully (Brussels: NATO), p.113.

Tammann, G., and Brauns, E., (1931), Z. Anorg. Allg. Chem., 200, 209.

CHAPTER FIVE

The Corrosion of Copper-Gold Alloys

5.1. Introduction

Like silver-gold alloys, copper-gold alloys satisfy many of the criteria for being suitable materials to study the phenomenon of selective dissolution. Copper dissolves vigorously in nitric acid, pure gold not at all, and the major corrosion product, copper nitrate, is extremely soluble and so should not reduce the corrosion reaction by forming a passivating surface film. There is, however, one very important respect in which copper-gold and silver-gold alloys are different and that is in their microstructure. As previously mentioned silver and gold form substitutional solid solutions as a single-phase, face-centred cubic material across the entire compositional range with hardly any attendant change in lattice parameter (0.02%). There is a more pronounced difference in the lattice parameters of pure copper and pure gold (which are 3.66 and 4.08 $\mathring{A}$ respectively) leading to a significant variation in lattice parameter with alloy composition and the possibility of complex phase changes. Consequently, when alloys dissolve lattice parameter changes will give rise to strain within the alloy and microstructural changes may well result from this. The micromorphology that develops on alloys after corrosion is therefore more difficult to interpret since it may arise directly because of the corrosion treatment or indirectly due to changes in alloy composition. It is therefore important to have a thorough understanding of the phase diagram of CuAu if unambiguous conclusions about corrosion micromorphology are to be made. Copper-gold alloys have a well characterised phase diagram (Hansen 1958). This is shown in Fig. 5.1.1. Copper and gold form a binary alloy system with a continuous solid solution at all compositions. At certain stoichiometric compositions these alloys form ordered structures; Cu_3Au, CuAu are the most notable examples but $CuAu_3$ has also been observed. Evidence for ordering has been provided by measurable reductions in lattice parameter at these stoichio-

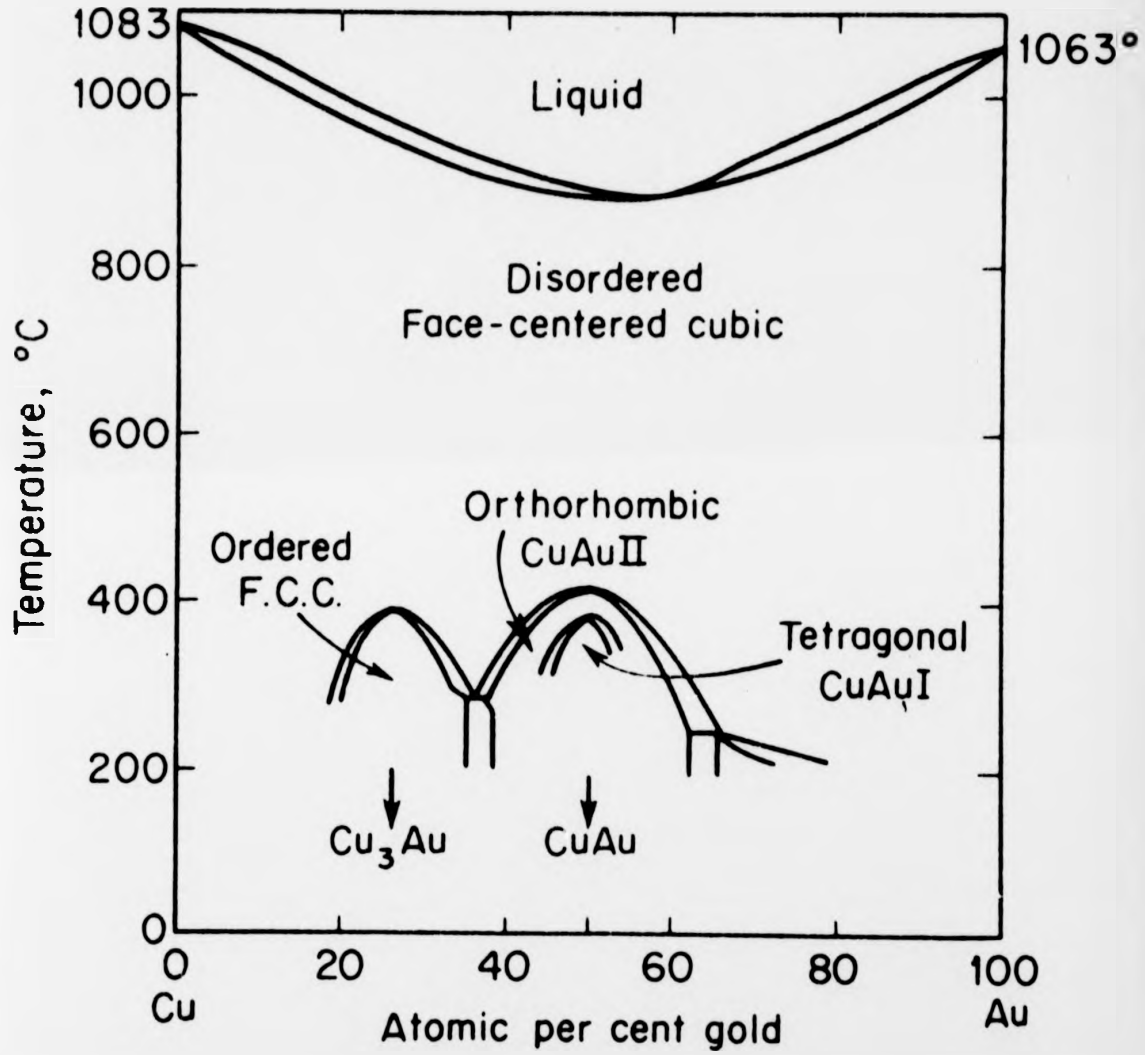

Fig. 5.1.1. Phase diagram for Au-Cu system (Hansen 1958).

metric compositions compared with those expected simply from compositional variations. Reductions of up to 0.2% have been observed for lattice parameters of ordered compared with the corresponding disordered structures (Flinn et al 1960). These changes are small compared with the uncertainties in measuring lattice parameter due to the electron microscope itself. Observations have been made on the kinetics and mechanisms of the order-disorder changes of state associated with ordered structures. According to Hansen (1958) the lattice constant of the f.c.c. Cu-Au phase shows a weak positive deviation from additivity so that the lattice constant progressively increases as gold is added to copper, Cu_3Au has a modified cubic structure. A plot of lattice parameter versus alloy composition was constructed from data given by Johnson and Linde (1975). The alloy CuAu, which has been extensively studied, for example, Glossop and Pashley (1959) and Pashley (1963), becomes ordered below a critical temperature (approximately 420°C) to give a modified f.c.c. structure CuAul in which the (002) planes contain alternately all copper and all gold atoms. The unit cell is then tetragonal with $^{c}/_{a} \sim 0.92$. If the alloy is annealed just below the critical temperature a further transformation is observed and an orthorhombic structure CuAu 11 forms. The unit cell of this structure is shown in figure 5.1.2. (after Pashley and Glossop (1959)). This contains 10 cells of the basic f.c.c. type aligned along a_1. Halfway along this a_1 axis the order of the gold and copper planes changes. Thus the structure is subdivided into domains with adjacent domains being in "antiphase". The antiphase domain boundaries are perpendicular to [100] and have a periodic arrangement, the period being $\frac{1}{2}$ a_1 or five unit cells of the original f.c.c. structure. It is possible to resolve these domains in the electron microscope using dark field techniques. The periodicity arising from antiphase domains gives rise to extra reflections in their electron diffraction patterns which Pashley and Glossop (1959) interpret in terms of double diffraction effects across the domain boundaries.

It is important to be aware of these ordered structures and how they are manifested both in electron diffraction patterns and in electron microscope

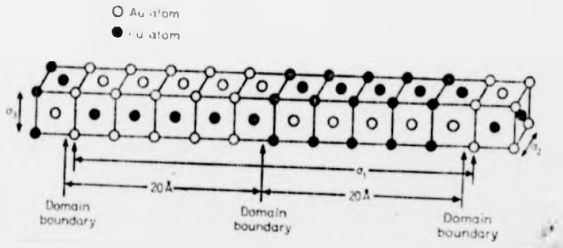

Fig. 5.1.2. The unit cell of the ordered CuAu II structure (after Glossop and Pashley, 1959).

images. Alloys prepared for the work to be described in this chapter sometimes showed evidence of ordering in their diffraction patterns particularly when they were at or about the stoichiometric compositions mentioned above. Later in this chapter evidence will be given to support the idea that corrosion of these alloys promotes ordering in certain circumstances even when the fairly complicated procedures normally required for their preparation (Glossop and Pashley 1959) were not followed.

5.2. The Formation of Moiré Patterns by Copper-Gold Alloys

A very important effect arising from the difference in lattice parameters of copper and gold is the appearance of moiré fringes in their electron microscope images. A brief description of the origin of moiré patterns will be given here since it will be referred to when the observations on copper-gold alloys are being discussed later in this chapter and also in the following chapter. Moiré patterns observed in the microscope can be formed in two distinct ways, first when two crystal lattices with dissimilar lattice parameters but in parallel orientation overlap, and secondly when two identical lattices are rotated relative to each other so that they are not in parallel orientation. Moiré patterns are also obtained by a combination of both the above processes i.e. when two lattices which are both dissimilar in lattice parameter and rotated relative to each other overlap. A simple view is to consider that fringes arise from the beating together of the two periodicities of the respective lattices and that the moiré pattern represents the periodicity with which the crystal lattices go in and out of register. In effect the moiré pattern is that produced by the two overlapping direct images assuming that they could be formed.

It has been shown (Bassett, Menter and Pashley 1958) that the condition for the formation of moiré patterns is that a beam which has been diffracted once by each set of lattice planes is allowed to contribute to the image. Figure 5.2.1.(a) shows that if P is the diffracted beam from the set of planes

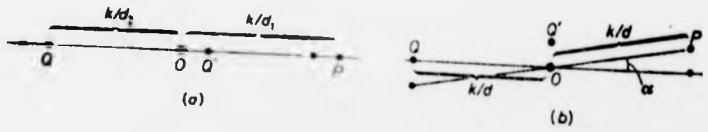

Fig. 5.2.1. The geometry of the double diffraction responsible for bright field moire patters: (a) parallel moire patterns; (b) rotation moire patterns. (After Hirsch et al 1965).

(interplanar spacing d_1) in the upper crystal, it is diffracted in the lower crystal by the parallel set of planes (interplanar spacing d_2) to give the beam Q^1, which is equivalent to the primary beam Q when the origin is displaced from 0 to P. If $0P = {}^{k}/_{d_1}$ and $0Q = {}^{k}/_{d_2}$ it immediately follows that $0Q^1 = k(d_1-d_2)/d_1d_2$. Thus Q^1 is equivalent to a Bragg reflection from a set of planes of interplanar spacing $d_1d_2/|d_1-d_2|$, i.e. the spacing of the moiré pattern. The same procedure can be applied to rotational moiré patterns and in this case $0Q^1$ is given by $(2\sin \frac{1}{2}\alpha)/d$, α being the angle of rotation. This is again equivalent to a Bragg reflection from a set of planes with a spacing equal to that of the moiré pattern.

Micrographs of copper-gold alloys before and after controlled corrosion, and for annealed as well as unannealed specimens, frequently showed moiré fringes and a careful and thorough analysis of them was required to understand what was happening to an alloy as it was treated in various ways. They are in effect an immediate means of obtaining structural information from these alloys. There is a drawback arising from the presence of these fringes in microscope images and that is that they tend to obscure the small scale microstructural features such as islands and other corrosion morphology which would otherwise be visible in these images. It is also important to distinguish moiré effects due to corrosion from those which exist before corrosion. An ideal situation would be to have a starting material which is a completely homogeneous single crystal alloy. This of course would not produce moiré fringes. However, once it had been treated in acid, say, the resulting compositional change should give rise to fringes providing information about the extent of corrosion and the distribution of any corrosion. A considerable amount of work was performed to try to obtain specimens in this form and this is described in the next section.

5.3. Preparation of Copper-Gold Specimens

Initially copper-gold alloys were prepared in the same way as the silver-gold alloys had been, that is to say by co-depositing copper and gold onto a gold:silver:mica substrate prepared in the usual manner (see Chapter 2) and held at a temperature of 285°C. The alloy composition was determined as before by choosing and monitoring the individual deposition rates for each metal. The specimen was then comprised of an alloy layer on top of a gold layer supported by a silver/mica base. Pieces of the composite specimen could be floated in nitric acid so that the gold and alloy layers were stripped from the mica, washed and mounted on electron microscope grids for viewing in the microscope (see Chapter 2). Figure 5.3.1. is fairly typical of copper-gold specimens prepared in the manner outlined above: it was a 200 Å thick layer of alloy (25% Au) on a 300 Å thick gold base. This micrograph shows a fairly extensive distribution of moiré fringes due to the two over-lapping phases (alloy and pure gold) as well as a quite well developed corrosion morphology indicating marked acid attack. A common feature of fringes observed on these specimens is that they were frequently discontinuous and irregularly shaped possibly due to dislocations and other imperfections in the sample (Bassett, Menter and Pashley 1958). These imperfections may be a result of specimen fabrication processes or due to the corrosive attack which occurred during stripping. They were not, however, associated exclusively with areas which had a well developed corrosion morphology.

Unstripped specimens of copper-gold alloys were examined using scanning electron microscopy. Figure 5.3.2. shows a scanning electron micrograph of such a specimen. The dark, rounded features had the same size and distribution as the holes shown in the corresponding T.E.M. images. This is similar to the observations made on silver-gold specimens (Chapter 2) and therefore the same conclusion can be drawn that these dark features correspond to the holes seen in transmission images and that they exist at all stages during specimen

Fig. 5.3.1. A transmission micrograph showing a 25% Au, Au-Cu alloy showing an extensive distribution of fringes due to overlapping phases of alloy and gold.

Fig. 5.3.1. A transmission micrograph showing a 25% Au, Au-Cu alloy showing an extensive distribution of fringes due to overlapping phases of alloy and gold.

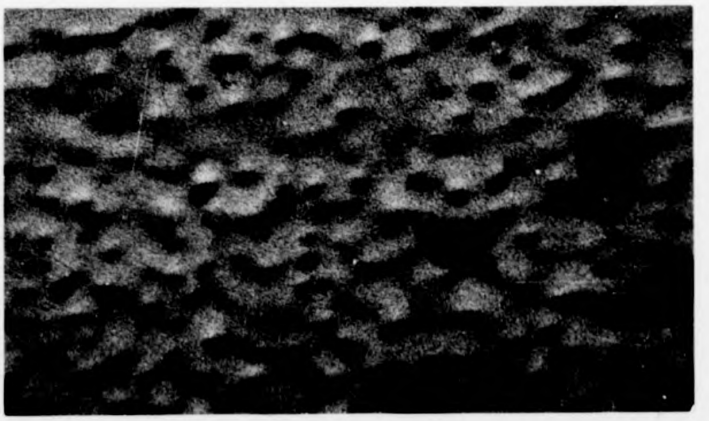

Fig. 5.3.2. Scanning electron micrograph of an unstripped film showing holes. This micrograph is directly comparable with the one showing the unstripped silver-gold alloy film. Fig. 2.5.1.

0.1μ

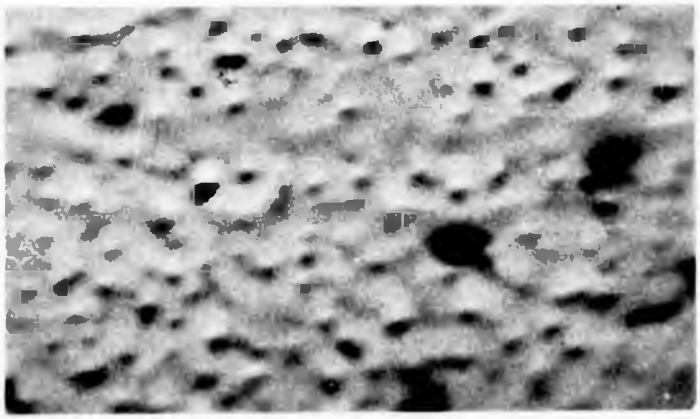

Fig. 5.3.2. Scanning electron micrograph of an unstripped film showing holes. This micrograph is directly comparable with the one showing the unstripped silver-gold alloy film, Fig. 5.5.1.

preparation. E.D.A.X. analysis did not indicate any unusual variation in copper concentration near hole regions or any other of the features resolved in the scanning pictures.

If a specimen prepared in the manner outlined above was stripped from its mica/silver substrate and mounted on a microscope grid, it could be annealed in a vacuum to allow the remaining gold and copper-gold phases to inter-diffuse. In this way a completely homogeneous specimen should be obtained. The microstructure and morphology would be simplified and any subsequent change due to a corrosive treatment would be readily recognised. This was a fairly successful method of producing homogeneous single crystals of copper-gold but the alloys produced contained typically 50 or more per cent gold. This was because a fairly thick ($\sim$ 300 Å) supporting layer of gold was required to protect the upper alloy layer from acid attack during stripping and also because the thickness of the uppermost layer was restricted to a few hundred angstroms so that the samples remained electron-transparent. Even if the alloy layer were practically all copper the resulting film after annealing would be approximately equiatomic. Furthermore it was necessary to retain some gold in the alloy layer to protect it against possible acid attack during stripping. Although it was a fairly simple matter to prepare alloys in this way, they were not particularly interesting from a corrosion point of view because of this high gold content.

Pashley and Glossop (1959), when studying ordering in copper-gold alloys, prepared them by depositing copper onto a stripped thin pure gold film which was prepared in the usual way (i.e. on silver/mica). It was then mounted on an electron microscope grid and held at a temperature of approximately 300°C. The copper was laid down in parallel orientation to the gold and after a one hour anneal the two layers completely interdiffused. They prepared these specimens *in situ* in an electron diffraction camera and were therefore able to monitor *in situ* the progressive interdiffusion of the two layers. Preparing samples in this way should enable more copper-rich alloys to be made since

the problem of dissolution of copper during stripping which occurred in the previous method of preparation should be avoided. This method of preparation has been used here but was only partially successful in producing the desired films. Frequently specimens were not completely inter-diffused in spite of annealing treatments of several hours (typically 5-10 hrs) at fairly high temperatures ($\sim$ 400°C). Very long annealing treatments yielded chemically homogeneous specimens but these were frequently polycrystalline. Pashley, in a private communication, has indicated that it is difficult to prepare samples more copper-rich than the equiatomic composition using this method, particularly when the initial gold films are in a (111) orientation. The gold films were extensively cold-worked during mounting onto microscope grids which themselves provided inadequate support for the films. This would be an important factor because stresses in the film could have a significant influence on re-crystallisation. The comparatively large amount of copper that was added might also lead to some re-arrangement or re-crystallisation of the films during annealing. Any ordering which may have occurred during the heat treatment must also be considered. It may be that these changes could also help to encourage re-crystallisation.

Another way of preparing alloy films was to evaporate copper and gold, simultaneously and with the required rates onto a single crystal of silver on mica, this having been prepared in the usual way. During stripping the acid would attack the copper-gold alloys as well as the silver and it was assumed that the dissolution of silver would not significantly affect the subsequent corrosion behaviour of the alloy. The extent of corrosion must be determined by the strength of acid used for stripping and the length of time that the specimen was in contact with the acid. The major drawback of this method of preparation is that the alloy cannot be examined using T.E.M. prior to corrosion and thus any features observed in these foils cannot be ascribed to the corrosive attack with the same degree of certainty as for films previously discussed. It remains a matter of judgement as to whether

a feature in the specimen arose because of corrosive attack or because of the way in which it was prepared.

To summarise, the aim in preparing alloys was to produce a completely homogeneous, single-crystal, thin film so that its initial microstructure was as simple as possible and any subsequent changes due to corrosion could be more easily determined. Several methods of achieving this have been described and each has its own advantages and limitations. Observations on alloys prepared by using the above methods will be described in the next section.

5.4. Observations on Copper-Gold Alloys Corroded in Nitric Acid

The introductory chapter of this thesis described some previous studies on the corrosion of copper-gold alloys. The work of Swann (1971) was particularly interesting. He used an electron microscope to study the corrosion behaviour of copper-gold alloys in corrosive environments known to cause stress corrosion cracking and his results showed the importance of corrosion tunnelling. One of the aims of the present work of copper-gold was to study the micromorphological changes brought about by corrosion and selective dissolution and attempt to correlate these with the occurrence of corrosion tunnelling.

Copper-gold alloys do indeed frequently exhibit a type of island/channel morphology, similar to that observed on silver-gold alloys. An example of this is shown in Fig. 5.4.1. This was a copper-gold alloy (25% Au) deposited onto a gold/silver/mica substrate as described in section 5.3. which had undergone corrosion as it was stripped from its mica/silver substrate in nitric acid. As in silver-gold alloys corroded during stripping in this way, the micromorphology was mainly confined to holes and boundaries. The T.E.M. image shows that the scale of the microstructure was finer i.e. the features have smaller dimensions (typical island diameter $\sim$ 150 Å) than for the corresponding silver-gold alloy (typical island diameter 2-300 Å). The free

Fig. 5 .4.1. Transmission electron micrograph of a copper gold alloy (25% Au) stripped in nitric acid.

Fig. 4.1. Transmission electron micrograph of a copper gold alloy (25% Au) stripped in nitric acid.

energy of formation ΔG_{fo} of silver nitrate is -34 kJ mole^{-1} and that for copper nitrate -120 kJ mole^{-1} suggesting higher reactivity for copper in nitric acid which may lead to the finer scale of corrosion morphology observed on copper-gold alloys compared to that on the corresponding silver-gold alloys. There were moiré fringes covering areas of the micrograph and these presumably arose from the two overlapping phases, Au and CuAu. The fringes were very irregular in shape and suggested a high concentration of imperfections in the metal structure. It is possible that these imperfections were simply coincidence lattice misfit dislocations formed at the interface of the two phases (see for example Macur and Vook 1980), or they may be due in part to the corrosion treatment. It is useful to remember that dislocations were frequently observed on corroded silver-gold alloys, particularly on silver-rich specimens. In addition dislocation networks were often found on corroded silver-gold alloys after they had been heat treated (Chapter 4). Figure 5.4.2. shows an enlargement of an area containing two distinct types of fringes, taken from the same specimen as in Figure 5.4.1. The first type of fringes are narrow and evenly spaced and the second type have a wider spacing and are broken and uneven.

In order to analyse the moiré fringe patterns measurements of the d spacings of the corresponding crystal structure are required. These can be obtained as follows:-

The diffraction pattern corresponding to figure 5.4.2. indicated, as expected, two overlapping face-centred-cubic structures, in parallel orientation. It is reasonable to assume that one phase was pure gold and the other copper-gold alloy. Taking a microdensitometer trace across the diffraction pattern which incorporates $2\bar{2}0$ reflections from both phases and assuming that the inner reflection was due to pure gold the camera constant can be determined from the relation $d_{hkl} = \frac{L\lambda}{Ro_{hkl}}$. For accurate determination of lattice parameters it is necessary to calibrate the electron microscope. Using a polycrystalline gold standard and a nominal camera length of 76 cm the variation in camera constant between the undiffracted and 222 reflections

Fig. 5.4.2. An enlargement of Fig. 5.4.1. showing an area containing two types of fringes, one narrow and even, the other broader and irregular.

0·1 μ

Fig. 5.4.2. An enlargement of fig. 5.4.1 showing an area containing two types of fringes, one narrow and even, the other broader and irregular.

was ± 0.6%. Measurements taken for use in this thesis were contained in this region of the diffraction pattern. Care was taken to place specimens in the eucentric position before diffraction patterns were recorded. Wear of the goinometer stage meant that there was, however, some small fluctuation in the height of the sample. These errors were, however, largely eliminated by using the pure gold phase of most specimens as an internal standard. Imperfections in foils affect the quality and nature of diffraction patterns and may cause a broadening or extending of reciprocal lattice reflections. This can give rise to an error of up to 1% (Hirsch et al 1965) in lattice parameter calculations. The distance between the undiffracted beam and the diffracted beam being measured (R_o) was obtained from microdensitometer traces of diffraction patterns. This was to reduce the error in R_o which was estimated at (0.4%). An overall error in lattice parameter measurements of ± 1% to account for shape effects in reciprocal lattice spikes and uncertainty in Ro was judged to be realistic.

Using the equation given above the d spacing of the alloy was found to be 1.33 ± 0.01 Å which corresponded to an alloy with lattice parameter a_o = 3.76 ± 0.04 Å. Reference to the known variation of lattice parameter with alloy composition revealed that the composition of this particular alloy was 26% ± 7% gold, which was in reasonable agreement with the nominal alloy composition of 25% gold. Moiré fringes obtained by beating both these $2\bar{2}0$ diffracted waves together should have a calculated spacing of 17 ± 5 Å. The uncertainty in the moiré fringes was obtained by combining the errors in the respective d values. The value measured from an enlarged print was 16 ± 1 Å. The origin of the wider spaced fringes which had an approximate measured fringe spacing of 70 ± 4 Å is uncertain. Calculations show that they may be accounted for by assuming the presence of an additional alloy phase with a composition of 35% gold. It is possible that this new alloy arose as a result of dissolution of copper from the original alloy. Pickering (1967) found from a detailed study of alloy composition by X-ray diffraction that when

copper-rich copper-gold alloys dissolved they tended to form an alloy having a gold content of between 30 and 40% gold, which persisted until all of the original alloy had been corroded. The wide fringes described here may be an indication that such an intermediate alloy was forming but this was not conclusively demonstrated. The irregularity of the fringes does seem to indicate poor epitaxial fit between the phases which give rise to them.

Figure 5.4.3. shows a T.E.M. micrograph of a specimen similar to the previous one but having a higher copper content (with only 11% gold). It had been stripped in 35% nitric acid in the usual way and once again a fine-scale form of island morphology was observed. Annealing foils of this type could change the corrosion micromorphology as was found in the case of silver-gold. For example, figure 5.4.5. shows the same specimen as illustrated in fig. 5.4.4. after annealing at 500°C for 100 minutes. This treatment should cause significant interdiffusion of the two layers yielding an alloy containing 40% gold. E.D.A.X. measurements indicated that this was in fact the composition obtained (± 5%). The micrograph shows two distinct regions or domains characterised by different diffracting conditions existing in each region. It can be seen that fringes were visible in one set of domains but not in the other set. By tilting the specimen those regions which did not formerly have the correct diffracting conditions to show fringes could be made to do so, and simultaneously the fringes disappeared from the other regions. This observation of sharply-defined regions with different diffracting conditions had not been observed in unannealed specimens and this led to the conclusion that the structure resulted from a redistribution of material during annealing. By comparison, annealing silver-gold alloys led only to a coarsening of the established morphology (Chapter 4). During the redistribution the initial micromorphology of the copper-gold alloys was apparently modified so that the islands (illustrated in fig. 5.4.3) developed into the irregularly shaped and inter-connecting areas shown in fig. 5.4.4. Because the fringes could be seen in all regions, depending on the particular orientation of the specimen, they must have arisen from re-formed phases present over the whole of the specimen.

Fig. 5.4.3. A copper-gold foil (11% Au) stripped in 35% nitric acid showing a fine-scale and modified island morphology.

Fig. 5.4.3. A copper-gold foil (11% Au) stripped in 35% nitric acid showing a fine-scale and modified island morphology.

Fig. 5.4.4. This micrograph shows the same foil viewed in fig. 5.4.4. after it has been annealed at 500°C for 100 minutes.

0·1μ

Fig. 5.4.4. This micrograph shows the same foil viewed in fig. 5.4.4. after it has been annealed at 500°C for 100 minutes.

It was possible that the material re-distributed during annealing was the gold-rich residue following selective dissolution of copper from the original alloy. Consequently, the strain imposed on the underlying structure due to compositional differences would locally alter the orientation of the underlying material. The resulting variation in diffracting conditions arising from the distortion was illustrated by the presence or absence of fringes in the T.E.M. images as shown in fig. 5.4.4. The spacing of the fringes in the diffracting regions was 25 ± 1 Å. A predicted moiré fringe spacing of 23 ± 6 Å could be obtained by assuming a pure gold phase and an alloy phase having approximately 40% gold. In addition to these morphological observations made on copper-gold alloys, changes in composition and structure which occurred during corrosion have also been studied.

In Chapter One of this thesis and briefly in this chapter reference is made to the work of Pickering on the selective dissolution of copper from copper-rich, copper-gold alloys. He made the interesting observation that, as copper was removed, an alloy of between 30 and 40% gold always formed, regardless of the original composition. This newly formed composition persisted until none of the original alloy remained. Only when all the original alloy had been attacked was copper dissolved from the newly formed alloy to produce a surface layer which was practically pure gold. Pickering used this observation to support his idea that vacancy-assisted volume diffusion was responsible for the transport of reactive material from the bulk of the alloy to the corroding surface. Volume diffusion would, however, be more likely to produce a gradient of chemical composition, becoming more gold-rich towards the corroding surface, and it was therefore surprising that an "intermediate" alloy formed in this way. This observation has been confirmed during the study of the copper/gold system presented here. When copper was dissolved from a copper-on-gold bimetallic specimen prepared by epitaxially depositing copper onto a heated single crystal of gold, an alloy of copper-gold was frequently observed as a corrosion product. This again tended to contain between 30 and 40% gold and did not appear to depend in any simple

way on the strength of corroding acid or alloy composition. These observations will be described fully later in this chapter.

In addition certain corroded copper-gold specimens showed superlattice reflections in their electron diffraction patterns indicating that a degree of ordering had taken place. The AuCu ordered structure, for example, has (002) planes which contain alternately all gold and all copper atoms, see figure 5.1.2. It is apparent from this that the true repeat distance along the [001] direction is doubled compared with the disordered alloy. Since gold and copper atoms have different scattering factors the 001 reflection becomes allowed. This is illustrated more clearly if the structure factor for a unit cell is obtained. From fig. 5.1.2. the four lattice points in the ordered f.c.c. unit cell are occupied by Cu at (000) and ($\frac{1}{2}\frac{1}{2}0$) and Au at ($\frac{1}{2}0\frac{1}{2}$) and ($0\frac{1}{2}\frac{1}{2}$).

The structure factor is given by:-

$$F_{hkl} = \sum_i f_i(0) \cos 2\pi (hu_i + kv_i + lw_i)$$

u_i, v_i, w_i being the fractional co-ordinates of the ith atom.
For the CuAu structure

$$F_{hkl} = f_{Cu} [\cos 2\pi (0+0+0) + \cos 2\pi (h/2 + k/2)] + f_{Au} [\cos 2\pi \left(\frac{h+1}{2}\right) + \cos 2\pi \left(\frac{k+1}{2}\right)]$$

$$= f_{Cu} [1 + \cos\pi(h+k)] + f_{Au} [\cos\pi(h+1) + \cos\pi(k+1)]$$

thus when hkl are odd odd even, or even even odd,

$$F_{hkl} = f_{Cu} (1+1) + f_{Au} (-1+-1)$$

$$= 2(f_{Cu} - f_{Au})$$

Therefore such reflections as $1\bar{1}0$ are allowed and their amplitudes will be proportional to $(f_{Cu} - f_{Au})$. As the degree of order is decreased the average scattering amplitude of the atoms on the two different sites becomes more

equal so that the intensity of the superlattice reflections diminishes. Other combinations (e.g. odd even odd) and even odd odd give $F_{hkl} = 0$, and so reflections such as $01\bar{1}$ and $00\bar{1}$ are not allowed. In the 111 reciprocal lattice section for an f.c.c. material there are six $2\bar{2}0$-type reflections symmetrically arranged around the zero-order beam (see for example Pashley and Stowell (1963)), these are $2\bar{2}0$, $0\bar{2}2$, $\bar{2}02$, $\bar{2}20$, $02\bar{2}$ and $20\bar{2}$. According to the argument outlined above only $1\bar{1}0$ and $\bar{1}10$ reflections are allowed; however, if the diffraction pattern arises from a large area it will contain contributions from three orientations of the ordered phase corresponding to an alignment of the c axis for CuAu I along the three principal axes of the original disordered material (a_1 a_2 and a_3) since they are equivalent. Superlattice reflections will be observed at all 110 positions since in general more than one orientation of the ordered structure is sampled by the electron beam at any one time.

For the case of $AuCu_3$ the atomic co-ordinates of the f.c.c. unit cell are Au at (000) and Cu at $(\frac{1}{2}\frac{1}{2}0)$, $(\frac{1}{2}0\frac{1}{2})$ and $(0\frac{1}{2}\frac{1}{2})$. This gives

$$F_{hkl} = f_{Au} + f_{Cu} \cos\pi (h+k) + \cos\pi (k+1) + \cos\pi (h+1)$$

It follows that for any combination of odd and even indices, $F_{hkl} = f_{Au} - F_{Cu}$ so that all such superlattice reflections will be allowed and they will consequently have approximately three times the intensity of the superlattice reflections from an equivalent volume of ordered CuAu $\underline{I}$. This difference is associated with the fact that CuAu loses cubic symmetry upon ordering (becomes tetragonal) whereas Cu_3Au remains cubic.

These observations of superlattice reflections and alloying during copper dissolution lead to several interesting ideas concerning the corrosion mechanisms applicable for copper-gold alloys dissolving in nitric acid. Figure 5.4.5. shows the electron diffraction patterns for a film of (111) gold which had a (111) copper overlayer deposited onto it in the manner described earlier in this chapter. Figure 5.4.5(a) shows the specimen before

Fig. 5.4.5. A film of (111) gold which has had a (111) copper overlayer deposited onto it (a) shows the specimen before exposure to acid and (b) after it has been exposed to 35% nitric acid for 15 s.

(a)

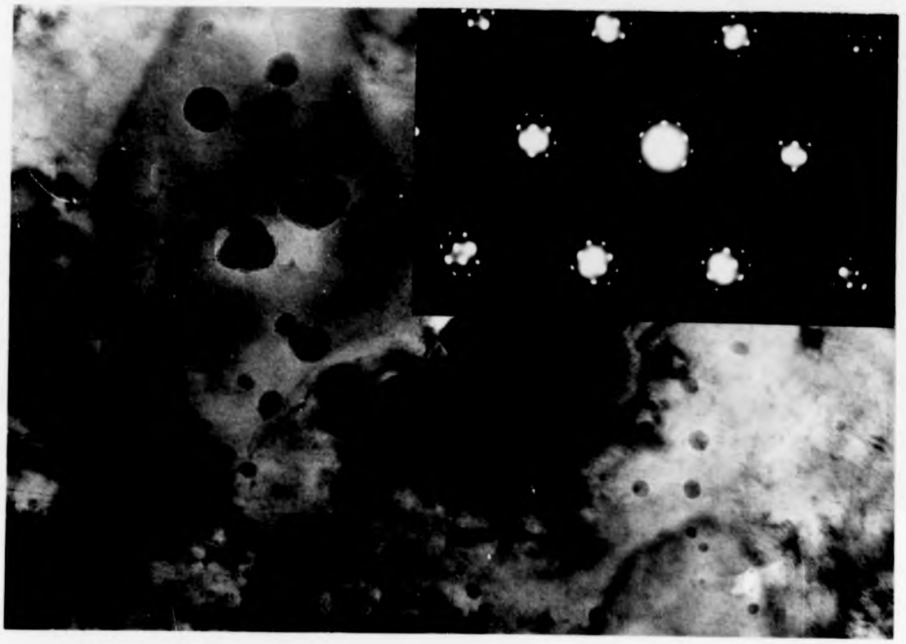

0·1 μ

(b)

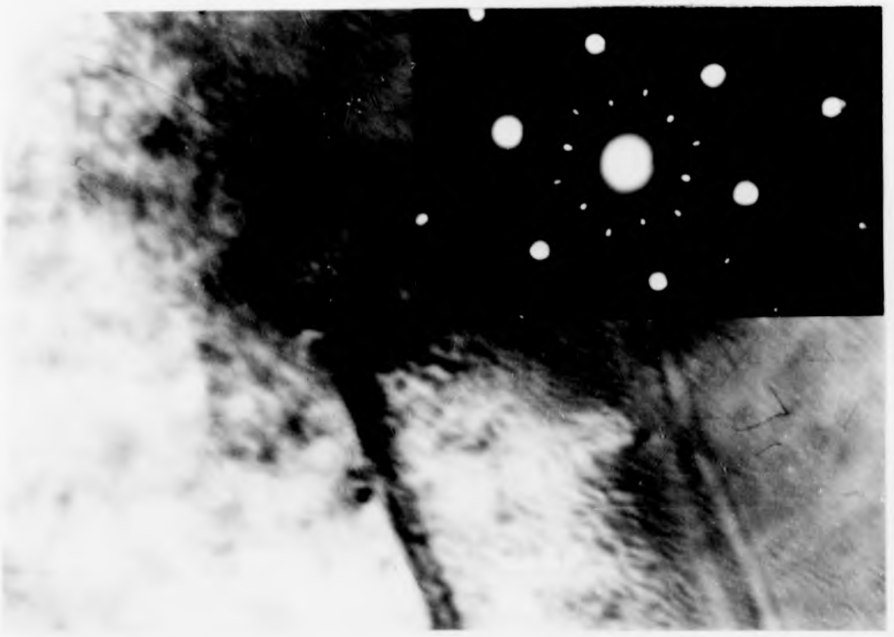

(a)

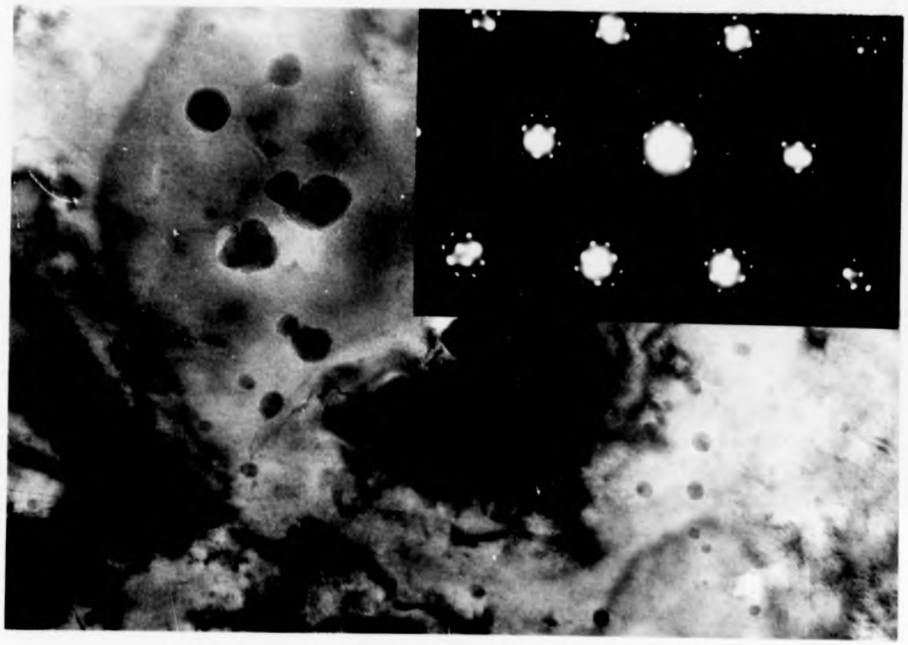

0·1 μ

(b)

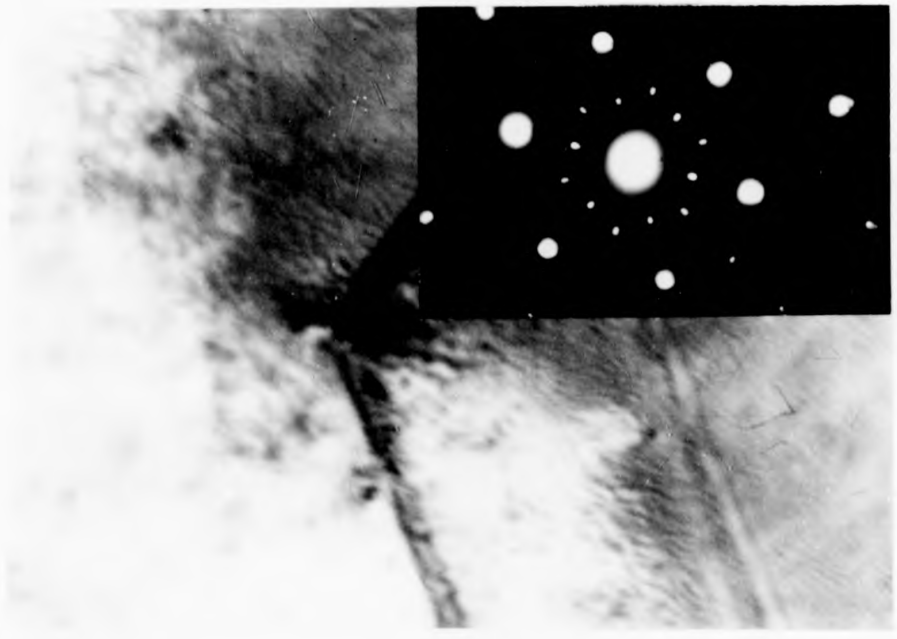

exposure to acid and 5.4.5(b) after it had been exposed to 35% nitric acid for 15 s. The diffraction pattern for 5.4.5(a) was that expected for two overlapping (111) oriented face-centred-cubic structures in parallel orientation. The pairs of main spots surrounding the undiffracted beam arose from the two separate phases, copper and gold, and the clusters of weaker spots around the main reflections could be accounted for by double diffraction. There was some intensity detectable at superlattice (i.e. $1\bar{1}0$) positions but this was found to be much enhanced when the specimen had been exposed to acid (fig. 5.4.5(b)). The diffraction pattern from this corroded specimen contained a $2\bar{2}0$ reflection close to the main gold $2\bar{2}0$ reflection, indicating alloy formation. This is shown more clearly in Fig. 5.4.6(a) and (b) which are microdensitometer traces taken from the above diffraction patterns. These results are consistent with the existence of separate phases of pure gold and pure copper before corrosion, and pure gold and an alloy containing 32 ± 7% gold after corrosion. It is worth noting that without depositing a standard onto these specimens then the designation of the two initial phases as pure copper and pure gold is a matter of judgement. It is of course possible that they contained up to a few percent gold or copper respectively. Since they were prepared as separate phases, it is assumed that before corrosion they are still best described as pure copper and pure gold.

Another example of alloy formation is illustrated in Fig. 5.4.7(a), (b) and (c). These TEM micrographs and the corresponding diffraction patterns are from the same copper-on-gold bimetallic specimen as shown in the previous figure. Figure 5.4.7(a) shows a specimen before immersion in acid, fig. 5.4.7 (b) after 5 s in 35% acid, and fig. 5.4.7(c) a similar sample after 15 s in 35% nitric acid. The diffraction patterns illustrate the progression from two phases before corrosion, shown in (a), to three phases (b) after a short exposure to acid. The third phase is indicated by an additional strong spot between the copper and gold $2\bar{2}0$ reflections, i.e. an alloy $2\bar{2}0$ reflection;

Fig. 5.4.6. Microdensitometer traces from the diffraction pattern shown in fig. 5.4.5. (a) corresponds to the untreated sample (Fig. 5.4.5 (a)) and (b) from the corroded specimen (Fig. 5.4.5(b)).

a

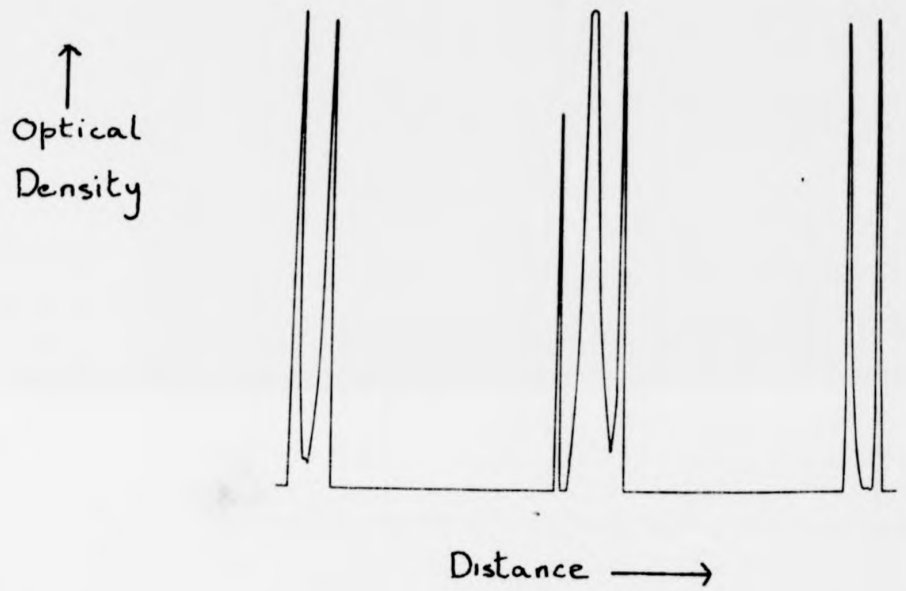

b

Fig. 5.4.7. Transmission electron micrographs of copper on gold bimetallic foil (a) before immersion in acid (b) after 5 s in 35% nitric acid and (c) after 2 5 s immersion in 35% nitric acid.

a

b

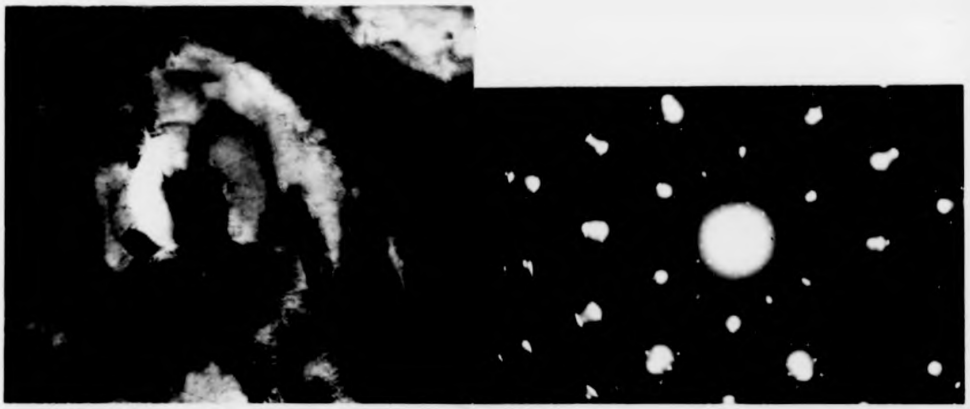

0·5μ

c

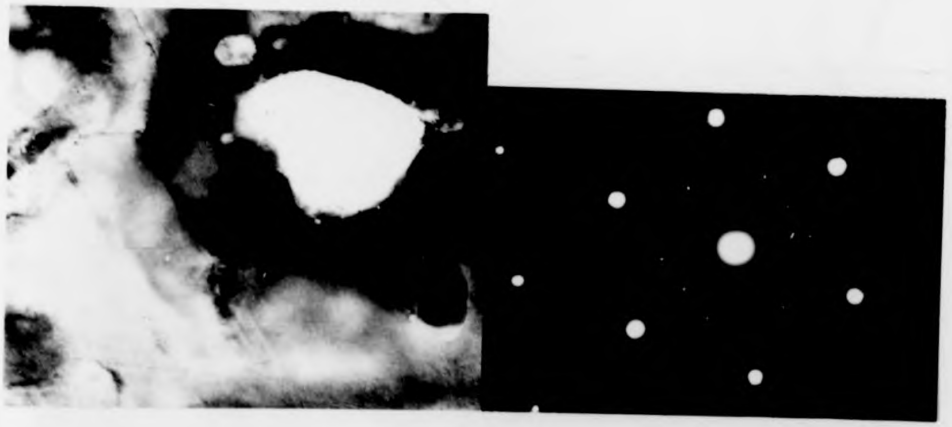

a

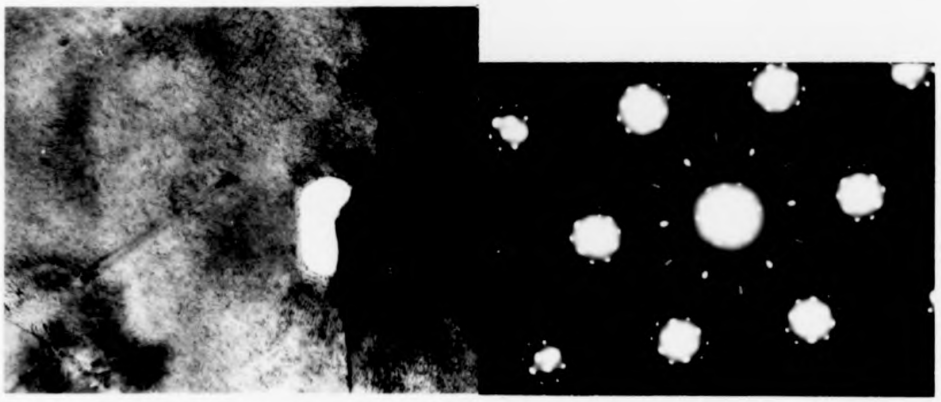

b

0·5μ

c

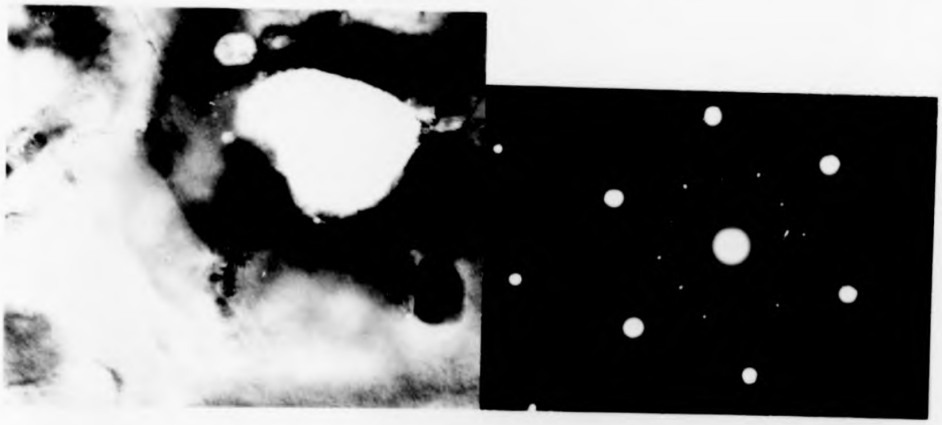

the composition of this alloy was found to be 38 ± 7% Au following the composition band generally observed for alloys formed in this manner. Finally, after a longer exposure to acid the film was composed of a pure gold phase and a second phase with a composition approaching that of pure gold (the $2\bar{2}0$ reflections from each phase were nearly coincident). Figure 5.4.8(a), (b) and (c) are microdensitometer traces across the electron diffraction patterns taken from a copper-on-gold specimen (a) before immersion in nitric acid, (b) after 10 s immersion and (c) 25 s immersion in 35% nitric acid. These traces show no evidence of an alloy formed before immersion but an alloy was formed during corrosion with a composition that remained the same (approximately 35% Au) even though copper dissolution appeared to continue as the corrosion progressed. E.D.A.X. measurements indicated the progressive removal of copper giving overall Au/Cu ratios for the specimen as a whole of 0.33 ± 0.06, 0.45 ± 0.08 and 0.52 ± 0.09 respectively. This shows that, although the amount of copper removed was directly dependent on the length of time the specimen was exposed to acid, the composition of the alloy which formed reaches a stable composition of about 35% gold.

A typical diffraction pattern from a copper-on-gold bimetallic foil after moderate exposure to acid is schematically represented in Fig. 5.4.9. It is included to clarify the interpretation of the diffraction patterns from these specimens, described above.

These observations of alloying and ordering in copper-gold specimens induced by corrosion and outlined above seem to indicate that, as in the case of silver-gold alloys, a very aggressive form of attack occurs and that the corrosion reaction involves gold as well as silver or copper. The gold component appears to be directly involved in a process initiated by the dissolution of copper which leads to a corrosion mixing (or alloying) of the two elemental phases. The fact that the alloy which forms during copper dissolution frequently shows evidence of ordering indicates a high

Fig. 5.4.8. Microdensitometer traces taken from a copper on gold foil (a) before immersion in nitric acid (b) after 10 s immersion and (c) 25s immersion in 35% nitric acid.

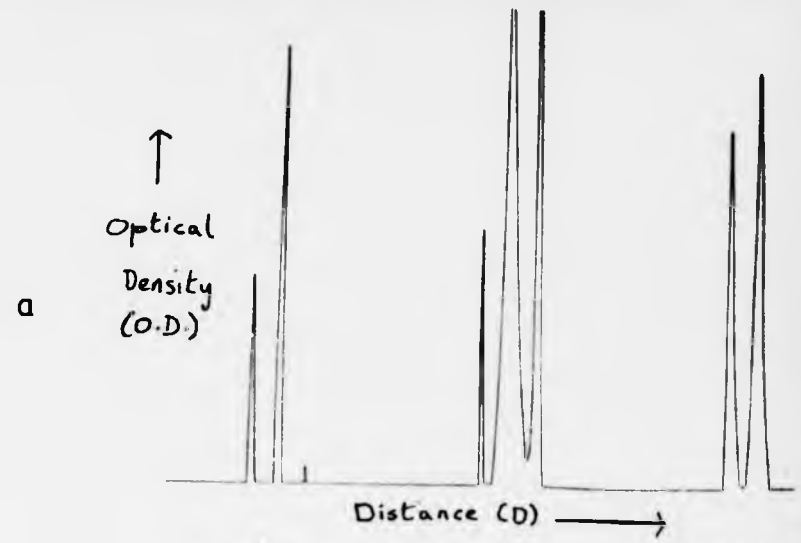
a
Optical
Density
(O.D.)
Distance (D)

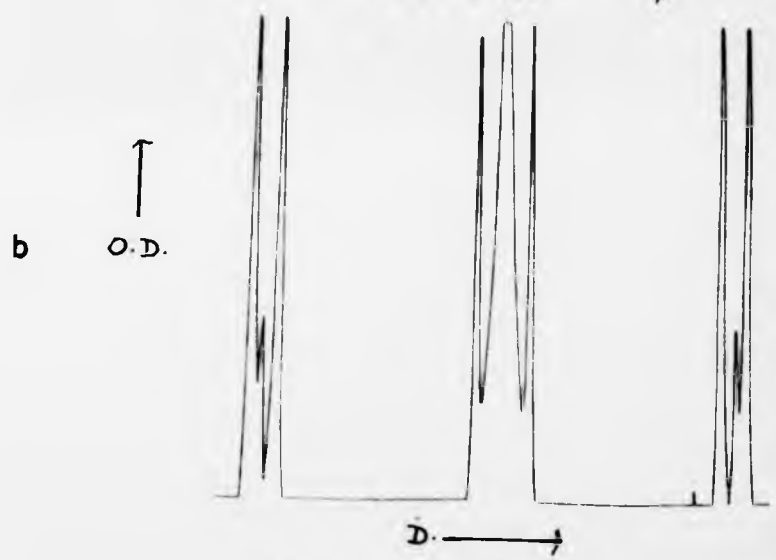
b
O.D.
D.

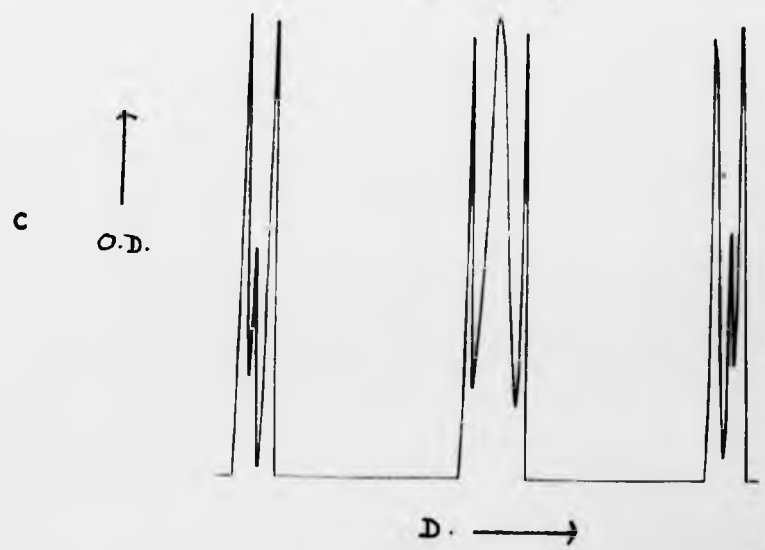
c
O.D.
D.

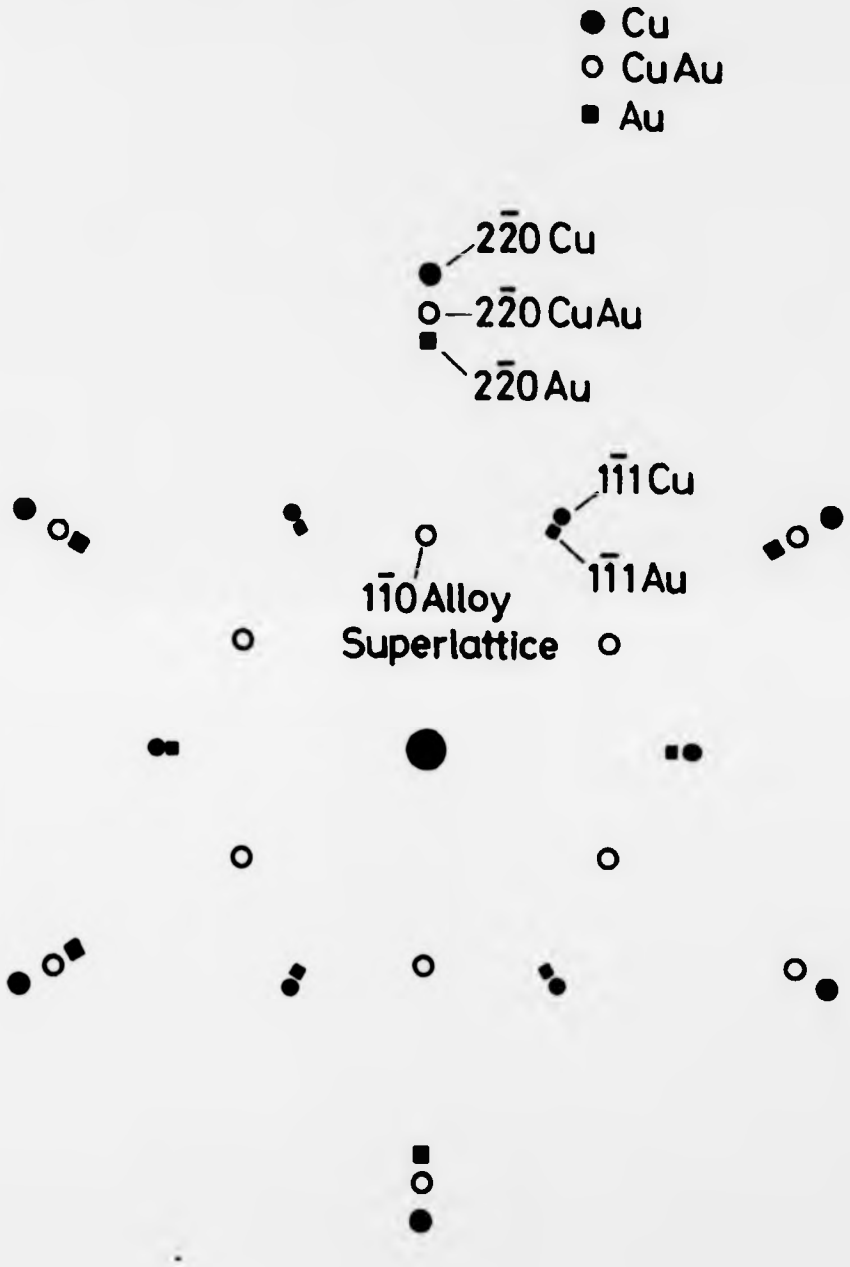

Fig. 5.4.9. A typical diffraction pattern from a corroded copper on gold bimetallic foil. It has been indexed according to the interpretation presented in the text (i.e. corrosion can induce alloying and a degree of ordering in these systems).

degree of disorder in the alloy so formed, sufficient to permit the ordering process to occur at room temperature. The exact mechanism of corrosion alloying and ordering must be a subject of speculation and remains for further discussion in Chapter Seven of this thesis.

References: Chapter Five

Bassett, G. A., Menter, J. W., and Pashley, D. W., (1958), Proc. Roy. Soc. A246, 345.

Flinn, P. A., McManus, G. M. and Rayne, J. A., (1960), J. Phys. Chem. Solids, 15, 189.

Glossop, A. B., and Pashley, D. W., (1959), Proc. Roy. Soc. A250, 132.

Hansen, M., (1958), Constitution of Binary Alloys, McGraw-Hill Book Co., N. York, p.198.

Hirsch, P. B., Howie, A., Nicholson, R. B., Pashley, D. W., Whelan, M. J., (1965), Electron Microscopy of Thin Crystals, London Butterworths.

Hunt, A. M., and Pashley, D. W., (1963), J. Australian, Inst. Met. Vol. 8 No. 1, p.61.

Johansson, C. H., and Linde, J. O. (1975), Ann. Phisik, 78, 439.

Macur, J. E., and Vook, R. W., (1980), Thin Solid Films, 66, 311-324.

Pashley, D. W., and Stowell, M. J., (1963), Phil. Mag., 8, 1605.

Pickering, H. W., (1967), Proceedings of the Conference on Fundamental Aspects of Stress Corrosion Cracking, Edited by R. W. Staehle, A. J. Forty, and D. van Rooyan (Houston N.A.C.E.), p.115.

Swann, P. R., (1971), Proceedings of the Conference on the Theory of Stress Corrosion Cracking in Alloys, ed. J. E. Scully,(Brussels: NATO), p.113.

CHAPTER SIX

Oxide formation during the corrosion of silver-gold alloys in nitric acid

6.1. Introduction

In Chapter Four of this thesis, observations were described of the micromorphological changes that occurred when silver-gold alloys were corroded in nitric acid. These show how the residue of gold left on the surface of an alloy after selective dissolution of silver by nitric acid becomes re-ordered to form gold-rich islands. The re-ordering process apparently occurs predominantly by surface diffusion which leads to the nucleation and growth of gold-rich islands. In this way further selective dissolution of silver becomes confined to the channels and pits left between islands. Eventually the channels "pinch-off" by coalescence of islands and actively dissolving pits remain in between the "pinched-off" regions. These observations are described fully by Forty and Durkin (1980) and an analytical model for corrosion-pitting and tunnelling based on these observations, has been developed by Forty and Rowlands (1981).

One of the reasons for choosing the silver-gold/nitric acid system as a model for the microscopic study of corrosion was the expected absence of insoluble products. The reaction products formed when pure silver is dissolved in nitric acid are primarily silver nitrate, which is extremely soluble in an aqueous environment, and gaseous nitric oxide (NO). This follows from the overall reaction: $3Ag + 4HNO_3 \rightarrow 3AgNO_3 + NO + 2H_2O$.

Therefore the corrosion reaction is not restricted by the formation of a passivating or semi-passivating film and, indeed, occurs by a vigorous autocatalytic process (see later). On the assumption that an analogous chemical reaction occurs in the selective dissolution of silver from silver-gold alloys, this should be an equally "film free" system, evidently suitable for a study of the basic processes involved in alloy dissolution. As previously described (Chapter 2) there are several other useful features

of the silver-gold alloy system. For example, the very small change in lattice parameter across the complete range of alloy compositions from pure silver to pure gold. This means that moiré effects in electron microscope images caused by compositional changes and discussed extensively in the preceding chapter for the case of copper-gold, should not occur. Furthermore, because the alloy remains a single phase (f.c.c.) at all compositions there are no complex microstructural changes accompanying selective dissolution. Thus, the interpretation of electron microscope images should be a fairly straightforward matter. This is not so, for example, for the observations made on copper-gold alloys described in Chapter 5 and for the alloy systems which have been used for microstructural and micromorphological studies of corrosion in the past (Pickering and Swann 1963; Pickering 1967).

In view of these considerations it is both surprising and interesting that, under certain conditions, the electron diffraction patterns for thin films of silver-gold alloys change dramatically as a result of the selective dissolution of silver in nitric acid. These changes are discussed in the following sections and evidence is given to support the idea that the formation of gold I oxide occurs and that this can account for the observed changes in the electron diffraction patterns of corroded specimens. A mechanism is suggested whereby the selective dissolution of silver creates a chemical environment in which the oxidation of gold becomes possible. The oxidation reaction is therefore promoted by the dissolution of silver, an example of coupled chemical reactions whose wider significance will be discussed more fully in the next chapter of this thesis.

6.2. Changes in electron diffraction patterns

The micromorphological changes that occurred as a result of corrosion were described fully in Chapter Four. The essential feature of a great many

observations, made on alloys having a wide range of compositions and corroded in nitric acid of various strengths, was the appearance of an island/channel morphology which partially covered the corroded surface. The islands, which were thought to be gold-rich, grew at a rate which seemed to depend on the concentration of gold in the alloy and the strength of nitric acid. However, the island morphology occurred only when alloys having between approximately 20 and 50 atomic percent gold were used. The more dilute alloys (i.e. < 20% Au) showed extensive general etching whilst more concentrated alloys (i.e. > 50% Au) appeared to be insoluble. At intermediate compositions the appearance and rate of growth of gold-rich islands depended on the strength of nitric acid; there was steady island growth in dilute nitric acid but in concentrated acid the growth and coalescence of islands occurred very rapidly. Imperfect coalescence of the islands led to the onset of corrosion pitting and eventually the pits developed into corrosion tunnels.

Under those chemical conditions which led to island formation a remarkable change in the electron diffraction pattern for the corroded alloy was observed. The patterns were transformed from the simple hexagonal pattern normally observed for gold and silver, to quite complicated arrays of spots. This is illustrated by Fig. 6.2.1. Fig. 6.2.1.a shows the normal pattern for a f.c.c. silver-gold alloy film in a (111) orientation, whereas Fig. 6.2.1.b was the pattern recorded for a similar film after corrosion in 50 per cent nitric acid solution for 10 seconds. The strong spots in fig. 6.2.1a correspond to $2\bar{2}0$-type reflections, and these are also evident as equally strong spots in fig.6.2.1b. As already remarked, there is little or no change of lattice parameter with changing alloy composition and consequently these $2\bar{2}0$ reflections give no information about the corrosion of the alloy. However, other features of the patterns are much more informative. The weak spots in fig.6.2.1a, occurring close to the positions expected for the "forbidden" 111 reflections are frequently observed for vapour deposited (111) films and have contributions to their intensity from double diffraction effects associated with double

Fig. 6.2.1. Transmission electron diffraction patterns for (111) films of 75 silver/25 gold at % alloy. (a) before corrosion, and (b) after corrosion in 50% nitric acid solution.

a

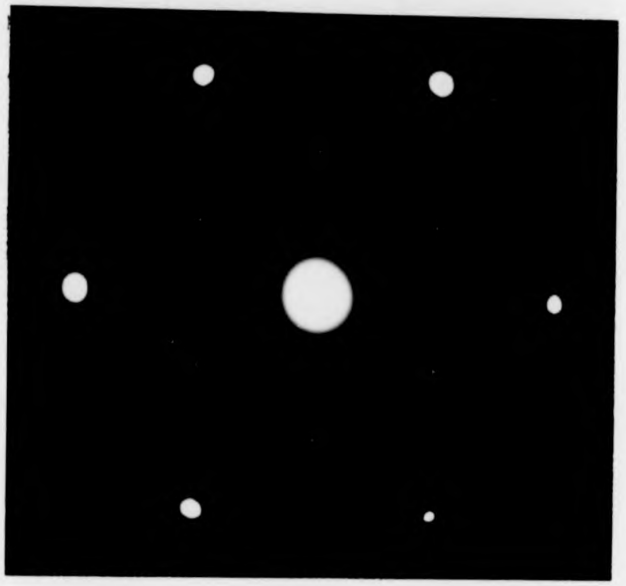

b

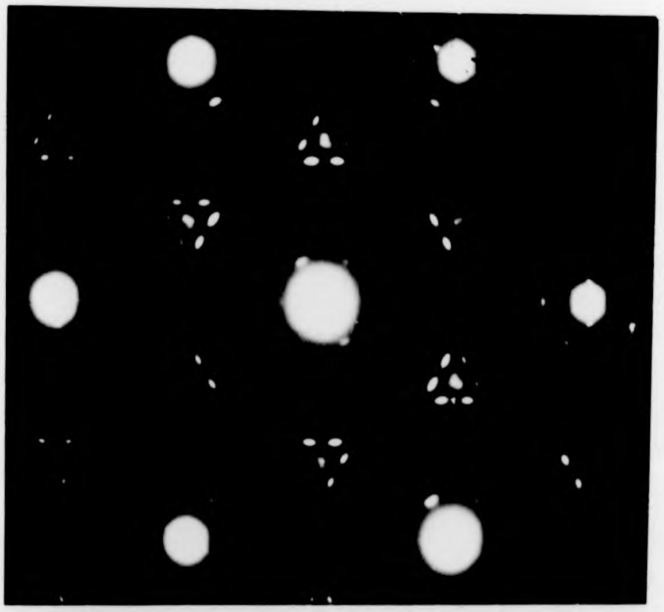

a

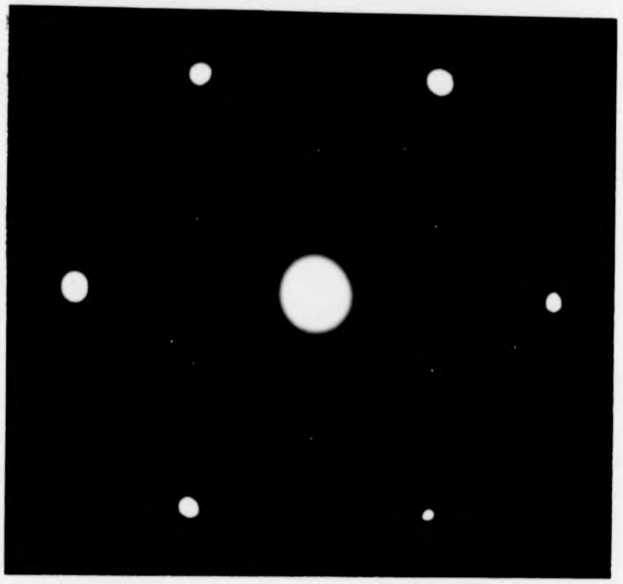

b

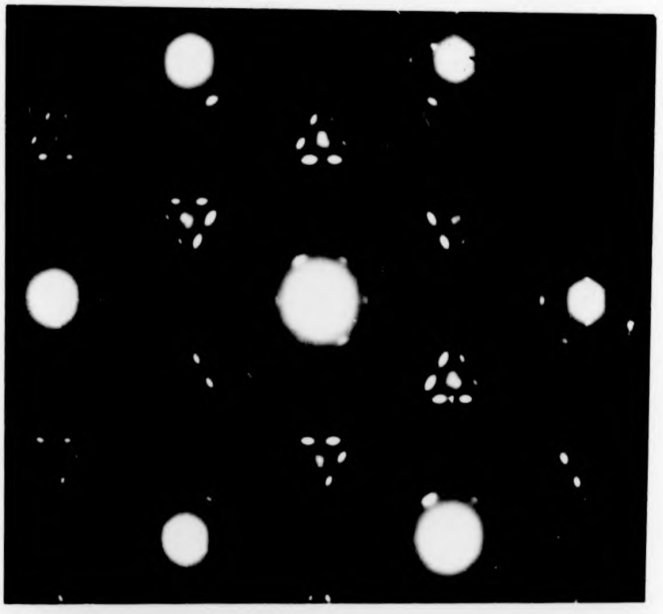

positioning twinned structures (Pashley and Stowell 1963). They can therefore be indexed as $^{1}/_{3}$ $(2\bar{2}4)$ reflections which are infact the $1\bar{1}1$ reflections of the secondary twin orientation indexed in terms of the co-ordinates of the primary twin orientation. Steps occurring on such films also contribute to the intensity of these reflections (Cherns 1974). Their intensity may therefore be indicative of the microstructure of the film surfaces. In the case of the corroded alloy (Fig. 6.2.1b) these weak spots were replaced by clusters of stronger spots also occurring in the vicinity of the forbidden 111 reflections. These clusters and also weaker reflections appearing in relation to the $2\bar{2}0$ reflections seemed to be geometrically related to the alloy reflections; a crystallographic relationship with the original alloy was therefore indicated. Each cluster consisted of a central spot surrounded by three symmetrically disposed pairs of more diffuse spots. The central spot in the cluster was, infact, four very closely spaced spots, as can be seen in the enlarged section of the diffraction pattern drawn out and indexed in fig. 6.2.2. This multiplicity was apparently associated with the 000 and neighbouring primary $2\bar{2}0$ diffracted beams from the alloy. Furthermore, the diffuse pairs of spots usually showed a tendency to form arcs, one pair around the direct 000 spot and the other two pairs around neigbouring $2\bar{2}0$ spots. Arcing of spots could arise for a variety of reasons some of which were mentioned briefly in Chapter Three. According to the interpretation of the diffraction pattern presented here the arced spots arose from the same phase that gave rise to the other additional reflections observed on these patterns. These, however, were not arced. It has not been possible to explain why this difference in spot shape should occur. These observations indicated that the reflections arising from the f.c.c. metal (gold substrate and uncorroded alloy) underwent a second or double diffraction in a new phase located on the surface of the film,the intensity of these extra reflections indicated that this effect was wide-spread. There were other extra spots in the diffraction pattern but these were relatively weak. They probably

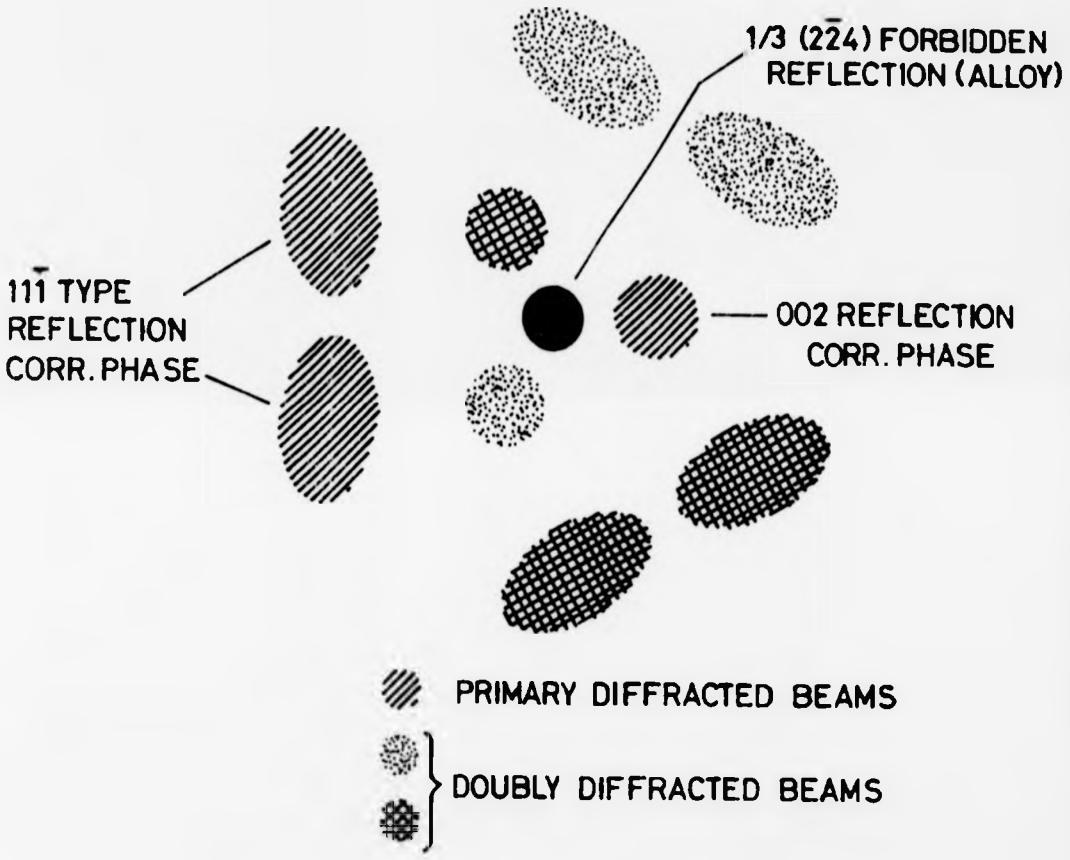

Figure 6.2.2. An enlarged drawing of the cluster of spots frequently observed on corroded silver-gold alloys. There are three spots shown which arise from primary diffraction in the corrosion phase. If neighbouring $2\bar{2}0$ alloy reflections act as primary beams and are doubly diffracted by the corrosion phase, three equivalent reflections displaced from the primary reflections will occur, in each case. These are also shown. In addition the forbidden alloy reflection ($^{1}/3$ $(2\bar{2}4)$) is drawn (central black spot).

arose from double diffraction and other dynamical effects which occurred so markedly, presumably because of the very high degree of symmetry which these metal crystals possessed. Three-dimensional information about the reciprocal lattice of a corroded specimen, obtained by rotating it about a [110] zone axis is illustrated in fig. 6.2.3. This shows a series of diffraction patterns taken from a Ag 25% Au alloy which had been stripped in 50% HNO_3. This sample was used because it yielded diffraction patterns in which the additional spots occurred with high intensity. As the specimen was rotated the intensity of the clusters of satellite spots, particularly those associated with second and third order diffracted beams, became reduced, eventually to zero. This, however, only occurred at large tilt angles (> 15°). The reduction in intensity of the "off-axis" $2\bar{2}0$ reflections was matched by a similar and proportional drop in the intensity of their associated satellite reflections. This illustrated the quality of the epitaxial match between the alloy and the additional phase. The general intensity of the satellite reflections indicated that for this sample the new phase was present in relatively large quantities.

6.3. Dark field electron microscope observations of the corrosion phase

Further insight into the origin of the extra spots in the diffraction pattern and hence into the nature of the corrosion phase, was obtained from dark field examination of the specimen using selected diffracted beams to form the TEM image. These showed that the extra phase existed in three distinct crystallographic orientations or domains with each domain giving rise to its own set of diffracted beams. The results of such an investigation are illustrated in 6.3.1. which shows a set of T.E.M. images again obtained from a 75 silver/25 gold atomic per cent alloy after it had been corroded in 50 per cent nitric acid solution. The bright field image (fig. 6.3.1a) shows the development of the gold island morphology described earlier. Figures 6.3.1b, c, d are dark field images of the same field of view using, in turn,

Fig. 6.2.3. A series of electron diffraction patterns taken from a Ag 25%Au alloy which has been stripped in 50% HNO_3 (a) with the incident electron beam along the [111] direction, (b) tilted 15° about a $1\bar{1}0$ zone axis, (c) tilted 19° about the zone axis, (d) tilted 23° about the zone axis.

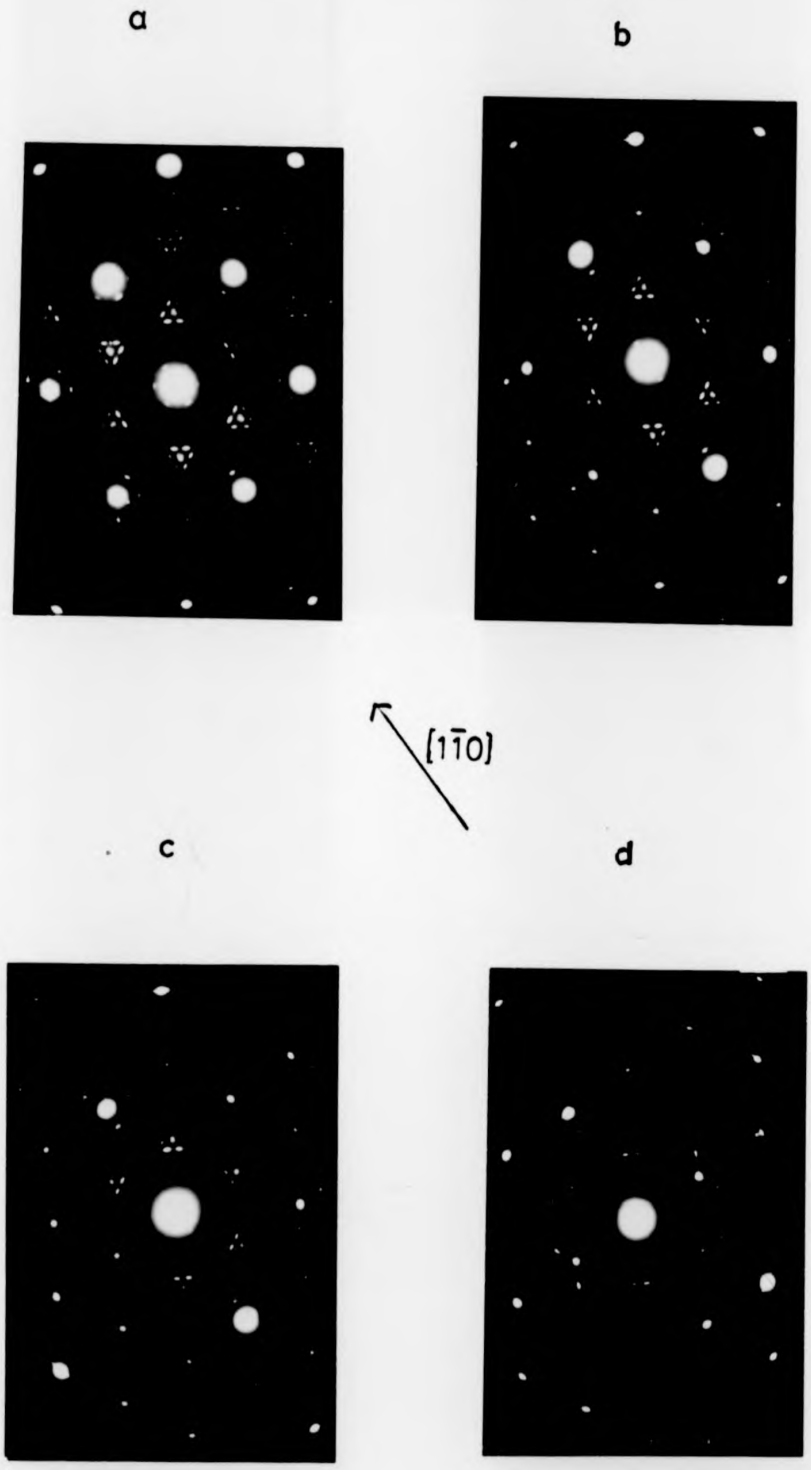
a
b
[1$\bar{1}$0]
c
d

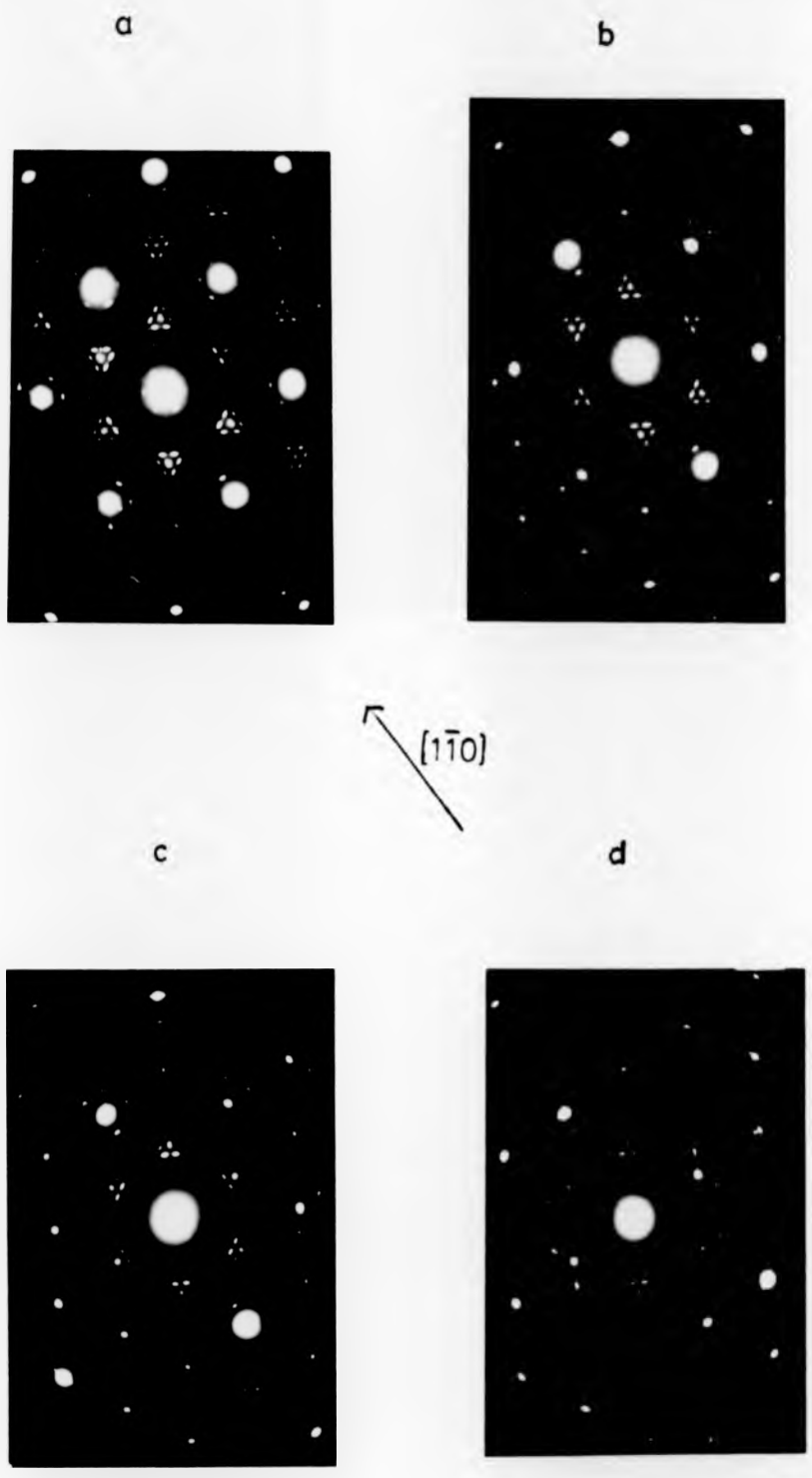
a
b
[1$\bar{1}$0]
c
d

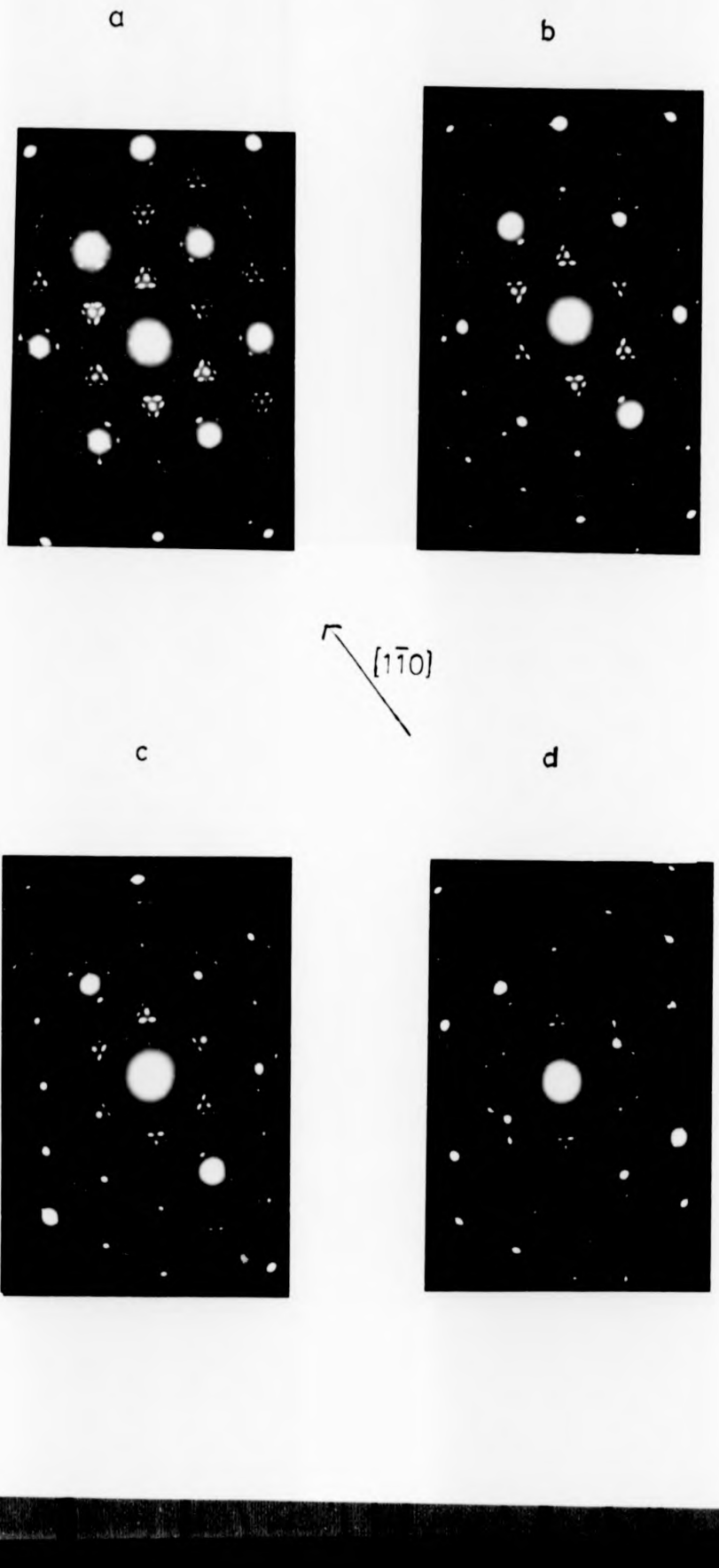
a
b
[1$\bar{1}$0]
c
d

Fig. 6.3.1. Bright field and dark field T.E.M. images of a 75 silver/25 gold at % alloy after corrosion in nitric acid solution: (a) bright field; (b) dark field using spot labelled b in the diffraction pattern which shows an enlarged section illustrating the detailed structure of the clusters of extra spots due to the corrosion phase, (c) dark field using spot c; (d) dark field using spot d; (e) a dark field image obtained when all three spots are used.

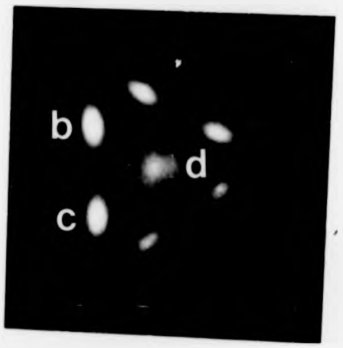

0·1 μ

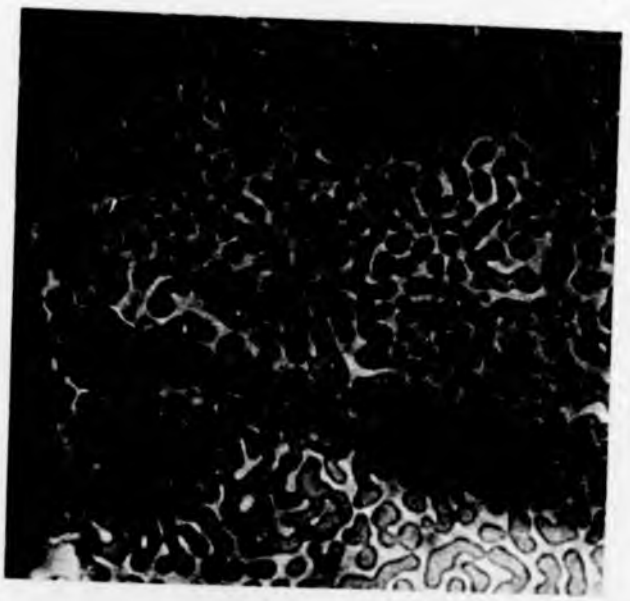

a

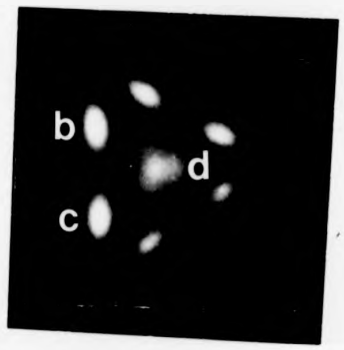

0·1 μ

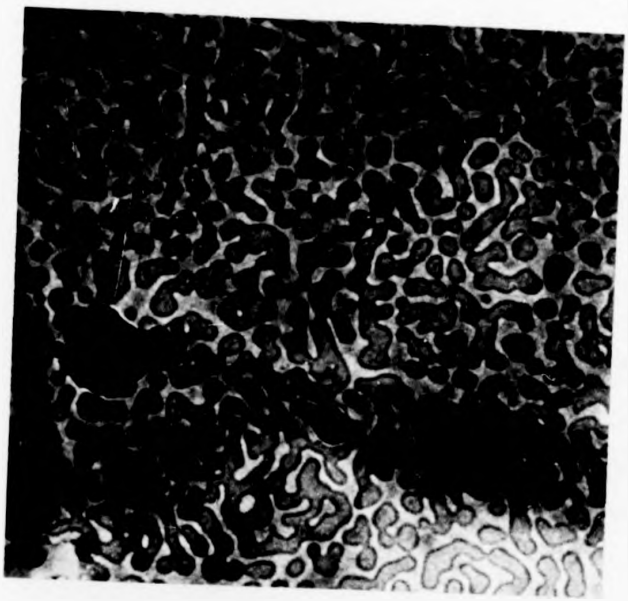

a

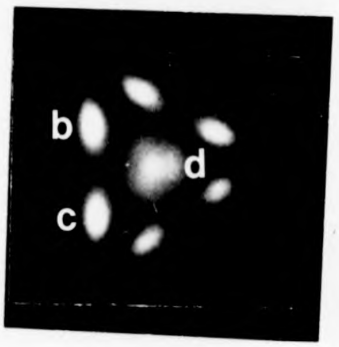

0·1 μ

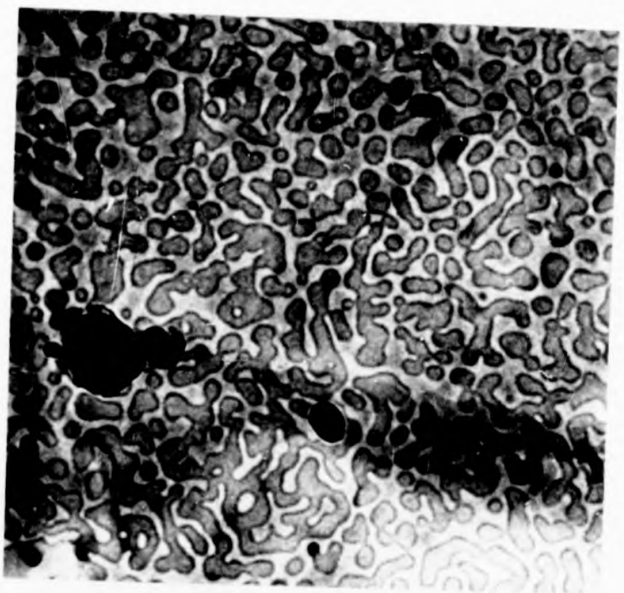

a

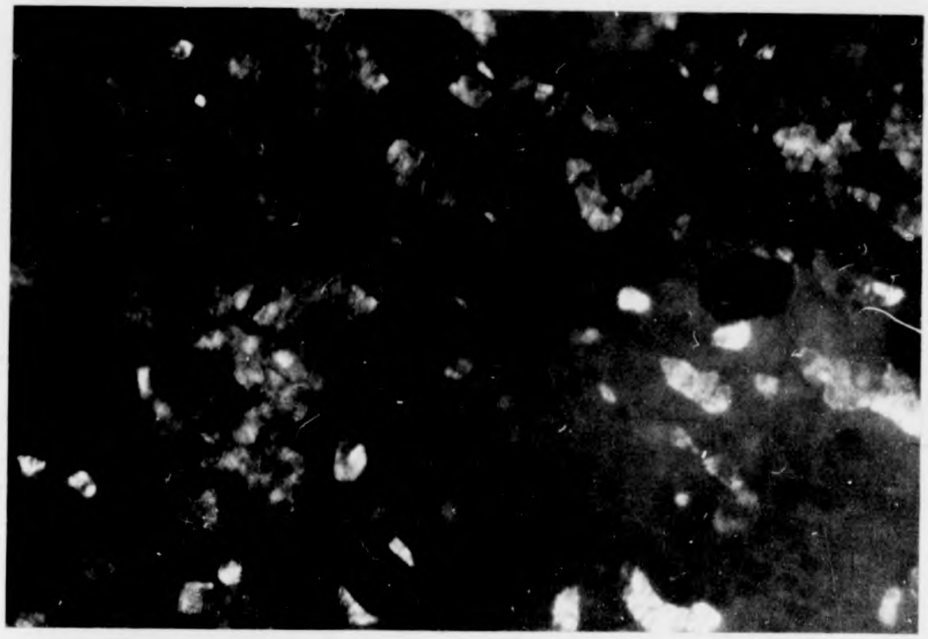

b

0·1μ

c

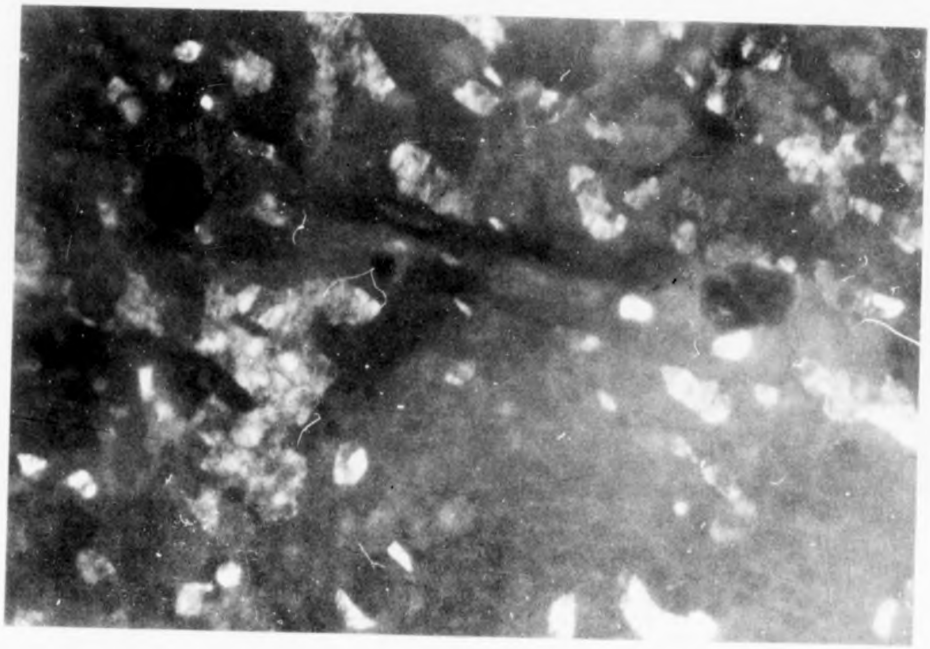

b

0·1 μ

c

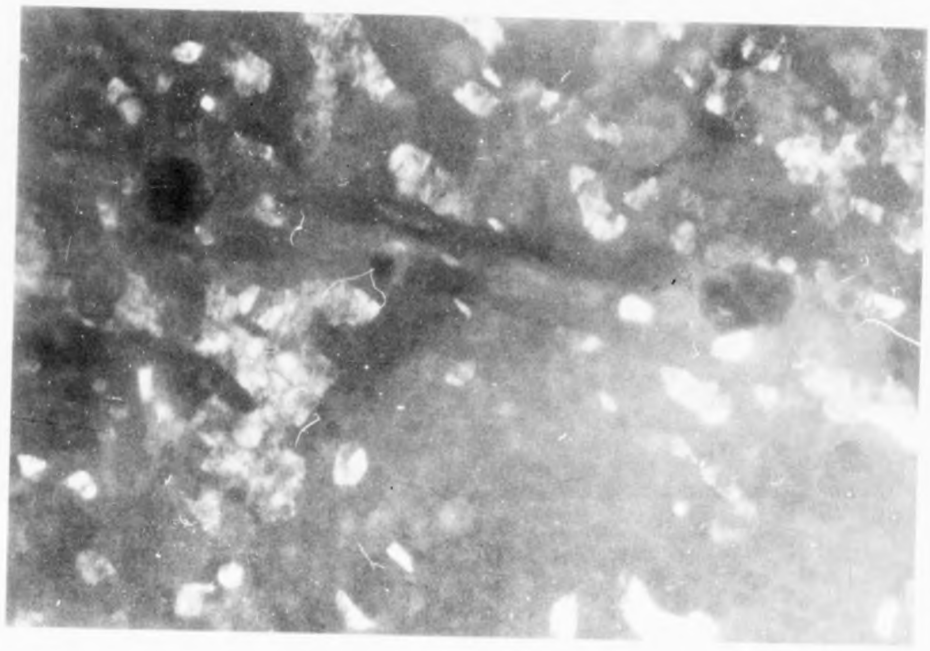

b

0·1 μ

c

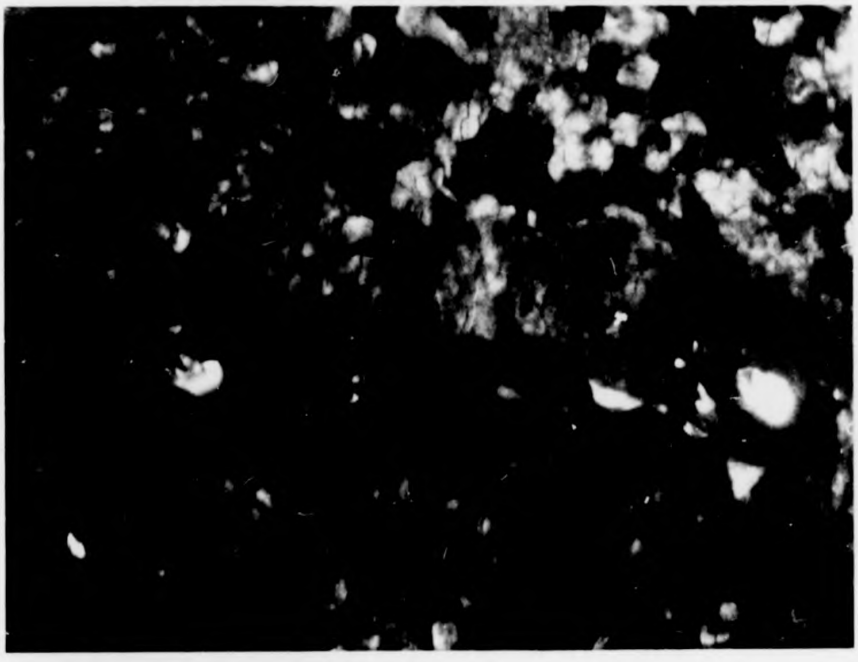

d

0·1 μ

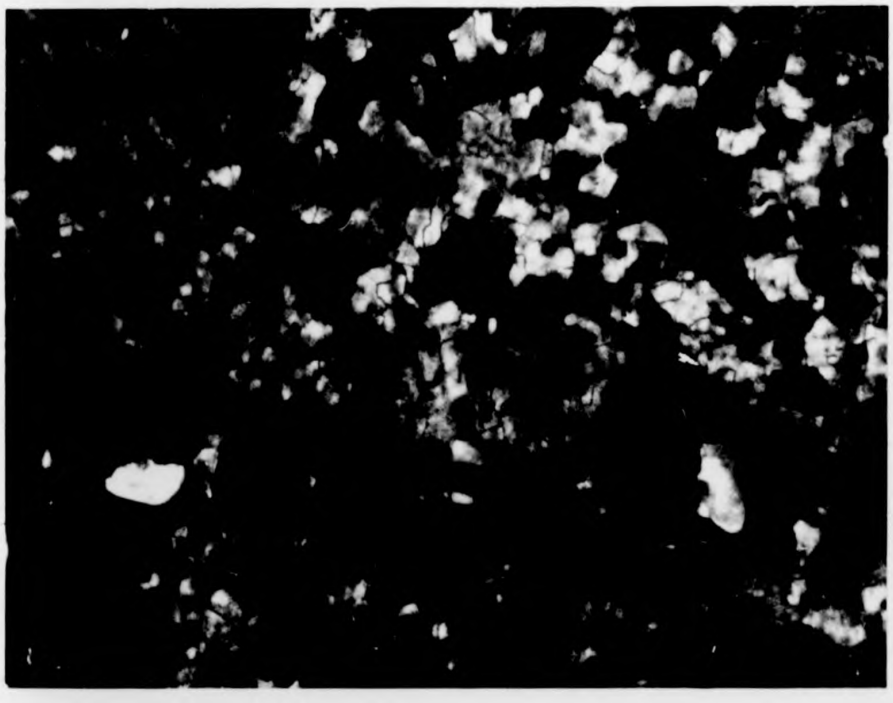

e

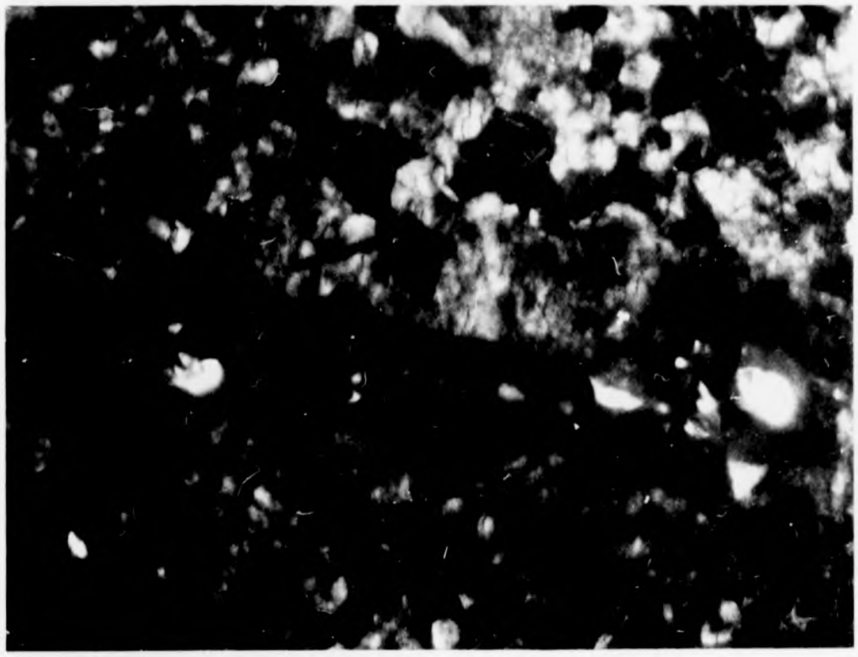

d

0·1μ

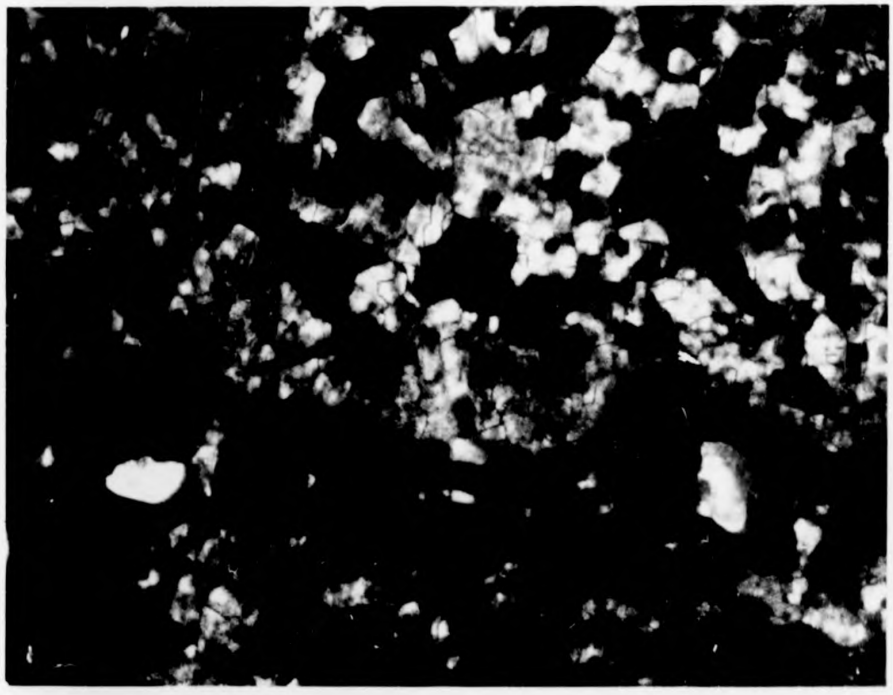

e

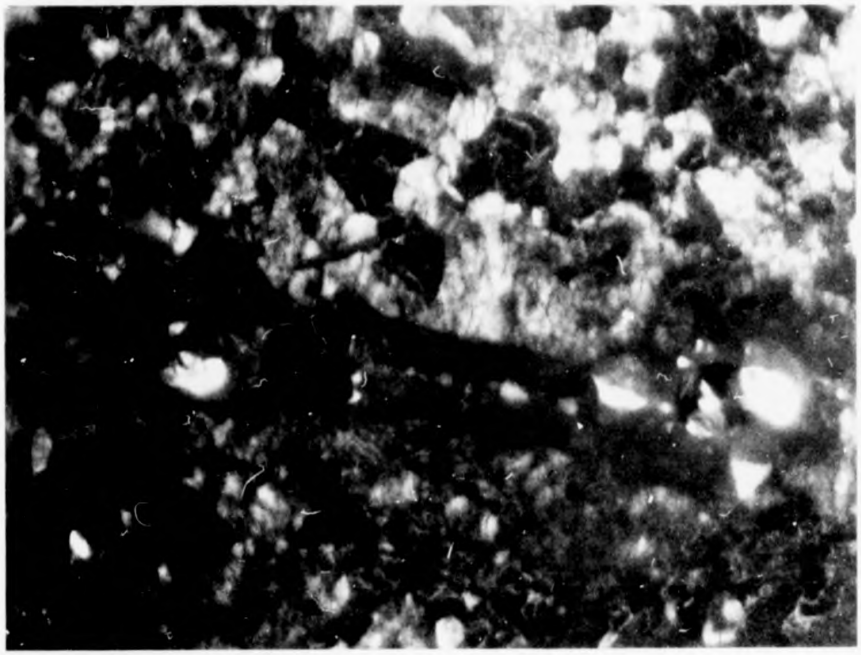

d

0·1 μ

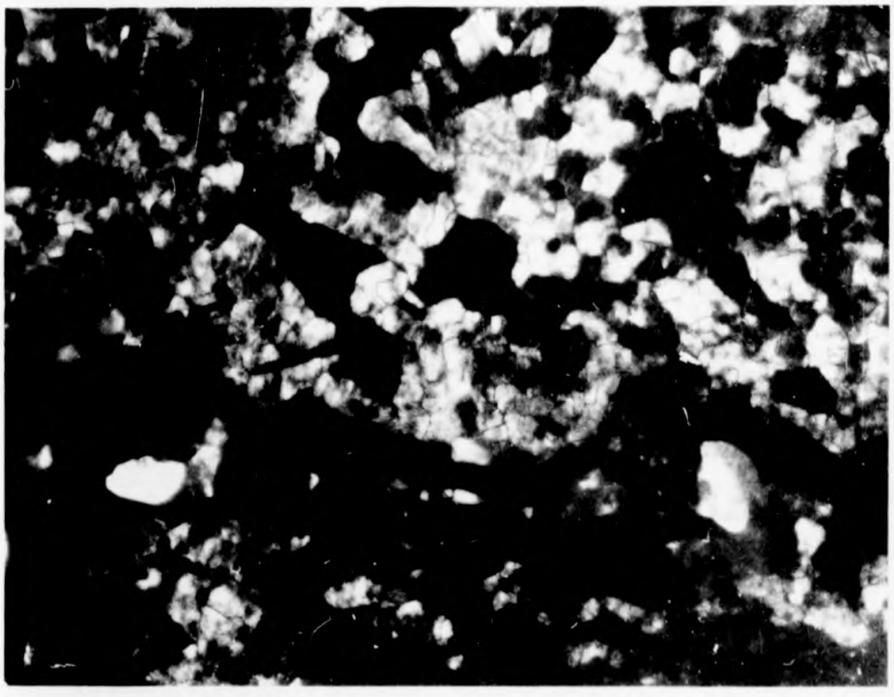

e

each of the extra diffracted beams labelled b, c, d on the accompanying diffraction pattern. Figures 6.3.1b, c show that the beams b and c arose from completely different domains of the corroded surface. Figure 6.3.1d shows a superposition of these two sets of domains together with a third set. This clearly reflects the multiplicity of spot d. All three sets of domains are shown more clearly in fig.6.3.1e. which is the dark field image formed by using beams b, c, and d together. A comparison of these dark field images showed clearly that the corrosion phase grew with a pronounced crystallographic domain structure, and that there were three distinct sets of domains, each of which gave rise to one of the three diffracted beams selected to form the dark field image. Identical sets of domains appeared in the dark field images formed from all such groups of extra diffracted beams. It could be concluded therefore that the corrosion process, involving the selective dissolution of silver and the re-distribution of the residual gold into islands, also led to a new phase being formed which grew epitaxially on the surface of the corroded alloy in three distinct but crystallographically related orientations. In the next section the possibility that this new phase was an oxide, probably gold (1) oxide is discussed, this being formed under the special conditions established in the aqueous environment by the selective dissolution of silver.

More information concerning the spatial distribution of the distinct crystallographic orientations of the domain structure in the corrosion phase could be obtained when dark field T.E.M. images were formed by selecting pairs of beams from the clusters of extra spots in the diffraction pattern. The interference between these beams gave rise to patterns of moiré fringes wherever their respective domains overlapped on the alloy surface. The micrograph shown in figure 6.3.2., which is an enlargement of figure 6.3.1e, was prepared in a similar manner but using the central spot and two of the arced spots in the characteristic cluster of spots. The fringes illustrated

0·05μ

Fig. 6.3.2. Moiré fringe patterns formed by the interference of three beams diffracted by the corrosion phase corresponding to the spots labelled b, c and d in the diffraction pattern shown in fig. 6.3.1. There are two orientations of fringes, corresponding to the overlap of two types of crystallographic domain in the corrosion phase with a third.

0·05μ

Fig. 6.3.2. Moiré fringe patterns formed by the interference of three beams diffracted by the corrosion phase corresponding to the spots labelled b, c and d in the diffraction pattern shown in fig. 6.3.1. There are two orientations of fringes, corresponding to the overlap of two types of crystallographic domain in the corrosion phase with a third.

Fig. 6.3.2. Moiré fringe patterns formed by the interference of three beams diffracted by the corrosion phase corresponding to the spots labelled b, c and d in the diffraction pattern shown in fig. 6.3.1. There are two orientations of fringes, corresponding to the overlap of two types of crystallographic domain in the corrosion phase with a third.

some degree of overlapping of the three sets of domains corresponding to these three diffracted beams. Thus, it was concluded that the corrosion phase grew with a complex microstructure of overlapping crystallographic domains. An additional explanation is possible (Hall, 1982 private communication). These alloy samples are in intimate contact with a layer of pure gold because of the way in which they were fabricated. Oxide could therefore grow on this gold surface as well as the upper, re-formed alloy surface. The overlapping domains observed using the dark field technique described above would therefore occur between oxide on both exposed surfaces of the specimen.

A dramatic example of the growth of the epitaxial corrosion phase is given in figure 6.3.3a. This shows a nominally pure gold foil stripped from a silver/mica base. This particular specimen had been allowed to stand for several weeks and interdiffusion at the gold/silver interface was thought to have occurred (see Chapter 2) so that a thin alloy layer existed between the two pure metal layers. After exposure to nitric acid during the stripping of the "gold" layer from the silver, rounded particles of the corrosion phase were clearly visible on this specimen. The diffraction pattern from such a sample is the same as that shown in fig. 6.2.1b and the dark field image (fig. 6.3.3b) which was formed using the satellite reflection described earlier, shows the particles in pronounced bright contrast against the dark alloy background. Figure 6.3.4. is an enlargement taken from figure 6.3.3b in which the fringes are clearly visible.

Moiré patterns such as those shown in figs. 6.3.2. and 6.3.3/4 are effectively spatial maps of the epitaxial relationship between the domains in the corrosion phase. The imperfections clearly visible in the fringe patterns indicate some local departures from good epitaxy at certain parts of the interface.

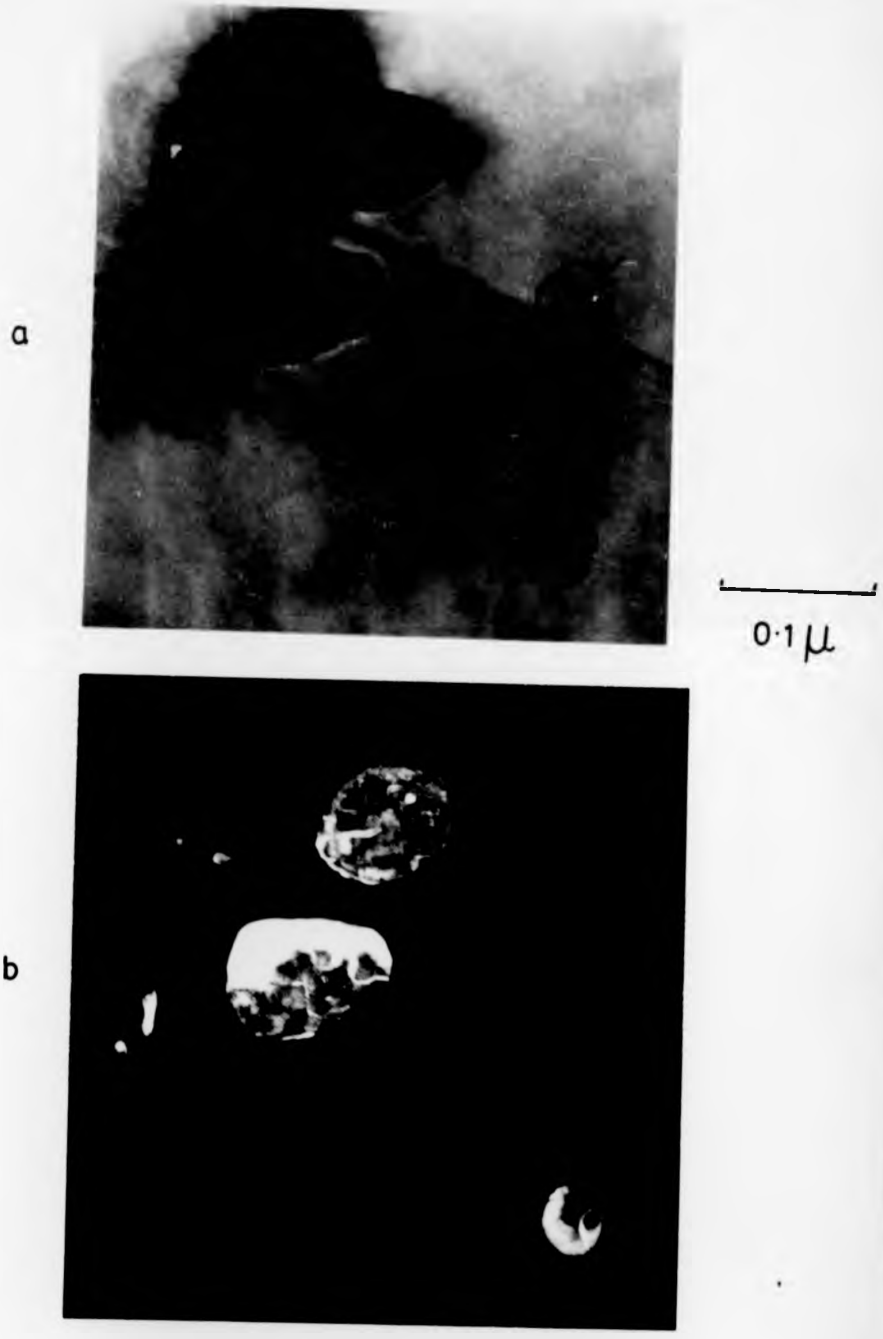

Fig. 6.3.3. Bright (a) and dark field (b) images of a nominally pure-gold foil stripped from a silver/mica base.

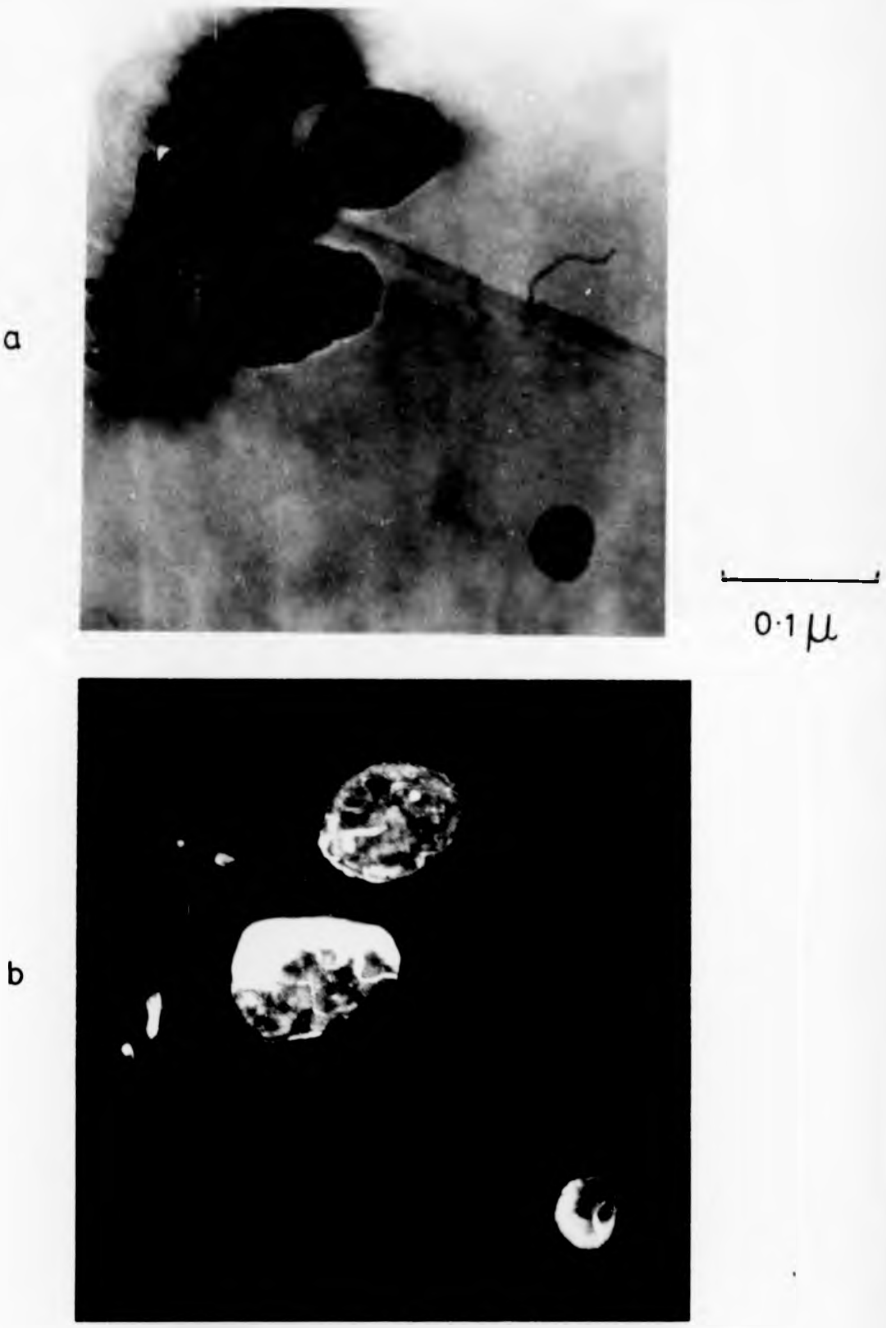

Fig. 6.3.3. Bright (a) and dark field (b) images of a nominally pure-gold foil stripped from a silver/mica base.

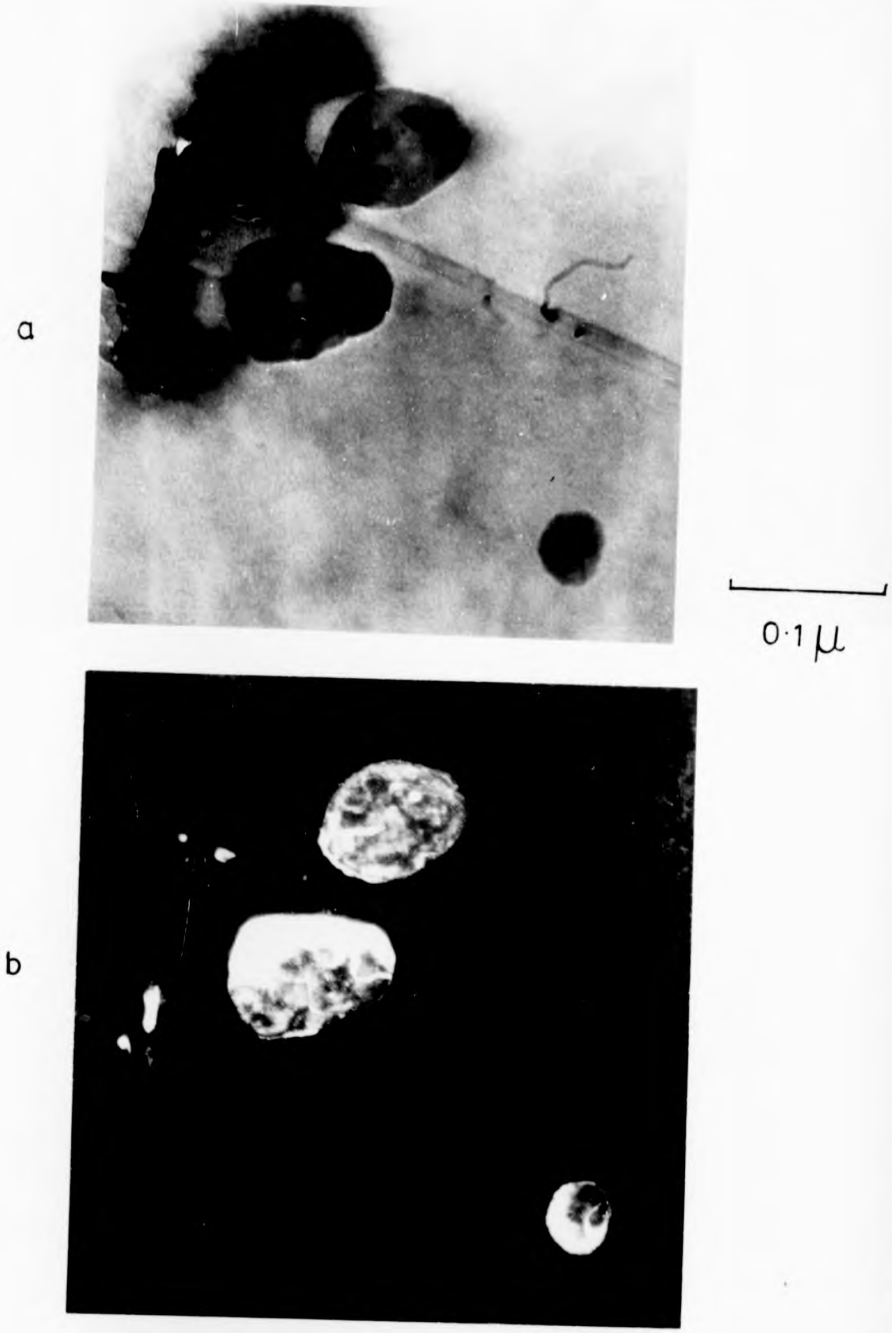

Fig. 3.3. Bright (a) and dark field (b) images of a nominally pure-gold foil stripped from a silver/mica base.

Fig. 6.3.4. This is an enlargement of fig. 6.3.3. in which moiré fringes are clearly visible which map out the epitaxial relationship between the corrosion phase and the underlying material.

0·05 μ

Fig. 6.4. This is an enlargement of fig. 6.3. in which moiré fringes are clearly visible which map out the epitaxial relationship between the corrosion phase and the underlying material.

0·05 μ

Fig. 6.4.4. This is an enlargement of fig. 6.4.3. in which moiré fringes are clearly visible which map out the epitaxial relationship between the corrosion phase and the underlying material.

6.4. Interpretation of Diffraction Patterns from Corroded Specimens

A more detailed analysis of the diffraction patterns from corroded specimens is given here. This, together with the evidence obtained from dark field images, leads to the conclusion that the corrosion of the alloy in nitric acid is accompanied by the formation of a surface overgrowth. In the next section the possible identification of the overgrowth as an oxide of gold is discussed.

The dark field microscope observations have shown that the corrosion phase was distributed in three distinct sets of crystallographic domains and each set of domains gave rise to particular extra spots in the diffraction pattern. The extra spots were arranged in clusters composed primarily of three spots. Six such clusters appeared around the 000 spots and this pattern was repeated about each of the $2\bar{2}0$ spots due to primary diffraction in the uncorroded alloy. This latter observation indicated, on a simple kinematical diffraction basis, that the corrosion phase was an overlayer formed on the surface of the alloy.

If it is assumed that the overgrowth had a simple cubic structure and that there was an epitaxial relationship between it and the (111) oriented alloy surface defined by $(110)\ [1\bar{1}0]_{\text{corr. phase}} \,||\, (111)\ [1\bar{1}0]_{\text{alloy}}$, then the unusual diffraction pattern observed for the corroded alloy can be constructed from a combination of the diffraction patterns for the silver-gold substrate and the corrosion phase. This is illustrated in fig. 6.4.1. There are in fact, three such expitaxial arrangements corresponding to setting the $[1\bar{1}0]$ direction in the corrosion phase parallel to each of the three close-packed $\langle 1\bar{1}0 \rangle$ directions in the (111) surface of the alloy. Thus the occurrence of the three distinct crystallographic domains in the corrosion phase, confirmed using dark field microscopy, was associated with these three epitaxial arrangements. The partially reconstructed diffraction pattern shown in fig. 6.4.1d, includes one of the clusters of spots formed by diffraction in the corrosion phase after primary $2\bar{2}0$ diffraction in the alloy (i.e. double

Fig. 6.4.1. The reconstruction of the diffraction pattern for a corroded silver-gold alloy assuming that the corrosion phase is a simple-cubic structure growing on the (111) surface of the alloy with three epitaxial relationships of the form $(110)\ [1\bar{1}0]_{\text{corr. phase}} \,||^{1}\, (111)\ [1\bar{1}0]_{\text{alloy}}$. The spots labelled with subscript 'a' are due to diffraction in the alloy; those labelled with subscript 'c' correspond to the corrosion phase. (a) Diffraction pattern for the alloy in a (111) orientation. The 'forbidden' $1\bar{1}1$ spots have been omitted. (b) Diffraction pattern for one type of crystallographic domain of the corrosion phase in a (110) orientation. (c) Diffraction pattern obtained by superimposing three domains of corrosion phase in (110) orientation on the (111) surface of the alloy with the $[1\bar{1}0]$ direction in the corrosion phase parallel to each of the three $\langle 1\bar{1}0\rangle$ directions in the alloy. (d) Reconstructed diffraction pattern including one cluster of extra spots containing pairs of arced spots formed by double diffraction of two of the primary $2\bar{2}0$ reflections in the alloy as well as the pair formed about the primary 000 beam. The full circles are $1\bar{1}1_c$ and 002_c reflections from the corrosion phase formed about the 000 beam; the thin circles are similar reflections formed by a second diffraction of the $2\bar{2}0_a$ beam from the alloy; the thick circles are similar reflections formed about a neighbouring $2\bar{2}0_a$-type beam. Note how the central 'spot' in each cluster is composed of three 002_c-type spots.


a
$2\bar{2}0_a$
000
b
$2\bar{2}0_c$
$1\bar{1}1_c$
002_c
c
$2\bar{2}0_a$
$2\bar{2}0_c$
$1\bar{1}1_c$
002_c
d

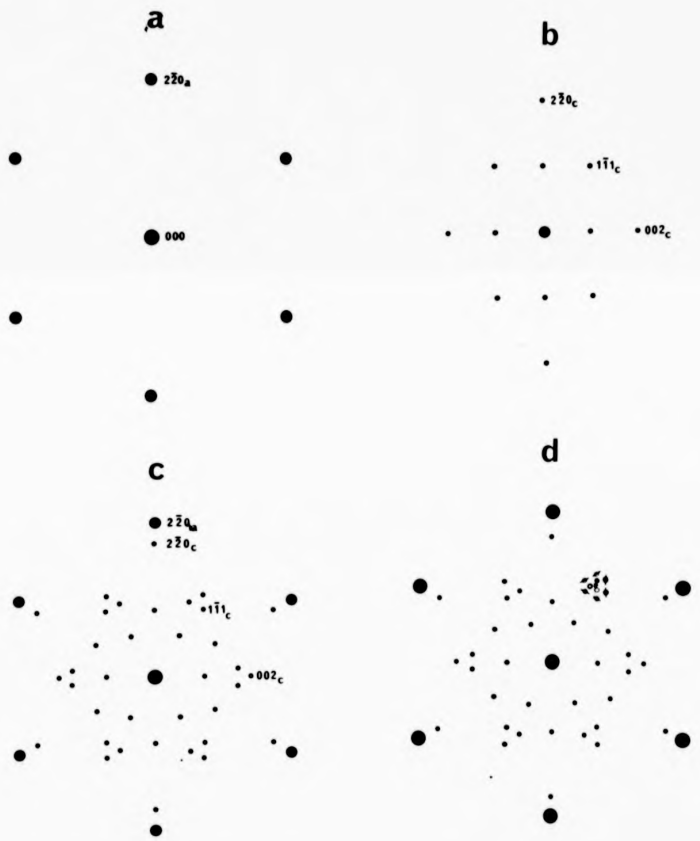
a
$2\bar{2}0_a$
000
b
$2\bar{2}0_c$
$1\bar{1}1_c$
002_c
c
$2\bar{2}0_a$
$2\bar{2}0_c$
$1\bar{1}1_c$
002_c
d

diffraction). This has been drawn to emphasise the fact that the 002 type spots in these clusters do not coincide precisely but are distributed about the forbidden $^1/3\ (2\bar{2}4)$ reflection from the alloy. As noted earlier, this multiplicity of the central spot in each of the composite clusters can be seen in the enlarged section of the observed diffraction pattern shown in fig. 6.3.1a, and schematically in Fig. 6.2.2. It is apparent when the dark field images shown in figs. 6.3.3.b, c and d are compared.

Having identified the structure of the corrosion phase in this way, its lattice parameter could be determined from the diffraction pattern. Taking the lattice parameter for silver-gold to be a_o = 4.08 Å, this means that the lattice parameter of the cubic structure assumed for the corrosion phase was a_o = 4.91 ± 0.05 Å. This could be checked for consistency with the spacing of the moiré pattern fringes observed in the dark field images. According to the foregoing interpretation of the diffraction pattern, the two sets of fringes in figure 6.3.2. could now be interpreted as moiré patterns, involving interference between the 002 diffracted beams from one type of domain and $1\bar{1}1$ beams from each of the other two domains of the corrosion phase. This gave a calculated fringe spacing of 14.0 ± 2 Å which agreed reasonably well with that measured (16 ± 1 Å). Moreover the d spacings of the 002 and $1\bar{1}1$ oxide planes and of the forbidden $^1/3\ (2\bar{2}4)$ alloy planes measured from calibrated diffraction patterns were consistent with the above structural interpretation. They were found to be 2.41 ± 0.02 Å; 2.83 ± 0.03 Å and 2.49 ± 0.02 Å respectively.

This interpretation of the diffraction pattern has been given further support by a high resolution examination of the corrosion phase, undertaken in collaboration with Smith and Freeman at Cambridge University using the 600 kV high resolution electron microscope (Smith et al 1981). Using a specimen similar to that illustrated by figure 6.3.3. it has been possible to observe directly the lattice planes of both the overlayer and the gold substrate. Optical diffractograms prepared from these high resolution micrographs reproduced the electron diffraction pattern and gave an oxide

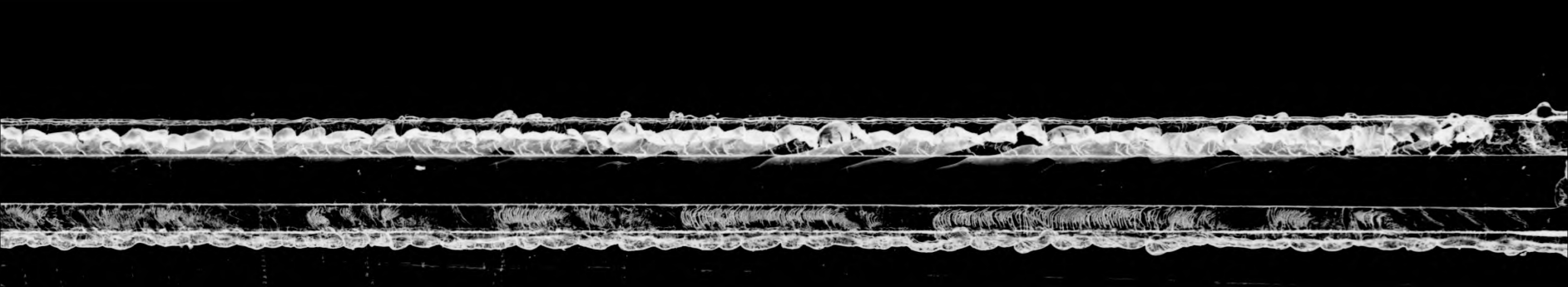

diffraction). This has been drawn to emphasise the fact that the 002 type spots in these clusters do not coincide precisely but are distributed about the forbidden $^1/_3$ $(2\bar{2}4)$ reflection from the alloy. As noted earlier, this multiplicity of the central spot in each of the composite clusters can be seen in the enlarged section of the observed diffraction pattern shown in fig. 6.3.1a, and schematically in Fig. 6.2.2. It is apparent when the dark field images shown in figs. 6.3.3.b, c and d are compared.

Having identified the structure of the corrosion phase in this way, its lattice parameter could be determined from the diffraction pattern. Taking the lattice parameter for silver-gold to be $a_o = 4.08$ Å, this means that the lattice parameter of the cubic structure assumed for the corrosion phase was $a_o = 4.91 \pm 0.05$ Å. This could be checked for consistency with the spacing of the moiré pattern fringes observed in the dark field images. According to the foregoing interpretation of the diffraction pattern, the two sets of fringes in figure 6.3.2. could now be interpreted as moiré patterns, involving interference between the 002 diffracted beams from one type of domain and $1\bar{1}1$ beams from each of the other two domains of the corrosion phase. This gave a calculated fringe spacing of 14.0 ± 2 Å which agreed reasonably well with that measured (16 ± 1 Å). Moreover the d spacings of the 002 and $1\bar{1}1$ oxide planes and of the forbidden $^1/_3$ $(2\bar{2}4)$ alloy planes measured from calibrated diffraction patterns were consistent with the above structural interpretation. They were found to be 2.41 ± 0.02 Å; 2.83 ± 0.03 Å and 2.49 ± 0.02 Å respectively.

This interpretation of the diffraction pattern has been given further support by a high resolution examination of the corrosion phase, undertaken in collaboration with Smith and Freeman at Cambridge University using the 600 kV high resolution electron microscope (Smith et al 1981). Using a specimen similar to that illustrated by figure 6.3.3. it has been possible to observe directly the lattice planes of both the overlayer and the gold substrate. Optical diffractograms prepared from these high resolution micrographs reproduced the electron diffraction pattern and gave an oxide

lattice parameter of 4.90 Å thereby confirming the foregoing analysis.

6.5. The Chemical Identification of the Corrosion Phase

It was found that both the micromorphology of the corroded alloy and the moiré patterns associated with the corrosion phase underwent a change during prolonged examination in the electron microscope, particularly when high beam currents were being used for dark field microscopy. This might be attributed to the heating effect of the electron beam causing a decomposition of the corrosion phase. As previously reported (Chapter 4) extensive growth and re-arrangement of the gold islands could be caused by heating the corroded alloy to a temperature of about 400°C. It was found that the extra spots in the diffraction pattern disappeared under these same conditions of heat treatment. Clearly there was a connection between growth of the gold islands and the thermal decomposition of the corrosion phase. This implied that the corrosion phase was some form of gold compound which was thermally unstable.

The lattice parameter of the cubic crystal structure obtained from the observed diffraction pattern for the corrosion phase (a_o = 4.91 ± 0.05 Å) is close to the value of 4.74 Å listed in the A.S.T.M. Index (1979) for silver I oxide (Au_2O being 3.6% larger). Silver oxide (Ag_2O) has a simple cubic structure, Wells (1975), consisting of interpenetrating face-centred-cubic silver and body-centred cubic oxygen lattices. This is known to be thermally unstable, decomposing at 160°C. The crystallographic evidence which required the overlayer to have a simple cubic structure, suggests therefore, that the corrosion phase might be silver I oxide, or a related compound.

A number of simple chemical tests designed to confirm this conclusion were performed. For example, the effect of strong acids on the corrosion phase was examined. Using the persistence of the diffraction pattern as an indicator of the stability of the compound, it was found that the phase

was quite stable in nitric acid, only partially soluble in sulphuric acid but very soluble in hydrochloric acid. This behaviour is unexpected for silver I oxide but is consistent with the reported properties of gold I oxide (Massey et al 1973). Furthermore, the corrosion phase was found to be soluble in potassium hydroxide whereas silver oxide should be insoluble.

The balance of evidence indicates, therefore, that the corrosion phase was gold I oxide. Unfortunately, there is no report in the literature of a study of the crystal structure of this compound. However, there is evidence from a comparison of the crystal structures of other compounds of monovalent silver I and monovalent gold I that they are isomorphic (e.g. Au_2S and the high temperature form of Ag_2S, both have a cubic structure the lattice parameter of Au_2S being ~3% bigger than for Au_2S. This is of the order of the measured difference in lattice parameters for gold and silver oxide (3.62%)). It is possible, therefore, that gold I oxide has a structure similar to that of silver oxide. Since both lattices consist essentially of a b.c.c. lattice of oxygen ions and the interpenetrating cations are small compared with O^{2-} it might be expected that the two structures will have similar lattice parameters. Using the values for ionic radii of Au^+, Ag^+ and O^{2-} given in the literature (Handbook of Chemistry and Physics 1981-1982) and using the structure outlined above, a lattice parameter of 4.82 Å for Au_2O is obtained. This is reasonably consistent with the measured value. The conclusion is therefore that the overlayer formed by the corrosion of silver-gold alloy in nitric acid is probably gold I oxide, having a simple cubic crystal structure and a lattice parameter $a_o = 4.91 \pm 0.05$ Å.

6.6. Some Implications of the Formation of Gold I Oxide During the Corrosion of Silver-Gold Alloys

If the observation that the corrosion phase is gold I oxide is correct some further discussion is necessary to find a mechanism whereby the oxidation

of gold might occur during the corrosion reaction. Furthermore, an explanation is needed of how both gold islands and the oxide overlayer could be formed as corrosion products of the same reaction. The islands and the oxide appeared as separate phases in the T.E.M. images but islands appeared to grow at the expense of the decomposing oxide when a corroded alloy was heated.

Pure gold is highly stable in nitric acid whereas silver is soluble. However, the possibility of a coupling of reactions in a dissolving alloy influencing the behaviour of gold has already been mentioned. The dissolution of silver in nitric acid is thought to proceed as follows (Evans 1960:-

Anodic reaction $Ag \rightarrow Ag^+ + e^-$

Cathodic reactions $H^+ + e^- \rightarrow H$ initially, followed by

$$H + HNO_3 \rightarrow H_2O + NO_2$$

$$NO_2 + e^- \rightarrow NO_2^-$$

$$NO_2^- + H^+ + \rightarrow HNO_2$$

$$HNO_2 + HNO_3 \rightarrow 2NO_2 + H_2O.$$

Thus two molecules of nitrogen dioxide (NO_2) are formed for every silver atom dissolved and they may in turn be reduced to NO_2^- enabling more silver to be dissolved. The reaction is said to be autocatalytic. The concentration of NO_2 would appear to rise indefinitely as long as silver is dissolving but several alternative reactions tend to reduce this concentration, these are:-

$$H + HNO_2 \rightarrow NO + H_2O$$

$$2HNO_2 \rightarrow 2NO + H_2O$$

Both these reactions remove nitrous acid which is necessary for the autocatalytic 'loop' to be complete and therefore act to lower the concentration of NO_2 formed during silver dissolution. When silver dissolves

from silver-gold alloy, it is most likely that the above series of auto-catalytic reactions are again set in motion and thereby generate a strongly oxidising environment for gold atoms adjacent to the dissolving silver. It has been shown (Finkelstein and Hancock 1974) that for gold to dissolve it is usual for it to be both oxidised and complexed. For example, HNO_3 is an oxidising reagent whilst chloride ion, Cl^- is an efficient complexing agent for Au^{3+} and hence Au is soluble in aqua regia ($1HNO_3$ + 3HCl). Nitrogen dioxide (NO_2) and the nitrite ion (NO_2^-) formed during silver dissolution are oxidising and complexing agents, respectively. It is also probably important that these species are produced in very close proximity to the residual gold atoms which are left after silver has dissolved. It is possible then that gold is taken into the first few layers of solution, adjacent to the corroding alloy, where it will be transported quickly away from the dissolving silver to more cathodic sites. The chemical conditions here are such that the gold "complex" becomes unstable i.e. the local concentrations of NO_2 and NO_2^- are lower, and the complex dissociates depositing gold. So this oxidised and mobile gold only forms in a quasi stable state at the actively dissolving regions of the alloy. Once it migrates elsewhere it dissociates depositing gold. An approximate estimate of the surface diffusivity of gold atoms required to account for the observed island growth (Forty and Rowlands 1981) shows that this must be greater than the value expected for a clean gold surface at room temperature. Consequently partial oxidation and solvation of the gold might well be essential in providing a mechanism for such rapid diffusion. The overall corrosion behaviour, and in particular the micromorphology that develops on silver-gold alloys, may be influenced, then, by this partial dissolution of gold. This is an important idea which will be developed in the following chapter of this thesis where similar ideas for the copper-gold system are also proposed.

This proposed transport mechanism for gold requires the cathodic reaction balancing the anodic dissolution of silver to occur vigorously in the vicinity of the anodic sites so that the NO_2 and NO_2^- species are readily

available at sufficiently high concentrations to oxidise the gold atoms at these sites. This might no longer be the case when islands have coalesced to form pits since the corrosion reaction will tend to be more inhibited; under these conditions the balancing cathodic reaction in the electrolyte producing NO_2^- might be expected to occur elsewhere on the surface. In this way a build up of NO_2^- might occur over the whole surface of the alloy, now generally gold-rich except inside the pits. In the absence of stirring this can lower the oxidation potential for gold so that the metastable oxide forms. Such an oxide layer would tend to stabilise the tunnelling mode of corrosion observed for these alloys, as is found in other examples of pitting and tunnelling corrosion.

Alternatively, it may be that the oxide forms at an earlier stage so that the sequence of events would be dissolution of silver, oxidation/transport of gold, solid oxide film formation and finally oxide decomposition into gold which forms islands. These processes can occur concurrently so that the island morphology develops as observed whilst the oxide layer continues to grow and decompose. In other words island growth is only a secondary result of the more important primary step of oxidation. Forty (1982) has used this idea to develop a structural model to account for the diffraction contrast of islands and also deformation structures observed in the transmission electron microscopy of corroded and deformed silver-gold alloys.

The importance of the coupling of the reactions controlling the dissolution of silver and the oxidation of gold, as suggested here, may have a more general significance in the corrosion of other binary alloys where selective dissolution is known to occur. It means that the noble metal component of the alloy plays a more direct role in the corrosion behaviour of such alloys.

References: Chapter Six

Cherns, D., (1974), Phil. Mag. 30, 549.

Evans, U. R., (1960), The Corrosion and Oxidation of Metals (London: Edward Arnold), p.326.

Finkelstein, N. P., and Hancock, R. D. (1974), Gold. Bull., 7, 72.

Forty, A. J. and Durkin, P., (1980), Phil. Mag. A, 42, 295.

Forty, A. J. and Rowlands, G., (1981), Phil. Mag. A, 43, 171.

Forty, A. J., (1982), Microdeformation Markings in T.E.M. Images of Silver Gold Alloys, submitted for publication.

Hall, C. R., (1982), private communication.

Massey, A. G., Johnson, B. F. G., Thompson, N. R., and Davis, R., (1973), The Chemistry of Copper, Silver, and Gold, (Oxford: Pergamon Press), p.97,

Pashley, D. W., and Stowell, M. J., (1963), Phil. Mag., 8, 1605.

Pickering, H. W., and Swann, P. R., (1963), Proceedings of the Second International Congress on Metallic Corrosion (Houston: NACE), P.128.

Pickering, H. W., (1967), Proceedings of Conference on Fundamental Aspects of Stress Corrosion Cracking, edited by R. W. Staehle, A. J. Forty and D. van Rooyen (Houston: NACE), p.159.

Smith, D. J., Freeman, L. A., Durkin, P. and Forty, A. J., (1981), Inst. Phys. Conf. Ser. No. 61, E.M.A.G., (The Institute of Physics, Bristol and London).

Weast, R. C., (1982), Editor, Handbook of Chemistry and Physics 62nd Edition, CRC Press, Florida.

Wells, A. F., (1975), Structural Inorganic Chemistry, 4th Edition, Clarendon Press: Oxford.

Powder Diffraction File Search Manual, (1979), File No. 12-793, (Pennsylvania, U.S.A.: Joint Committee on Powder Diffraction Standards).

CHAPTER SEVEN

General Discussion

In this chapter some of the implications of the observations made on silver-gold and copper-gold corroded alloys and on the formation of gold oxide, described in chapters 4, 5 and 6 are discussed. The ideas previously mentioned briefly will be discussed more fully and subsequently drawn together in a general discussion on selective dissolution.

7.1. A Simple Corrosion Disordering-Reforming Model for Selective Dissolution of Silver from Silver-Gold Alloys Corroded in Nitric Acid

Observations on silver-gold alloys corroded in nitric acid reveal island structures which are remarkably similar to the structures seen in vapour-deposited thin gold films during their initial stages of growth on cleavage surfaces (Pashley 1965). This suggests that corrosion gives rise to surface disordering due to silver being removed. This is followed by a reforming of the residual material by surface diffusion, in a manner analogous to the growth of deposited metal islands during thin film growth by vapour deposition. For simplicity the proposed model assumes that disordering and reforming are discrete and sequential processes, so that a smooth layer-by-layer attack occurs.

The structural aspects of selective dissolution from an ideal terrace, ledge, and kink, surface have been outlined in the introduction to this thesis. For the specimens described here, the (111) surface can be considered to be terraced with monoatomic steps separating atomically smooth regions. There is support for this, since loops of mono-atomic steps have been revealed on gold films prepared by a similar vapour deposition method by Cherns (1974) using weak beam transmission electron microscopy. This step structure is consistent with the layer-by-layer way in which

CHAPTER SEVEN

General Discussion

In this chapter some of the implications of the observations made on silver-gold and copper-gold corroded alloys and on the formation of gold oxide, described in chapters 4, 5 and 6 are discussed. The ideas previously mentioned briefly will be discussed more fully and subsequently drawn together in a general discussion on selective dissolution.

7.1. A Simple Corrosion Disordering-Reforming Model for Selective Dissolution of Silver from Silver-Gold Alloys Corroded in Nitric Acid

Observations on silver-gold alloys corroded in nitric acid reveal island structures which are remarkably similar to the structures seen in vapour-deposited thin gold films during their initial stages of growth on cleavage surfaces (Pashley 1965). This suggests that corrosion gives rise to surface disordering due to silver being removed. This is followed by a reforming of the residual material by surface diffusion, in a manner analogous to the growth of deposited metal islands during thin film growth by vapour deposition. For simplicity the proposed model assumes that disordering and reforming are discrete and sequential processes, so that a smooth layer-by-layer attack occurs.

The structural aspects of selective dissolution from an ideal terrace, ledge, and kink, surface have been outlined in the introduction to this thesis. For the specimens described here, the (111) surface can be considered to be terraced with monoatomic steps separating atomically smooth regions. There is support for this, since loops of mono-atomic steps have been revealed on gold films prepared by a similar vapour deposition method by Cherns (1974) using weak beam transmission electron microscopy. This step structure is consistent with the layer-by-layer way in which

these metal films thicken after the initial nucleation stage on the mica substrate. In the first instance silver atoms at kink sites in these surface steps will be dissolved when the alloy is brought into contact with nitric acid. Eventually all such atoms will be removed and the kink sites at steps will thereafter be occupied by gold atoms. Dissolution at the step can only continue if atoms exchange places along the steps to renew silver occupation of the kink sites. For silver-gold alloys migration of atoms along steps should occur readily even at room temperature so dissolution can continue. As more silver is removed the stepped terraces will shrink to form discs of gold-rich material. These will be small, possibly only clusters of a few atoms since Auger electron spectroscopy shows that the surfaces of these specimens are enriched with silver. There is some evidence that enrichment can occur slowly even at room temperature (Forty 1982, private communication) and it is possible that this may have an important effect during corrosion. After these discs are formed, further dissolution requires that silver atoms are removed from newly exposed terrace sites in the alloy surface. This requires a greater activation energy (or dissolution potential), but is clearly possible since observations show that corrosion continues. It is the removal of silver from this surface layer which leads to disordering. This disorder may be considered as either a high concentration of gold ad-atoms or of surface vacancies. The former is a better description for a silver-rich alloy and the latter for a gold-rich one. In any case the surface mobilities of the remaining gold atoms have to be sufficiently high to induce growth in the tiny residues formed from corrosion of the previous layer. In this way, islands slowly grow as successive cycles of selective dissolution of silver and surface diffusion of residual gold occur. Surface diffusion coefficients at room temperature must be high enough to account for a typical distribution of islands. It is possible that the transport of disordered gold over the

surface of the alloy is assisted by the electrolyte (aqueous nitric acid and of course complex ions). This argument was developed in Chapter Six and will be referred to later in this Chapter. This process of island growth results in the removal of surface atoms which will therefore reveal a fresh surface to the acid, so that further selective dissolution of silver can proceed. This gives rise to more surface disorder, further surface migration and consequently further growth of islands. Figure 7.1.1. shows diagrammatically how the surface disordering and reforming occur at successively deeper atomic planes in the alloy. The overall result is a re-distribution of the alloy during which silver is dissolved, the gold-rich islands grow and the channels between them deepen by corrosive action. Eventually the islands should coalesce and merge to form pits trapped between them. The pits remain as active areas of corrosion. In this way redistribution of the alloy continues and the pits continue to shrink but deepen. The model presented so far explains in crude terms the basic morphologies which have been observed on these alloys.

The thermodynamic driving force for the re-ordering of the residual disordered gold is the lowering of surface energy when islands and eventually pits form from a disordered surface. The TEM images of corroded specimens show that the edges of islands and pits are quite well defined. Pits are often hexagonally-shaped, having edges parallel to the principal $\langle 1\bar{1}0 \rangle$ directions in the alloy. It is likely that in any case the faces of islands and pits are relatively close packed and so will have low surface energies. Although compositional differences are expected between various corrosion induced morphological features, these are probably less important than geometrical and structural factors in determining morphology. The surface energies of silver and gold are similar and so compositional differences will not in themselves significantly affect the overall surface energy of an alloy.

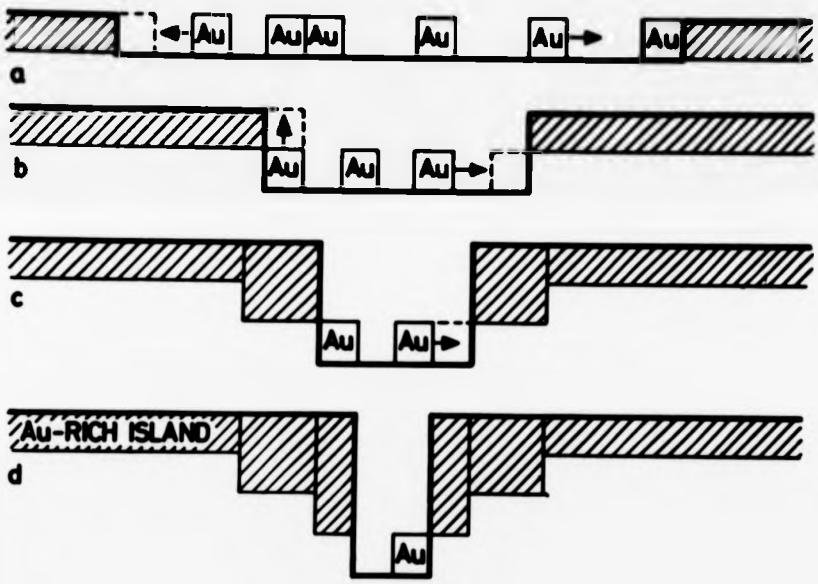

Fig. 7.1.1. Schematic representation of island growth and pit formation according to the corrosion disordering/diffusion reordering model.

To summarise, the surface morphologies observed for a wide range of silver-gold alloys after exposure to various concentrations of nitric acid, and in some cases a subsequent heat treatment, can be used to provide a model for selective dissolution. Dissolution of silver leads to a disordered, gold-rich surface layer, which then reforms by surface diffusion of the gold ad-atoms into an island and channel structure. This structure can develop further into a pit morphology when the islands coalesce. The formation of pits occurs only in the silver-rich alloys and appears to do so more readily for higher concentrations of silver and with stronger acid.

7.2. Further Models for Selective Dissolution

Forty and Rowlands (1981) have devised an analytical model to account for the variation of morphology with alloy composition and this is summarised below. In this model, several simplifying assumptions have been made. The first assumption is that only the less-noble component is dissolved by the acid, leaving the noble component as a disordered distribution of adatoms on the surface of the alloy. It is also assumed that only those less-noble atoms situated in the surface of the alloy are dissolved. Thus the possibility that diffusion of silver from the underlying layers of the alloy contributes to the dissolution at the surface is ignored. The second step in the sequence involves diffusion of the residual noble metal adatoms over the surface and eventually the nucleation of islands. This second stage is assumed to be the rate-determining stage. A further assumption is that all the noble metal atoms remaining in the disordered surface eventually migrate to form islands. Furthermore none of the less noble atoms left on the surface are assumed to participate in island growth. This is probably unrealistic because these too should have a relatively high surface mobility. In order to analyse the growth process the assumption is made that these steps of chemical disordering and diffusive

re-ordering occur sequentially. This is only valid if the surface re-ordering occurs sufficiently rapidly.

This model has enabled predictions to be made about the conditions under which the surface becomes completely passivated. At high concentrations of noble metal (> 50% Au), the island layer should form a complete coverage of the surface in a definite time, so that corrosion eventually stops. At low concentrations (< 50% Au), the islands never completely cover the surface. The channels and pits which form as a result of incomplete merging of the islands shrink at an ever decreasing rate. A critical composition, (50% gold), corresponds to the parting limit of the alloy.

In the case of dilute alloys, the model predicts a critical radius below which a shrinking pit develops into a tunnel. This depends on among other things, the concentration of noble metal in the alloy. Swann (1969; 1971) has also observed corrosion tunnelling. He used copper-gold alloys exposed to ferric chloride solution and arrived at a model linking tunnel radius with alloy composition. However, the Forty-Rowlands model produces calculated radii which are in better quantitative agreement with experiment than those of Swann (Forty and Rowlands 1981).

Two important features emerge from the Forty-Rowlands model. The first is that the morphology which eventually develops on silver-gold alloys is critically dependent on the thickness (m) of the island nuclei which form in the initial stages of corrosion. A significant weakness of the model is that this cannot be predetermined with a great deal of accuracy. Although this should depend on alloy composition in a consistent way, artefacts in specimens (such as surface segregation of silver and other discontinuities of composition or structure) can give rise to variations in m for a given alloy composition. The other feature which emerges from this model is the thickening of the rim of an island as it grows, resulting from the layer-by-layer removal of material from the

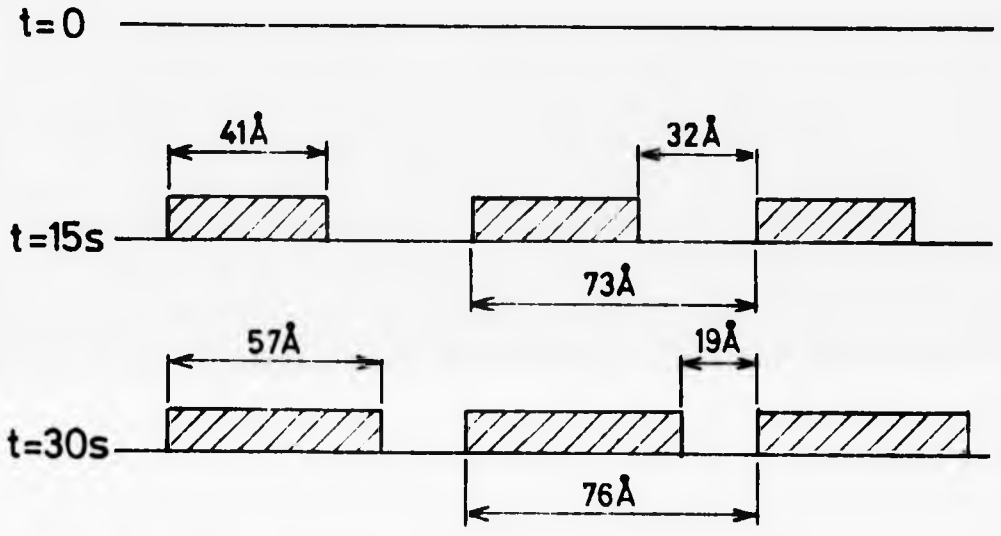

Fig. 7.2.1. This is a representation of the development of corrosion morphology on a 50% Au, Ag-Au alloy (specimen 3 as described in section 4.9) corroded in 35% nitric acid. It shows the condition of the surface directly after stripping and after immersion in nitric acid for 15 s and a further 15 s. It is constructed so that the morphology consists only of islands having the measured average diameter and separation.

surrounding surface. This is important because it reduces the rate of lateral growth. Consequently, the coverage of the surface by an island occurs in progressively smaller steps, as a result of both the reduction in the corroding surface area and the deepening of the island walls.

Thus the model implies two stages of corrosion: the first in which island nuclei are established, and the second in which they grow according to the layer-by-layer processes discussed above. Measurements described in Chapter Four indicate that the number of islands observed does indeed increase with increasing exposure to acid (60% in the example quoted). Obviously the simplifying assumptions on which the model is based will give rise to some discrepancies between what is predicted and what is observed. Other measurements described in Chapter Four do, however, provide some support for the model and these are discussed below.

It was possible to obtain an average island diameter for a 50:50 alloy after it had been exposed to 35% nitric acid for 0, 15 and 30 s respectively (Chapter Four). In addition, it was possible to obtain an average channel width (i.e. distance between the edges of islands) in the same way. If the alloy surface is considered to be composed of a statistically averaged morphology then it can be represented as shown in Fig. 7.2.1. This shows that the distance between island centres after 15 s and 30 s exposure is remarkably consistent. These measurements can be used to test the Forty-Rowlands model and a value for the surface diffusivity of gold can be obtained in this way. Furthermore the number of disordered atomic layers (n) represented by each morphology can also be calculated.

The numerical values obtained for surface diffusivity and n will be critically dependent on the value chosen for the thickness of the initial island nucleus (m). Several examples have been calculated corresponding to several values of m. These are given on the next page.

Table 7.1.1. To show the dependence of the values of surface diffusivity and n (number of disordered layers) on the original thickness m of island nuclei according to the Forty-Rowlands model (Forty and Rowlands 1981).

Thickness (m) of initial island nuclei (in atom layers)	time (s)	number of disordered atom layers (n)	Surface Diffusivity of gold ($cm^2\ s^{-1}$)
m = 1	15 s	6	1.68×10^{-14}
	30 s	17	1.32×10^{-14}
m = 4	15 s	18	6.20×10^{-14}
	30 s	58	5.18×10^{-14}
m = 7	15 s	31	1.09×10^{-13}
	30 s	102	8.97×10^{-14}

The number of atomic layers in the alloy cannot be greater than 127, (i.e. the total alloy thickness of the specimen being corroded). This implies that m cannot be greater than seven since in the case of the alloy exposed to acid for 30 s this would yield values of n corresponding to thicknesses in excess of the original alloy thickness. Obviously the minimum value for m must be one. These values of m can be used to define the corresponding maximum and minimum values of surface diffusivity of gold. Thus the surface diffusion coefficient for gold lies between 10^{-14} and 10^{-13} $cm^2\ s^{-1}$. These values are high compared with the value obtained by extrapolating from high temperature measurements (i.e. 1.5×10^{-15} $cm^2\ s^{-1}$).

These measurements should not be considered definitive and ideally many more attempts should be made to obtain information of this kind. They do, however, yield reasonably consistent values for surface diffusivity in the two cases of exposure to acid discussed (i.e. 15s and 30s). Perhaps

Table 7.1.1. To show the dependence of the values of surface diffusivity and n (number of disordered layers) on the original thickness m of island nuclei according to the Forty-Rowlands model (Forty and Rowlands 1981).

Thickness (m) of initial island nuclei (in atom layers)	time (s)	number of disordered atom layers (n)	Surface Diffusivity of gold ($cm^2\ s^{-1}$)
m = 1	15 s	6	1.68×10^{-14}
	30 s	17	1.32×10^{-14}
m = 4	15 s	18	6.20×10^{-14}
	30 s	58	5.18×10^{-14}
m = 7	15 s	31	1.09×10^{-13}
	30 s	102	8.97×10^{-14}

The number of atomic layers in the alloy cannot be greater than 127, (i.e. the total alloy thickness of the specimen being corroded). This implies that m cannot be greater than seven since in the case of the alloy exposed to acid for 30 s this would yield values of n corresponding to thicknesses in excess of the original alloy thickness. Obviously the minimum value for m must be one. These values of m can be used to define the corresponding maximum and minimum values of surface diffusivity of gold. Thus the surface diffusion coefficient for gold lies between 10^{-14} and 10^{-13} $cm^2\ s^{-1}$. These values are high compared with the value obtained by extrapolating from high temperature measurements (i.e. 1.5×10^{-15} $cm^2\ s^{-1}$).

These measurements should not be considered definitive and ideally many more attempts should be made to obtain information of this kind. They do, however, yield reasonably consistent values for surface diffusivity in the two cases of exposure to acid discussed (i.e. 15s and 30s). Perhaps

the most significant factor to emerge from this analysis is that the surface diffusivity necessary to account for the observed morphology is higher than that obtained from extrapolation using high temperature measurements. This is in keeping with the ideas presented in Chapter Six concerning the possibility that gold atoms might be partially ionised and solvated in the presence of the electrolyte.

The simple corrosion disordering-surface re-ordering model discussed so far requires modification to allow for the possibility of ionisation and solvation of gold and to incorporate a phase of gold oxide. Fig. 7.2.2. is an attempt to illustrate a more complex corrosion mechanism involving temporary ionisation of gold as discussed in Chapter Six. This diagram shows the early stage of corrosion when an island morphology is expected Fig. 7.2.2.(a) and also the later stage where a pit morphology is expected Fig. 7.2.2.(b). For clarity, the ion paths of gold and silver have been drawn separately, but in the real case they would obviously overlap. Figure 7.2.2.(a) indicates that the cathodic and anodic reactions are occurring in close proximity to each other during the initial stages of corrosion. Gold is not contributing to the overall dissolution current of the reaction, it is simply moving from a channel to an island region with the assistance of the electrolyte (Chapter Six). In the later stages of corrosion Fig. 7.2.2.(b) the anodic and cathodic reactions are separated. Anodic dissolution of silver occurs at the bottom of the pit/tunnel and the balancing reduction of nitrogen dioxide occurs on the upper surface of re-formed gold. The build up of NO_2^- over this surface is thought to lower the oxidation potential for gold, enabling a layer of gold oxide to form. If this cathodic reaction occurs at the lower specimen surface (i.e. on the surface of the pure gold supporting film exposed to acid), then a layer of oxide may be formed there as well. Gold is once again transported from a pit to a re-formed region via the electrolyte, with no nett contribution to the dissolution current. Whether the gold is deposited as the

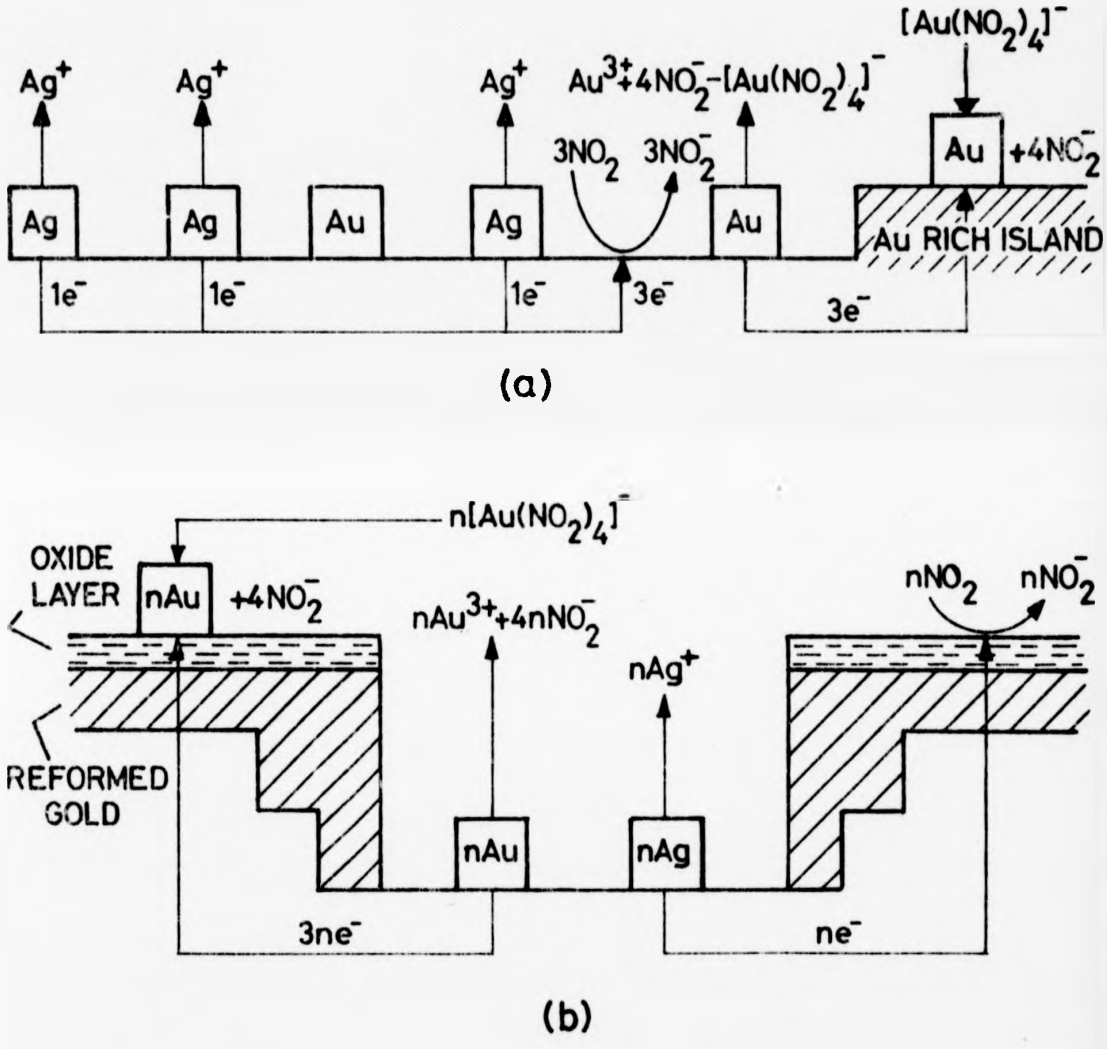

Fig. 7.2.2. A schematic representation showing the dissolution of silver and the electrolyte-assisted transport of gold (a) during the early stages and (b) during the later stages of corrosion.

metal and then oxidised or laid down directly as the oxide can only be a matter of speculation at this stage.

Swann (1969), in his model for tunnelling corrosion in copper-gold alloys, assumes that gold is redeposited only on the walls of tunnels, rather than on the alloy surface as indicated by the model given here. This model depends on an almost complete coverage of the surface with an increasing thickness of noble metal in the vicinity of pits. The observations of island nucleation and growth provide good support for this hypothesis. As tunnels grow deeper, then the assumption that all residual gold from the previous corrosion cycle will have re-ordered before further dissolution occurs, may break down. Some accretion of gold within the tunnels themselves may then occur. Swann (1969) observed small particles of gold, about 60 Å in diameter, inside corrosion tunnels in 25% Au, copper-gold alloys. This is not inconsistent with the ideas contained in the model given here. This model neglects the time required for diffusion of gold up the side walls of tunnels in estimating the rates of shrinkage of channels and pits. Provided the pits are shallow, this should not result in serious error. Indeed, this model gives better agreement with measured values of tunnel radii than the Swann model (Forty and Rowlands, 1981).

7.3. A Discussion of the Principal Observations Contained in the Thesis

The idea of enhanced surface mobility of gold was discussed in the previous section. Other observations given here also indicate that residual gold can be directly involved with the corrosion reaction. A dramatic indication of this direct involvement of gold in the corrosion process is the observation of a corrosion phase which, according to electron diffraction patterns and dark-field TEM images of corroded samples may be gold oxide. Oxidation of gold has already been indicated by the enhanced surface diffusivity mentioned earlier (7.2) and the structural and chemical evidence presented in Chapter Six of this thesis points fairly conclusively

to the formation of gold I oxide as a corrosion phase. There is independent evidence that gold oxide can form on these alloys when they dissolve, from electrochemical measurements made by Gerisher and Tischer (1954). Gerisher and Tischer were investigating the occurrence of resistance limits i.e. the possibility that there are alloy compositions at which no dissolution of the active constituent could be detected, irrespective of the corrosion parameters operating. They obtained current versus voltage curves for a range of silver-gold alloys in various oxidising acids (e.g. perchloric and acetic acids). They considered that kinks (i.e. increase of resistance) in these curves indicated the formation of a gold oxide. They identified this as Au_2O, from measurements of the potential at which it formed and also because this potential shows a dependence on the pH of the electrolyte (unlike the potential at which Au_2O_3 forms which is found to be independent of the pH of the electrolyte). If the applied potential required to dissolve silver, say, is greater than that at which Au_2O forms, then obviously, an oxide will grow. Although this influences the kinetics of the corrosion reaction, the film need not be completely passivating. Gerisher and Tischer found that the passivating effect of the film increased with increasing gold content of the alloy. They emphasise the critical influence of oxidising agents in solution in determining whether or not any oxide layer which forms is passivating. They also claim that in the absence of the formation of an oxide film, passivation may eventually occur by the formation of a dense gold layer (usually on alloys with a high gold content). To summarise, if the potential of the dissolving alloys is raised higher than that required to form gold oxide, then an oxide film forms. This film may or may not be passivating, depending on the exact nature of the oxidising species in solution. If the oxide does not form, dissolution will proceed unabated or a passivating layer of gold metal will form, depending on the composition of the alloy. They also noted evidence of passivating behaviour

to the formation of gold I oxide as a corrosion phase. There is independent evidence that gold oxide can form on these alloys when they dissolve, from electrochemical measurements made by Gerisher and Tischer (1954). Gerisher and Tischer were investigating the occurrence of resistance limits i.e. the possibility that there are alloy compositions at which no dissolution of the active constituent could be detected, irrespective of the corrosion parameters operating. They obtained current versus voltage curves for a range of silver-gold alloys in various oxidising acids (e.g. perchloric and acetic acids). They considered that kinks (i.e. increase of resistance) in these curves indicated the formation of a gold oxide. They identified this as Au_2O, from measurements of the potential at which it formed and also because this potential shows a dependence on the pH of the electrolyte (unlike the potential at which Au_2O_3 forms which is found to be independent of the pH of the electrolyte). If the applied potential required to dissolve silver, say, is greater than that at which Au_2O forms, then obviously, an oxide will grow. Although this influences the kinetics of the corrosion reaction, the film need not be completely passivating. Gerisher and Tischer found that the passivating effect of the film increased with increasing gold content of the alloy. They emphasise the critical influence of oxidising agents in solution in determining whether or not any oxide layer which forms is passivating. They also claim that in the absence of the formation of an oxide film, passivation may eventually occur by the formation of a dense gold layer (usually on alloys with a high gold content). To summarise, if the potential of the dissolving alloys is raised higher than that required to form gold oxide, then an oxide film forms. This film may or may not be passivating, depending on the exact nature of the oxidising species in solution. If the oxide does not form, dissolution will proceed unabated or a passivating layer of gold metal will form, depending on the composition of the alloy. They also noted evidence of passivating behaviour

for the copper-gold system, which they further discuss as evidence of the formation of gold oxide. However, no direct evidence for the formation of gold oxide has been observed on copper-gold specimens in the work described in Chapter 5, and it may be that in the copper-gold system passivation is achieved by some other means, although this seems less likely. Gerischer and Tischer conclude that although passivation does depend on alloy composition, a shift in the 'resistance' (parting) limit can be achieved by altering the pH and changing the oxidising agents in solution. This conclusion implies that any physical processes which operate to keep the active component dissolving (e.g. surface and volume diffusion), can be modified by the chemistry of the electrolyte in contact with it. This is in keeping with the findings of this thesis.

Either an oxide or a noble metal layer on the surface of alloys can have a profound influence on their corrosion behaviours. Copper-gold and silver-gold alloys are susceptible to stress corrosion failure when they are immersed in environments which will lead to the formation of gold-rich surface layers, (Pugh 1967). Reagents in which gold exists in a stable form as a complex ion (e.g. 10% KCN-H_2O_2), and which will therefore dissolve gold readily, do not give rise to stress corrosion failure. Stress corrosion attack is thought to proceed by the following stages: a gold-rich film forms initially on the surface. This is ruptured by the emergence of slip-steps. Corrosion of the metal along the slip trace leads to localised attack and this gives rise to an incipient crack. Rupture occurs at this weakened site under the applied stress. The underlying material then undergoes a similar sequence of events, so that the "crack" tends to propagate in a quasi-continuous way. Swann (1963) ascribes the mechanical weakening of the material to the formation of corrosion tunnels; it has already been observed (Chapter 4) that a tunnelling mode is eventually reached during the corrosion of silver-gold alloys, this presumably being stabilised by an oxide or passive layer as in other

examples of pitting and tunnelling corrosion.

We have seen how the preceding discussion leads to the idea that during the corrosion of gold alloys, gold can be either oxidised, partially ionised, or even partially dissolved. This leads to greatly enhanced mobility of the residual gold atoms. It is however, difficult to explain how an alloy of copper-gold forms when a layer of pure copper is dissolved off a gold layer. A possible indication of the way in which it happens may be obtained from the observation that marked variations in thickness occur in corroded silver-rich silver-gold alloys, as indicated by pronounced differences of electron absorption contrast in the TEM images (Chapter 4). This suggests that the sequence of processes represented schematically in figure 7.3.1. may occur. The reaction of pure copper proceeds via the autocatalytic cycle previously mentioned and it is reasonable to suppose that this will also cause marked variations in the thickness of the dissolving copper layer. That is, the autocatalytic reaction becomes established at certain strongly anodic sites on the copper surface. Material in the vicinity of these sites is quickly dissolved because of the autocatalytic reaction and consequently pits, extending deep into the material, are established. When the gold interface is reached, gold is taken into solution because of the strongly oxidising conditions established by the autocatalytic reaction, but is quickly re-deposited on the less actively dissolving regions. Alloying with copper occurs during deposition. These regions where the alloy forms are less anodic than regions of pure copper elsewhere on the surface and there will therefore be a tendency for subsequent autocatalytic cycles to be established only in these pure copper regions. Consequently more gold is dissolved and further alloy forms in the regions between those where the alloy was first formed. This process continues until a fairly uniform covering of alloy is reached (Fig. 7.3.1). Thereafter, the alloy layer itself is reduced to gold by a slower process of selective dissolution.

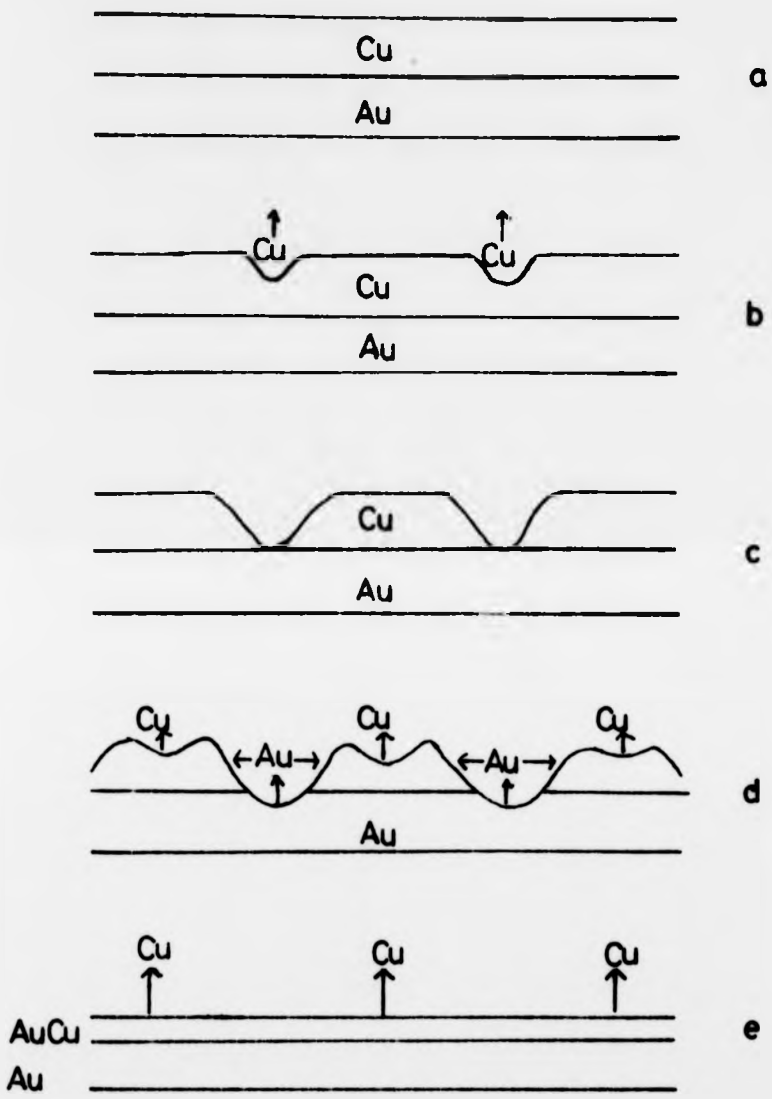

Fig. 7.3.1. A schematic representation of the sequence of processes which are thought to lead to the formation of an alloy layer when a layer of pure copper is dissolved off a layer of pure gold.

It should be emphasised that this explanation of the phenomenon of "corrosion alloying" is put forward only tentatively. One very interesting feature of the observations described in Chapter Five is that the composition of the alloy that forms always lies within a well-defined range of between 30 and 40% gold. This might indicate the alloy composition at which a sharp increase in resistance to selective dissolution occurs, possibly because a layer of gold oxide forms rapidly at this stage. That is, selective dissolution of copper occurs easily through the initially copper-rich alloy until the resistance limit of between 30 and 40% gold is reached. Thereafter, a rapid build-up of oxide markedly reduces the rate of selective dissolution, which tends to stabilise the alloy composition at this value. Although this is a plausible explanation, it must be remembered, however, that so far it has not proved possible to obtain evidence of gold oxide on copper-gold alloys.

Pickering (1967) also noted the formation of an alloy of this same composition from X-ray diffraction studies of copper-rich copper-gold alloys (between 5 and 10 atomic percent gold) after a period of corrosion by selective dissolution. An explanation can now be given in terms of partial oxidation and re-deposition of gold at the same time as dissolution of copper. This will continue until an alloy of this intermediate composition is obtained. Thereafter, dissolution is impeded (i.e. the kinetics of the corrosion reaction are affected) by oxide formation. Dissolution can continue at a fast rate from the uncorroded regions of the original copper-rich alloy until none of this remains. Copper is then more slowly dissolved from the new intermediate alloy, continuing at this much lower rate until only a layer of gold remains.

The suggestion that the formation of a quasi-stable alloy composition of approximately 35% gold during the dissolution of copper-rich alloys and of copper-on-gold bimetallic foils is due to the growth of a partially passivating oxide is supported to some extent by the observations of gold oxide formation on silver-gold alloys described in Chapter Six. In that

case oxide forms rapidly at an alloy composition of 25% gold or greater, but not at more silver-rich compositions. It is interesting to speculate that the corrosion of silver-rich silver-gold alloys or silver-on-gold bimetallic layers might also lead to "corrosion alloying" with a quasi stable alloy composition of 25% gold. However, it is not possible to investigate this possibility by electron or X-ray diffraction because silver, gold and silver-gold alloys all have closely similar lattice parameters.

It is interesting to observe that stress corrosion susceptibility, which is thought to require the initial formation and subsequent rupture of a passive film, reaches a maximum value for an alloy composition of 25% gold in the case of silver-gold and 35% gold in the case of copper-gold. This shows a notable correlation with the observations discussed above.

Further evidence for the degradation of the structure of an alloy during selective dissolution is found in the observation that dislocations and, sometimes, dislocation networks are created in corroded specimens. For example, Fig. 7.3.2 shows a TEM image of a copper-on-gold bimetallic foil after the copper has been completely dissolved, so that the diffraction pattern indicates that the residue is a single-crystal of pure gold. The micrograph shows many dislocations which extend over wide regions of the specimen. It has previously been observed (Chapter 5) that irregularities in the moiré fringes commonly observed in TEM images of copper-gold alloys may be due to a high concentration of dislocations which occur as a result of the corrosion reaction. In addition, dislocation networks are clearly visible on corroded silver-gold alloys which are subsequently annealed (Chapter 4). Thus the alloy structure appears to be considerably perturbed during corrosion and the formation of high concentrations of point defects is indicated. In Chapter Four the possibility that handling specimens introduces dislocations was discussed. Dislocations are not universally observed in specimens although they all receive similar handling during preparation. The observations discussed above, however, should be viewed with this in mind.

0·1μ

Fig. 7.3.2. T.E.M. image of a copper-on-gold bimetallic foil after the copper has been completely removed. This shows many dislocations which extend over wide regions of the specimen.

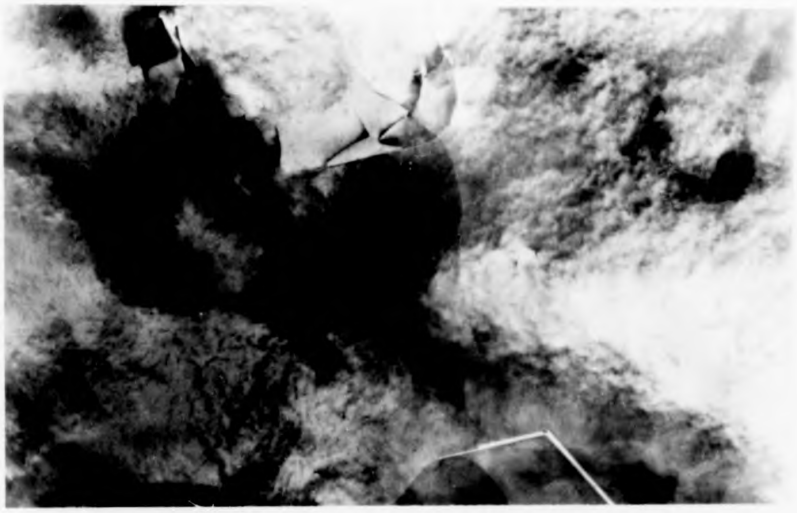

Fig. 7.3.2. T.E.M. image of a copper-on-gold bimetallic foil after the copper has been completely removed. This shows many dislocations which extend over wide regions of the specimen.

Dark-field TEM images of corroded copper-gold alloys formed using the forbidden $1\bar{1}1$ type reflections, seem to indicate an irregular and atomically 'roughened' surface after corrosion. Cherns (1974) has shown that surface steps on such films, or indeed any regions which have a thickness corresponding to a non-integral number of unit cells, contribute to the intensity of the $1\bar{1}1$ reflections. The intensity of these reflections, which do not appear in the reciprocal lattice section of perfect crystals, is an indication of the degree of surface roughening. Observations have been made in the present work which show that the intensity of the $1\bar{1}1$ spots in diffraction patterns from corroded specimens is frequently directly related to the extent of corrosion. Furthermore, by using these diffracted beams to form dark-field images, it has been possible to observe directly surface roughening by corrosion. Fig. 7.3.3.b is a dark-field image formed in such a manner (i.e. using a $1\bar{1}1$ reflection), while fig. 7.3.3.a is the corresponding bright field image. If the contrast in the dark field image is due to incremental variations in sample thickness of one atomic layer, then the shape and scale of the light and dark regions indicates that corrosion of the alloy is producing a surface which is highly disordered and severely roughened on the atomic scale.

7.4. Discussion of Selective Dissolution

In Chapter One, the various mechanisms proposed for preferential dissolution in binary alloys were outlined. The central problem concerns the transport processes which enable continued replenishment of the dissolving component at the corroding surface. These mechanisms are now discussed with reference to the observations contained herein.

At the time of commencement of this study the volume diffusion mechanism seemed the most satisfactory explanation of selective dissolution. Pickerings observations of chemical and phase changes accompanying selective

(a)

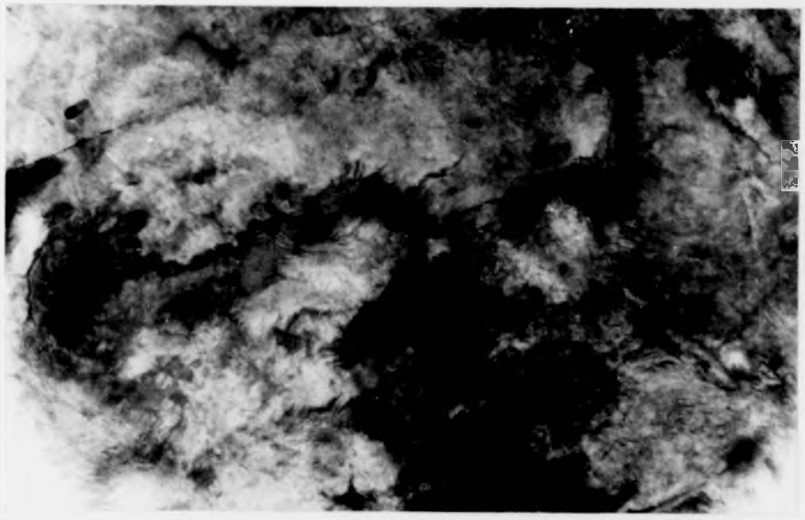

0·1μ

(b)

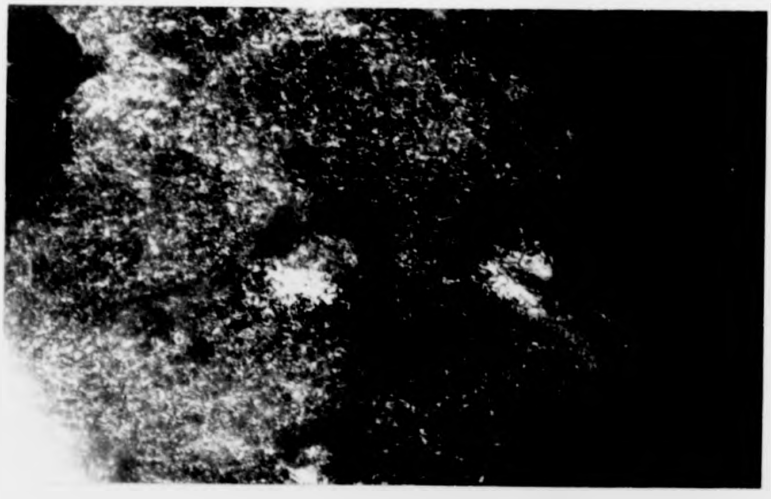

Fig. 7.3 3(a) T.E.M. of a copper-gold alloy (40% Au) immersed in 50% HNO_3 for 10 s. (b) Corresponding dark field image obtained using a forbidden $\bar{1}11$ reflection.

(a)

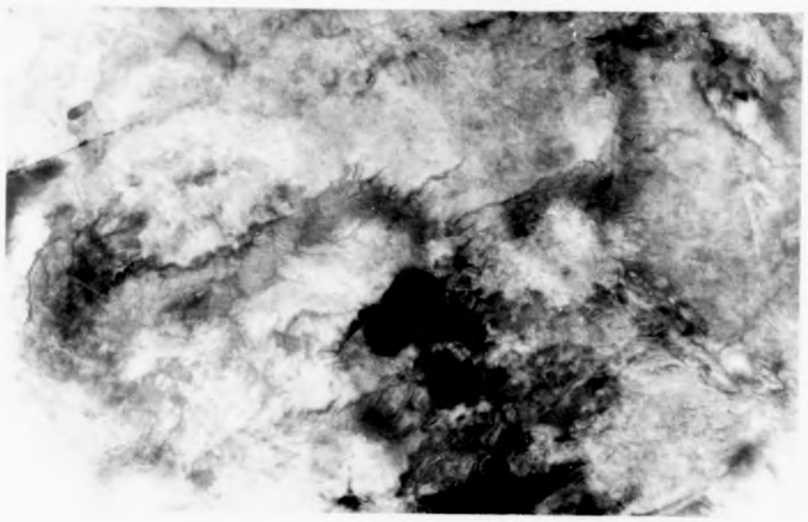

0·1 μ

(b)

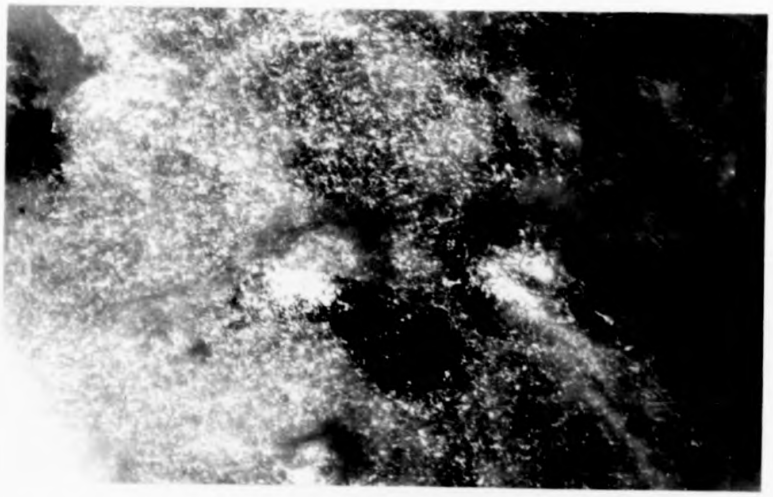

Fig. 7.3 3(a) T.E.M. of a copper-gold alloy (40% Au) immersed in 50% HNO_3 for 10 s. (b) Corresponding dark field image obtained using a forbidden $\bar{1}\bar{1}1$ reflection.

dissolution from copper-gold and brass alloy systems (1967, 1968, 1970) provided good support for this mechanism. Swann (1967) and Vermilyea (1967), however, expressed reservations about Pickerings conclusions and favoured the ionisation/precipitation mechanism and the surface diffusion mechanism respectively.

Morphological observations presented here clearly demonstrate the occurrence of surface diffusion under the conditions studied. Measurements seem to indicate that the surface diffusion of gold may be enhanced by an interaction with the electrolyte. That is, gold may be partially ionised during the course of corrosion, the degree of ionisation depending on the "aggressiveness" of the corrosion reaction. Thus the boundary between the surface diffusion mechanism and the ionisation/precipitation mechanism is not a clear one. If this idea is extended it is possible that all three transport processes, discussed in Chapter One, operate during selective dissolution, the balance between them varying according to the chemical activity of the system. An appraisal of the various models for selective dissolution follows, which contains an indication of the contribution of this work to the understanding of preferential dissolution in alloys.

Pickerings observations (1967, 1968, 1970) of chemical and phase changes as one component is selectively removed from an alloy indicate that there has been considerable rearrangement of material in the bulk of the alloy. He assumes that the active component diffuses to the corroding surface and the noble metal into the bulk of the alloy, thus creating the chemical and structural changes observed using X-ray and electron diffraction. The major criticism of this model is that it is necessary to invoke volume diffusion via divacancies and even this is insufficient to account for the high dissolution currents which he measured. The occurrence of volume diffusion during anodic dissolution of Cu-Au alloys should lead to severe

roughening of the surface, according to theoretical considerations by Harrison and Wagner (1959). It is this which Pickering uses to account for the large currents mentioned above. It is interesting to speculate whether the pit and tunnel morphologies described here, which would also increase the measured surface area and which do not need to invoke volume diffusion for their formation, would provide a better quantitative agreement between theoretical and measured dissolution currents.

The corrosion disordering surface re-ordering model given here is based on the much faster process of surface diffusion. The main evidence for this model comes from the micromorphological features which are observed on corroded specimens. These are interpreted as islands of re-ordered material on the upper surface of the alloy, which grow and merge as corrosion proceeds (Chapter 4). It has not been possible to positively identify the island features as gold-rich relative to the alloy. This is because the percentage difference in gold between the two regions is less than the uncertainty in the measurements (Chapter Four). An alternative explanation of the morphology is that it represents a condensation of vacancies which were injected when silver atoms were removed from terrace sites in the alloy crystal lattice. The observed morphologies are not typical of vacancy aggregates but bear a remarkable resemblance to the structures seen during the nucleation and growth of vapour deposited metal films on cleavage surfaces (Pashley 1965). Furthermore there was no obvious structural discontinuity within the samples at which vacancies could condense. In addition Forty (1982) has been able to interpret the observed contrast in corroded specimens in terms of an island morphology. For these reasons the observed morphologies are interpreted in terms of the island structures discussed in Chapter Four.

The analytical model based on the surface re-ordering mechanism of corrosion (Forty and Rowlands 1981) has been tested. The results are given in a previous section (7.2). These provide a measure of support

for the model, although it is obviously desirable to have more than the single set of measurements available in this case. The surface diffusion coefficient of gold obtained using the above model is between one and two orders of magntidue greater than that obtained from extrapolation of high temperature diffusivities. This supports the idea that during corrosion gold may be partially ionised and have increased mobility. The exact degree of ionisation is critically dependent on factors such as the reactivity of the less-noble constituent in the alloy, the composition of the alloy and the strength of the corroding acid.

The discussion so far has illustrated how the surface re-ordering model can account qualitatively and to a certain extent quantitatively, for most of the observations presented herein. The alloys used were, however, relatively thin (less than 200 atomic distances). Pickerings samples (1967, 1968, 1970) were much thicker, being typically several microns. This leads to the interesting possibility that volume diffusion may have an increasing contribution to selective dissolution with prolonged exposure of thick samples to acid. According to the conclusions of the models given here pit/tunnel regions will remain active even in thick alloys, provided they contain sufficient silver (Forty and Durkin 1980, Forty and Rowlands 1981). A contribution to dissolution from surface re-ordering of gold in these regions is thus expected, in addition to that due to volume diffusion. This seems a more satisfactory description of the large dissolution currents which Pickering obtained (1967) and which were difficult to explain simply in terms of volume diffusion.

It may be, then, that the three mechanisms for selective dissolution are best considered as complementary. Thus the surface re-ordering model may need to be modified to account for the possibility that diffusion of silver from the underlying layers of the alloy contributes to the dissolution at the surface. It has already been shown that a high degree of dissolution may create the conditions necessary for transport of gold in the electrolyte.

Finally the observations on thick samples of dissolution currents which are large compared with the quantity of dissolvable metal that could be expected to have been removed simply by invoking volume diffusion, indicate that more than one transport process may be operating. The balance in the contribution from the three transport processes will be critically dependent on the overall chemical activity of the system. Thus changes of alloy system, alloy composition, strength and time of exposure of corroding acid will all influence the respective contributions of each transport process. In general, a vigorous and extensive dissolution is expected in the initial stages of corrosion when the processes of ionisation/redeposition and surface diffusion of gold will dominate. As corrosion continues and much of the surface becomes covered with a layer of noble metal enriched material (i.e. the tunnelling mode of corrosion is attained), then the reaction will slow down. The contribution to dissolution from volume diffusion would consequently be increased. In order to understand selective dissolution it is necessary to be able to assess the relative contribution of the three transport processes.

References: Chapter Seven

Cherns, D., (1974), Phil. Mag. 30, 54.9.

Forty, A. J., and Durkin, P. (1980), Phil. Mag. 42, 295.

Forty, A. J., and Rowlands, G., (1981), Phil. Mag. 43, 171.

Forty, A. J., (1982), Private Communication.

Gerisher, H., Tischer, R. P., Z. Electrochem (1954), 58, 819.

Harrison, J. D., and Wagner, C. (1959), Acta Met. 7, 722.

Pashley, D. W., (1965), Adv. Phys. 14, 327.

Pickering, H. W., (1967), Proceedings of the Conference on Fundamental Aspects of Stress Corrosion Cracking, edited by R. W. Staehle, A. J. Forty, and D. van Rooyan (Houston: N.A.C.E.), p.159.

Pickering, H. W., (1968), J. Electrochem. Soc., 115, 690.

Pickering, H. W., (1970), J. Electrochem Soc., 117, 8.

Pugh, E. N., Craig, J. V. and Sedinks, A. J., (1967), Proceedings of the Conference on Fundamental Aspects of Stress Corrosion Cracking, edited by R. W. Staehle, A. J. Forty, and D. van Rooyan (Houston: N.A.C.E.), p.118.

Swann, P. R., and Pickering, H. W., (1963), Corrosion, 19, 369.

Swann, P. R., (1967), Proceedings of the Conference on Fundamental Aspects of Stress Corrosion Cracking, edited by R. W. Staehle, A. J. Forty, and D. van Rooyan (Houston: N.A.C.E.), p.176.

Swann, P. R., (1969), Corrosion, 25, 147.

Swann, P. R., (1971), Proceedings of Conference on the Theory of Stress Corrosion Cracking in Alloys, edited by J. C. Scully, (Brussels: N.A.T.O.), p.113.

Vermilyea, D. A. (1967), Proceedings of the Conference on Fundamental Aspects of Stress Corrosion Cracking, edited by R. W. Staehle, A. J. Forty and D. van Rooyan (Houston: N.A.C.E.), p.177.

CHAPTER EIGHT

General Conclusions

8.1. A Summary of the Principal Observations Contained in this Thesis

Observations on silver-gold alloys corroded in nitric acid revealed characteristic and well developed morphologies. These were first accounted for using a simple model based on the nucleation and growth of islands, from gold residues left on the alloy surface, when silver was selectively dissolved from it. This model assumed that the islands grew by surface diffusion of the gold, which was left behind when successive layers of the alloy were attacked. A qualitative description of the way the morphology develops was thus obtained. Measurements indicated that it was difficult to account for the development of morphology using the accepted value for the surface diffusivity of gold. A more complex interaction between gold and the electrolyte was indicated.

A further and stronger indication of direct interaction between residual gold and the electrolyte (nitric acid) was given by the observation of a corrosion phase, gold I oxide, found on silver-gold alloys. This was always found on alloys which exhibited the island-channel morphology. It was also observed in a less extensive form on pure gold foils where an island morphology did not occur. In this case the oxide phase probably occurred because of some small degree of local alloying due to interdiffusion of silver into gold at the silver/gold interface, a result of the way in which these films were manufactured (Chapter 2). There was structural and chemical evidence to support the existence of gold I oxide on corroded specimens. This had implications concerning the origin of the islands formed during corrosion. Both observations, the quantity of gold re-distributed into islands and the formation of gold oxide, indicated strongly that some oxidation, or partial ionisation, or even temporary dissolution

of gold occurred during corrosion.

A surprising observation made on the copper-gold system, was the formation of an alloy during the dissolution of copper from copper-on-gold bimetallic foils. An alloy of between 30 and 40% gold formed as the copper dissolved. This alloy eventually underwent selective dissolution to yield practically pure gold as the final product of corrosion. Some mixing of the two constituents had clearly occurred and it is interesting to speculate how exactly this could have happened.

These observations have led to an increased understanding of selective dissolution in binary alloys. Gold appears to be directly involved in the corrosion reaction under certain circumstances. In addition the importance of surface diffusion processes in selective dissolution has been demonstrated.

8.2. Summary of the Achievements of the Work Contained in this Thesis

The main achievements of the work described herein are itemised below.

1. The technique devised by Pashley (1959) for making single-crystal metal films of gold and extended by Forty (1980) to make gold alloy films has been shown to be successful in enabling electron transparent films to be produced. These are not typical of bulk materials but are relatively easily prepared and have mirror smooth surfaces. Chemical segregation and major structural singularities in these specimens have been investigated.
2. An investigation of the corrosion micromorphology which develops on silver-gold alloys corroded in nitric acid has been undertaken. A model is developed on the basis of these observations on silver-gold, which eventually leads to pit and tunnel morphologies similar to those observed elsewhere (Swann and Pickering 1963).
3. Estimates given here of the quantity of residual gold involved in surface diffusion during corrosion imply that the transport is much faster than simple ad-atom migration. It is suggested that this

arises from a strong interaction between the electrolyte and the corroding sample and the remaining uncorroded material (gold).

4. A corrosion phase is observed on silver-gold alloys and a thorough examination of its structure and epitaxial growth has been made. It is identified as gold I oxide. Some diffraction spots arising from this phase are streaked and this is not fully understood.
5. An observation of "corrosion-alloying" has been made. This leads to the idea of an intimate coupling of the chemical reactions involving the separate components of an alloy or a bimetallic foil. The narrow band of composition in which the quasi-stable alloy forms, points to the controlling influence of a passive layer.

The observations discussed here indicate that gold can be directly involved in the corrosion reaction. Thus it may be partially solvated and oxidised during dissolution. In addition to a corrosion morphology dislocation networks and point defects observed in corroded samples point to an aggressive rearrangement of the alloy crystal lattice. Normal solid state bulk and surface diffusion processes are unlikely to be sufficient to account for the extensive re-structuring of the alloy which apparently occurs during corrosion. It should be remembered that because the alloys are thin it is the relatively early stages of corrosion which are being observed where high dissolution currents would be expected. Furthermore the dissolution of silver and copper in nitric acid proceeds via an autocatalytic reaction which is not common in most corrosion situations. The observations, therefore, should be viewed in the light of these two factors.

Notwithstanding the specialised nature of the particular corrosion systems dealt with in this thesis, considerable weight has been added to the importance of surface diffusion during selective dissolution. In addition the possibility of electrolyte assisted surface diffusion has

been demonstrated. A model based on surface re-ordering of gold predicts features which are in fairly good agreement with the observed morphologies, even though many simplifying assumptions are made in the model. An important consequence of the model is that provided the concentration of silver is sufficiently high, then tunnel regions will remain active and not passivate even after extensive corrosion. If this were the case then a contribution to the dissolution current from surface diffusion processes as well as volume diffusion processes would be expected in the case of prolonged dissolution of bulk samples. The volume diffusion mechanism (Chapter 1) provides a good explanation for the observed chemical and phase changes accompanying selective dissolution (Pickering 1967, 1968, 1970). Pickering found it difficult, however, to account for the observed dissolution currents in terms of volume diffusion alone.

8.3. Future experiments

Several interesting experiments arise from the foregoing discussion. It would be desirable to examine thicker alloy films in the transmission electron microscope so that later stages of corrosion may be observed. Specimens have to be electron transparent but if they could be prepared without the gold supporting layer then alloy thickness could be approximately doubled. This would confer the additional advantage of enabling small local changes of gold concentration to be measured. One possible way of achieving this would be to deposit alloy directly onto a very thin slip of mica. The mica/alloy composite specimen could then be viewed directly in the electron microscope and no stripping would be necessary. Specimens would not necessarily be single crystals when prepared in this way.

A discussion of the Forty-Rowlands model (1981) in Chapter Seven revealed the importance of the initial distribution and thickness of island nuclei, on the subsequent corrosion morphology which developed. In view

of this it would be useful to obtain high resolution information using a microscope such as the one at Cambridge (600 kV operating voltage) so that any fine scale morphology developed in the very first stages of corrosion could be resolved. In the systems studied here it has been difficult to limit corrosion and arrest it in the very early stages but if the stripping process were dispensed with it may be possible to achieve this. In this way a more complete assessment of selective dissolution would be possible.

More information concerning the development of corrosion morphology is required. The effects of varying exposure time, alloy composition and strength of corroding acid need to be determined in a more quantitative way. This could be achieved by potentiostatically controlling experiments. However, it is possible, with patience, to obtain such information under open circuit conditions, as described in chapters four and seven. The relative contribution of the three transport processes to dissolution at various stages of corrosion ought to emerge from such a study.

Several more specific experiments might follow from the work described here. More extensive investigation should be undertaken to discover whether oxide growth can be detected on copper-gold alloys. The observation of dislocations in micrographs of corroded specimens of various noble metal alloys needs further investigation. This should lead to a greater understanding of the way in which the microstructure of an alloy is affected by corrosion. In conjunction with this, further use could be made of dark-field microscopy to obtain information about atomic roughening of surfaces by selective dissolution corrosion.

It is well known that many noble metal alloys are susceptible to stress corrosion cracking. The work described in this thesis has recently been extended to a study of this very important phenomenon. Selective dissolution is thought to play a crucial role in stress corrosion cracking phenomena and therefore this is a logical extension of the work already undertaken.

References: Chapter Eight

Forty, A. J., and Durkin, P., (1980), Phil. Mag. 42, 296.

Forty, A. J., and Rowlands, G., (1981), Phil. Mag. 43, 171.

Pashley, D. W., (1959), Phil. Mag. 4, 324.

Pickering, H. W. (1967), Proceedings of the Conference on Fundamental Aspects of Stress Corrosion Cracking, edited by R. W. Stachle, A. J.Forty and D. van Rooyan (Houston: N.A.C.E.), P.159.

Pickering, H. W., (1968), J. Electrochem Soc., 115, 690.

Pickering, H. W., (1970), J. Electrochem Soc., 117, 8.

Swann, P. R., and Pickering, H. W., (1963), Corrosion, 19, 369.